CIVIL ENGINEERING STUDIES
Structural Research Series No. 442

STUDIES ON THE SEISMIC DESIGN OF LOW-RISE STEEL BUILDINGS

by
C. JAMES MONTGOMERY
and
WILLIAM J. HALL

Technical Report of Research
Supported by the
NATIONAL SCIENCE FOUNDATION (RANN)
under Grant No. AEN 75-08456

DEPARTMENT OF CIVIL ENGINEERING
UNIVERSITY OF ILLINOIS
AT URBANA-CHAMPAIGN
URBANA, ILLINOIS

JULY 1977

BIBLIOGRAPHIC DATA SHEET	1. Report No. NSF/RA-770318	2.	3. Recipient's Accession No. PB276733

4. Title and Subtitle
Studies on the Seismic Design of Low-Rise Steel Buildings

5. Report Date
July 1977

6.

7. Author(s)
C. J. Montgomery, W. J. Hall

8. Performing Organization Rept. No. SRS442

9. Performing Organization Name and Address
University of Illinois at Urbana-Champaign
Department of Civil Engineering
Urbana, Illinois 61801

10. Project/Task/Work Unit No.
UILU-ENG-77-2012

11. Contract/Grant No.
AEN7508456

12. Sponsoring Organization Name and Address
Research Applied to National Needs (RANN)
National Science Foundation
Washington, D.C. 20550

13. Type of Report & Period Covered

14.

15. Supplementary Notes

16. Abstracts

The seismic analysis and earthquake resistant design of steel low-rise shear buildings, moment frame buildings, and x-braced frame buildings are studied. A number of two- and three-story buildings were designed according to the recommendations of modern building codes. The forces and deformations generated in the buildings under the North-South component of the El Centro 1940 earthquake were assessed by means of time-history analysis. It was found that the base story was the critical link in the lateral seismic load resisting system for the shear buildings, the moment frame buildings proportioned with weak columns, and the x-braced buildings considered. Two simpler methods of analysis, the modal method used in conjunction with inelastic response spectra and the quasi-static building code approach modified to explicitly taking inelastic behavior into account, were evaluated for use in calculating response quantities. The authors concluded that the quasi-static building code approach is the most appropriate procedure for use in the practical design of low-rise steel buildings of the types considered. Finally, the application of the results of these studies to the practical design of low-rise steel buildings is discussed.

17. Key Words and Document Analysis. 17a. Descriptors.

Earthquakes
Earthquake resistant structures
Buildings
Design standards
Construction
Steel construction
Earth movements
Seismology

17b. Identifiers/Open-Ended Terms

Low-rise steel buildings
Non-linear dynamic analysis
Earthquake resistant design
Seismic design

17c. COSATI Field/Group

18. Availability Statement	19. Security Class (This Report)	21. No. of Pages
NTIS	UNCLASSIFIED	181
	20. Security Class (This Page) UNCLASSIFIED	22. Price A09 - A01

ABSTRACT

This report presents studies on the seismic analysis and earthquake resistant design of steel low-rise shear buildings, moment frame buildings, and X-braced frame buildings.

In the first portion of the study, a number of two- and three-story buildings were designed according to the recommendations of modern building codes. The forces and deformations generated in the buildings under the North-South component of the El Centro 1940 earthquake were assessed by means of time-history analysis. It was found that the base story was the critical link in the lateral seismic load resisting system for the shear buildings, the moment frame buildings proportioned with weak columns, and the X-braced buildings considered. For the moment frame buildings proportioned with strong columns and weak beams, inelastic response was distributed fairly uniformly throughout the beams of the buildings. From the results of the time-history studies, it appears that inelastic deformations can be estimated from the elastic deformations by means of the design rules that have been developed for single-degree-of-freedom systems.

In addition, two simpler methods of analysis, the modal method used in conjunction with inelastic response spectra and the quasi-static building code approach modified to explicitly take inelastic behavior into account, were evaluated for use in calculating response quantities.

it was concluded that the quasi-static building code approach is the most appropriate procedure for use in the practical design of low-rise steel buildings of the types considered.

In the last section of the report, the application of the results of these studies to the practical design of low-rise steel buildings is discussed. A simplified design procedure that is in part similar to the quasi-static building code approach presently recommended by the Applied Technology Council III study is discussed; the procedure appears to be applicable at least to two- and three-story buildings. Comments concerning other factors (redundancy, reserve strength, and so forth) that should be considered in the design of low-rise steel buildings are made.

ACKNOWLEDGMENT

This report is based on the doctoral dissertation of C. James Montgomery submitted to the Graduate College of the University of Illinois at Urbana-Champaign in partial fulfillment of the requirements for the Ph.D. degree. The study was directed by William J. Hall, Professor of Civil Engineering, as a part of the research program "Design for Protection Against Natural Hazards", sponsored by the National Science Foundation (RANN) Grant No. ENV 75-08456 to the Department of Civil Engineering, University of Illinois at Urbana-Champaign. In the early stages, the study was supported in part by the Department of Civil Engineering through John I. Parcel funds. Also, computer services support was supplied in the early stages through the Research Board of the Graduate College of the University of Illinois at Urbana-Champaign. The above noted support is gratefully acknowledged.

Any opinions, findings, and conclusions or recommendations expressed in this publication are those of the authors and do not necessarily reflect the views of the National Science Foundation.

The authors extend their appreciation to Professors N. M. Newmark, D. A. W. Pecknold and J. E. Stallmeyer for advice during the course of the study.

TABLE OF CONTENTS

Page

LIST OF TABLES

LIST OF FIGURES

1. INTRODUCTION

1.1 Objectives of the Investigation

A major proportion of society's investment in building construction is consumed on low-rise buildings. Most people spend some portion of each day -- sleeping, working or living -- in buildings which can be classified as low-rise. In the past, many of the available techniques of seismic analysis and design have not been applied to this class of structures mainly because the additional design costs are large relative to the value of the buildings, the consequences of failure are considered to be small, or the dynamic properties cannot be expressed simply in mathematical terms. Thus, there is a need for procedures consistent with earthquake engineering theory that can be simply applied to the design practice of low-rise buildings.

The objective of the first portion of this investigation was to determine the behavior of some low-rise buildings when subjected to earthquake base motion. Step-by-step numerical integration of the governing equations of motion (time-history analysis) was used for these studies. In the second portion of this investigation, simplified analytical procedures, specifically the modal method and the quasi-static building code approach, were evaluated for use in predicting the dynamic response of low-rise buildings. The objective of the final portion of the investigation was to discuss the application of the results of the studies in this report to the design of buildings. The major emphasis of the studies was on inelastic response as it affects the seismic design of low-rise buildings.

This study was limited in scope to planar two- and three-story shear buildings, moment frame buildings, and X-braced frame buildings subjected to one horizontal component of earthquake ground motion. It was assumed that nonstructural components had an insignificant influence on the seismic response, and that torsional and soil-structure interaction effects could be ignored. A number of assumptions regarding the structural properties were made in order to simplify the problem of analysis to one of tractable proportions.

Although the studies were limited to a relatively small sampling of buildings subjected to only one base motion, it is hoped the conclusions drawn are general enough that certain limitations in current design procedures might be isolated, and the gap between complicated methods of analysis and simplified procedures of design might be lessened.

1.2 Previous Work

The problem of determining the dynamic behavior of building structures during earthquake motion has been approached by a number of experimental and analytical investigators. It has long been recognized that seismic behavior cannot be reconciled on a purely elastic basis. Thus, much of the recent research effort has been directed towards the determination of the lateral load carrying capacity of structures in the inelastic range. In the remainder of this section, reference is made to (a) pertinent experimental and analytical investigations which lay the foundation for the selection of the structural idealizations used in chapters to follow, (b) analytical studies which have given insight into the earthquake resistant design of buildings, and (c) some of the current methods of earthquake design.

1.2.1 Behavior of Steel Members and Frames -- Considerable effort in the development of the plastic design of steel theory has been directed towards the determination of the collapse load of moment frames. Tests (see for example Arnold, et al., 1968) have shown that the monotonic lateral load-deformation path observed in experiments can be closely predicted by second-order elastic-plastic analysis (Galambos, 1968).

Recently much emphasis has been placed on determining the cyclic hysteretic behavior of steel moment frame structures. The results of tests by Popov and Bertero (1973) on girder subassemblages, by Carpenter and Lu (1973) on frames, and others have shown hysteretic behavior to be remarkably stable. The results indicate that after a number of load cycles, the experimental ultimate strength can exceed the calculated monotonic load by 30 percent or more. This increase in load carrying capacity is primarily due to strain hardening and the beneficial effects of gravity axial loads acting on column members. Stiffness deteriorates as the number of load cycles increases because of the Bauschinger effect.

Local buckling of the flange or web of flexural members can lead to strength and stiffness degradation on cyclic loading, and this must be protected against in the proportioning of moment frames.

Analysts have attempted to use the results of cyclic load tests in formulating structural models to account for the hysteretic behavior of flexural members (Clough, et al., 1965; Giberson, 1969). Some success has been achieved in using these types of models in nonlinear time-history analysis procedures to predict the behavior of dynamically loaded steel frames (Tang, 1975).

The cyclic inelastic behavior of steel X-bracing is relatively new and not well defined. The load history of a steel brace extends from tensile yielding through compressive buckling. Although recent tests (Hanson, 1975) indicate that models with more complicated hysteretic behavior should be developed, the most commonly used is the elastoplastic model with tensile yielding and zero buckling strength. Igarashi, et al. (1973) have shown that this type of model predicts the dynamic behavior of steel diagonal braces well, provided the slenderness ratios of the braces are relatively large.

In summary, some of the basic factors which control the inelastic response of steel members and frames to earthquake base motions have been determined. It appears that more research is needed before simple analytical models can be developed to account for many of these factors.

1.2.2 Analytical Investigations -- Inelastic analytical studies generally fall in two categories: those based on spring-mass or shear-beam systems, and those based on more complicated finite element models.

The former type of study attempts to model the macroscopic behavior of a real structure. Work with single-degree-of-freedom systems with elastoplastic resistances has led to the inelastic response spectra proposed by Newmark (Veletsos et al., 1965; Newmark and Hall, 1973 and 1976). Veletsos (1969) summarizes the results of investigations on single-degree-of-freedom systems with various resistance functions. Bazán and Rosenblueth (1974) have studied the combined effect of two resistances in parallel, one representing frame action and the other representing X-bracing. Penzien (1960), Veletsos and Vann (1971), and

others have used elastoplastic shear-beam models to represent multi-degree-of-freedom systems.

Studies on shear-beam systems are usually carried out over a wide range of parameters with a minimum of expense. Design forces that would be consistent with a given amount of nonlinear behavior during an earthquake can be estimated for many one-story buildings directly from published results. Unfortunately, the results give little indication of the individual member ductility requirements.

The latter type of study uses finite elements to model tall buildings. Time-history calculations by Clough and Benuska (1967) on concrete frame buildings and Goel and Hanson (1972) on a series of lightly braced steel frames are representative of this class of investigation.

Studies using finite elements give insight into the ductility requirements of the individual members of a frame. The behavior of specific structures is indicated, but it is difficult to generalize the results and apply them to the design of other structures.

1.2.3 Present Methods of Design -- In the quasi-static building code approach (NBC, 1975; SEAOC, 1975; UBC, 1976; and so forth), the design lateral base shear is calculated and the distribution of the base shear as lateral loads over the building height is determined. These lateral loads are applied to the building and a static analysis is performed; members are proportioned to resist the forces thus obtained elastically.

The code design approach has evolved empirically from observations of building behavior during past earthquakes, and it is generally

consistent with more complicated methods of analysis and design (Newmark, 1968). Buildings designed according to the lateral force provisions of modern codes are expected to deform inelastically, withstanding ductilities of 4 to 6 without collapse during major earthquakes.

The modal method used in conjunction with response spectra provides a slightly more complicated procedure for determining lateral design forces, but one which is consistent with the principles of dynamic behavior. Unfortunately, since superposition is used, the modal method is only rigorously correct for linear elastic systems. However, Newmark and Hall (1973) note that, if design response spectra are modified to account for nonlinear behavior, the method can be used to approximate inelastic response quantities. In fact, some of the modern building codes (NBC, 1975; ATC, 1977) recommend this approach for complicated or important structures.

It is appropriate to mention that the development of procedures for the estimation of inelastic response quantities using the modal method is presently an area of active research (Anderson and Gupta, 1972; Luyties et al., 1976; Shibata and Sozen, 1976).

In short, it is apparent that design procedures for low-rise buildings must be simple and similar to present practice in order to be utilized by design engineers. It is likely that the quasi-static building code approach, modified to explicitly take into account inelastic behavior, is at present the most appropriate procedure for use in the design of low-rise buildings.

1.3 Scope of the Investigation

This report summarizes the methods used in, and the results of, detailed studies on the seismic response and the earthquake resistant design of low-rise steel buildings. It should be appreciated that for the sake of brevity and understanding the methods and results are presented in condensed form.

In Chaper 2 a series of two- and three-story low-rise steel buildings are designed according to the quasi-static procedures recommended by modern building codes. Also contained in Chapter 2 is a description of the ground motion used for time-history calculations and the development of design response spectra consistent with the ground motion. Appendix A contains supplementary data pertaining to the building properties described in Chapter 2.

The analytical procedures used for time-history analysis, modal analysis, and the quasi-static building code approach calculations are described in Chapter 3. Appendices B, C and D contain detailed descriptions of the analytical procedures discussed in Chapter 3.

The results of very interesting studies on the dynamic response of two-degree-of-freedom systems subjected to pulse base motion are contained in Appendix E; the intent of these special studies was to provide a theoretical basis on which to view the results of studies on more complicated building systems.

In Chapter 4 the results of time-history calculations on the building designs are summarized with particular attention being paid to the inelastic response, the story shear distributions, and the story displacements and drifts. Also contained in Chapter 4 is an evaluation of the modal method of analysis and the quasi-static building code approach for

estimating the base story shear. Appendix F contains the detailed results of the time-history calculations discussed in Chapter 4.

The application of the results of the studies recorded in this report to the design of low-rise buildings is discussed in Chapter 5. Procedures for proportioning structures to resist seismic motion with an adequate margin of reserve strength are discussed.

To the authors' knowledge, this is one of the few studies that has been directed specifically towards determining the inelastic response of low-rise steel buildings of practical proportions to earthquake ground motion. The studies have indicated that complicated methods of analysis are in general not necessary for use in analyzing commonly employed low-rise building frames. Also, the studies carried out have provided further confirmation of the fact that the design rules applicable to single-degree-of-freedom systems can be used to predict the dynamic response of (and can be used in the design of) low-rise buildings. In addition, in contrast to studies on simple systems, these studies on framing systems have pointed out clearly areas where additional research impacting practical design is required. For example, there is a tendency for yielding to be concentrated in the columns of well-designed low-rise buildings. As yet there are no easy-to-use and reliable procedures for evaluating the strength-deformation capacities of yielded columns subjected to thrust and end moment, especially where bracing against instability is lacking. Also, the role of secondary resisting systems, redundant resisting systems, and methods for evaluating the margin of safety or reserve strength under dynamic load reversal remain to be investigated.

1.4 Notation

The symbols used in the text are defined where they are first introduced. For reference purposes, they are also defined here. A superscript dot above a symbol indicates one differentiation with respect to time. A Greek delta prefix to a symbol indicates an incremental quantity.

a = maximum ground acceleration, or inelastic hinge length

A = cross-sectional area

A_n = spectral acceleration for the n-th mode of vibration

$[A]$ = pseudostatic structural stiffness matrix

b = coefficient of proportionality between mass and damping

$\{B\}$ = pseudostatic structural load vector

c_i = coefficient relating the yield displacement of the i-th spring to the maximum relative displacement observed when the system responds elastically

$[C]$ = structural damping matrix

d = maximum ground displacement

D_n = spectral displacement for the n-th mode of vibration

D.L. = dead load

E = modulus of elasticity

E.Q. = earthquake load

f = frequency of vibration for a single-degree-of-freedom system

f_n = frequency of vibration for the n-th mode

F_a = axial stress permitted in the absence of bending moment

F_b = bending stress permitted in the absence of axial force

F_x = design lateral force at the x-th floor

F_y = yield stress

$\{F\}$ = vector of design lateral forces, or vector of resisting forces due to structural stiffness

$[F]$ = structural flexibility matrix

$\{g\}$ = end moment vector for a simply supported (constrained) flexural element

$\{G\}$ = total element end force vector

$\{G_E\}$ = element end force vector calculated from material properties

$\{G_G\}$ = element end force vector calculated from geometric properties

$\{G_o\}$ = element fixed end force vector

h = story height

h_i, h_x = height of the i-th or x-th story

I = moment of inertia

k = story stiffness, or stiffness of a spring

k_A, k_B, k_C = entries to the simply supported (constrained) flexural element stiffness matrix

L = length of a flexural element, or horizontal length between columns

L_b = length of an X-brace

L.L. = live load

m = mass, or mode number

m_i = mass of the i-th story, or mass concentrated at the i-th degree-of-freedom

M_p = plastic moment capacity

M_{pc} = plastic moment capacity reduced to take axial load effects into account

$[M]$ = mass matrix

$\lceil M \rfloor$ = diagonal mass matrix

n = mode number, or number of cycles of iteration in the initial stress procedure

N = number of lateral translational degrees-of-freedom, number of stories, or axial force used to obtain the element geometric stiffness matrix (positive in compression)

P = axial force (positive in compression)

P_y = yield axial force

$\{P\}$ = structural load residual vector used in the initial stress procedure

q_m, q_n = generalized coordinate in the m-th or n-th mode of vibration

Q = story shear capacity, or story shear resisted by an X-brace subassemblage

Q_i = force in the i-th spring

$(Q_i)_{code}$ = force in the i-th spring calculated using the quasi-static building code approach

$(Q_i)_{max}$ = force in the i-th spring calculated by combining modes using the sum of the absolute values of modal quantities approach

$(Q_i)_o$ = maximum force in the i-th elastic spring

$(Q_i)_{prob}$ = force in the i-th spring calculated by combining modes using the square root of the sum of the squares of modal quantities approach

$(Q_i)_y$ = yield force in the i-th elastoplastic spring

$(Q_i)_{1st}$ = force in the i-th spring in the first mode

$\{R\}$ = structural load residual at the beginning of a time step

$[S]$ = complete structural stiffness matrix

$[S^*]$ = structural stiffness matrix condensed to include only story displacements

$[S_E]$ = element stiffness matrix calculated from material properties

$[S_G]$ = geometric element stiffness matrix

t = time

t_1 = measure of the duration of the pulse base motion

$[T_1]$ = transformation matrix

$[T_2]$ = transformation matrix

u = relative story displacement, or relative spring displacement for a single-degree-of-freedom system

u_i = relative displacement of the i-th spring

u_m = maximum relative story displacement, or maximum relative displacement for a single-degree of-freedom system

u_{ps} = permanent set

u_y = story yield displacement, or yield displacement for a single-degree-of-freedom system

$(u_i)_m$ = maximum relative displacement of the i-th elastoplastic spring

$(u_i)_{max}$ = maximum relative displacement of the i-th spring calculated by combining modes using the sum of the absolute values of modal quantities approach

$(u_i)_o$ = maximum relative displacement of the i-th elastic spring

$(u_i)prob$ = maximum relative displacement of the i-th spring calculated by combining modes using the square root of the sum of the squares of modal quantities approach

$(u_i)_y$ = yield displacement of the i-th spring

$\{u\}$ = total end rotation vector for a simply supported (constrained) flexural element

$\{U\}$ = element end displacement vector

v = maximum ground velocity

$\{v\}$ = structural story displacement vector relative to the base

$\{v^{(m)}\},\{v^{(n)}\}$ = structural story displacement vector relative to the base in the m-th or n-th mode of vibration

V = design base shear

V_y = measure of the yield displacement of an elastoplastic spring in a single-degree-of-freedom system

$(V_i)_o$ = measure of the maximum relative displacement of the i-th elastic spring

$(V_i)_y$ = measure of the yield displacement of the i-th spring

w_i, w_x = weight of the i-th or x-th story

W = building weight

W.L. = wind load

x = base (ground) displacement

Z = plastic section modulus

α_m = maximum inelastic hinge rotation

$\{\alpha\}$ = inelastic (hinge) end rotation vector

β = parameter in Newmark's β-Method equations

γ = parameter in Newmark's β-Method equations

γ_n = participation factor for the n-th mode of vibration

ε_n = phase angle for the n-th mode of vibration

θ_h = inelastic hinge rotation capacity

$\{\theta\}$ = structural rotation vector

μ = story ductility, or ductility for a single-degree-of-freedom

μ_i = ductility of the i-th spring

ξ_n = percent critical viscous damping in the n-th mode of vibration

ϕ_{av} = average curvature in the inelastic region of a beam during its critical loading

ϕ_p = plastic curvature

ϕ_p^* = design plastic curvature

$\{\phi^{(m)}\}, \{\phi^{(n)}\}$ = mode shape of the m-th or n-th mode of vibration

$\tilde{\phi}_i^{(n)}$ = normalized amplitude of the n-th mode shape at the i-th story

$\{\tilde{\phi}^{(n)}\}$ = normalized mode shape of the n-th mode of vibration

ω = circular frequency of vibration for a single-degree-of-freedom system

ω_n = circular frequency of vibration for the n-th mode

ω_{dn} = damped circular frequency of vibration for the n-th mode

$\{0\}$ = zero vector

$\{1\}$ = unit vector

$[I]$ = identity matrix

$\{\ \}^T$ = transposed vector

$[\ ]^T$ = transposed matrix

2. BUILDING DESIGNS

2.1 Introduction

In this chapter several two- and three-story buildings are designed to resist earthquake motion using the quasi-static building code approach to determine lateral loads, and the steel design specifications of the AISC (1969) to size members. The buildings designed provide the ensemble of structures used in the analytical and behavioral studies discussed in Chapter 4. Also presented is a description of the base motion used for time-history analysis, and the construction of the Newmark-Hall elasto-plastic design response spectra used for modal analysis and building code calculations in Chapter 4.

2.2 Ground Motion

The North-South component of the El Centro 1940 earthquake is believed to be representative of a strong base motion which has a reasonable probability of occurrence in a highly seismic zone. The particular digitalized accelerogram used in this study had a maximum ground acceleration (a), velocity (v) and displacement (d), of 0.318 g, 13.0 in./sec and 8.40 in., respectively. The maximum ground motions and the elastic response spectrum for this record are shown in Fig. 2.1. Also shown are elastic and elastoplastic design spectra, consistent with the maximum ground motions listed above, constructed using the rules given by Newmark and Hall (1973). All spectra are plotted for 5 percent critical viscous damping.

The ductility factor for a single-degree-of-freedom elastoplastic system is defined as

$$\mu = \frac{u_m}{u_y} \tag{2.1}$$

in which u_m and u_y denote the maximum displacement of the oscillator relative to the ground during seismic motion and the maximum elastic or yield displacement, respectively. The design spectra plotted in Fig. 2.1 represent the peak elastic response (acceleration and yield displacement) for a series of elastoplastic oscillators.

2.3 Design Criteria

The base shears, V, used in seismic design were selected on the basis of recommendations contained in modern building codes. The base shear coefficients recommended by several building codes for use in calculating design forces in zones of maximum earthquake hazard are tabulated in Table 2.1. The entries to the table represent the limiting (maximum) values of the base shear normalized by the building weight, W, for low-rise buildings on stiff ground. The base shear was distributed over the building height according to the following formula:

$$F_x = V \frac{w_x h_x}{\sum_{i=1}^{N} w_i h_i} \tag{2.2}$$

in which w_x, w_i and h_x, h_i represent the story weight and height of the building at the x-th or i-th story, and N denotes the total number of stories. Since it is generally not required by the building codes for low-rise buildings, no concentrated lateral force at the top of the structure was included in Eq. (2.2).

The design external pressure due to wind on the buildings was assumed to be 20 psf. For design the lateral deflection of the buildings

per story arising from wind and gravity loading was limited to 1/500 of the story height.

Member sizing was accomplished by the specifications of the AISC using type A36 steel with a yield stress, F_y, of 36 ksi and a modulus of elasticity, E, of 30,000 ksi. The members were designed for dead plus gravity live loading (D.L. + L.L.), dead plus gravity live plus earthquake loading (D.L. + L.L. + E.Q.), and dead plus gravity live plus wind loading (D.L. + L.L. + W.L.), the loads for the latter two cases being multiplied by a 0.75 probability factor. *

Beam members in moment frame buildings were assumed to be capable of developing their plastic moment capacities. For moment frames and shear buildings, it was assumed that column members could develop their reduced plastic moment capacities calculated according to the strength interaction formula (AISC Formula 2.4.3)

$$M_{pc} = 1.18 \left(1 - \frac{P}{P_y}\right) M_p \leq M_p \qquad (2.3)$$

in which M_p $(= F_y Z)$ denotes the plastic moment capacity and P_y $(= F_y A)$ denotes the yield axial load capacity of the section. In Eq. (2.3), Z and A represent the plastic section modulus and the cross-sectional area of the member. The axial load, P, acting on the column during dynamic motion was obtained using the concept of tributary area** and was assumed to be constant.

---

* For convenience in this study, rather than increasing the resistance function by a factor of 1.33 for the (D.L. + L.L. + E.Q.) and (D.L. + L.L. + W.L.) loadings, the loads were multiplied by a factor of 1/1.33 = 0.75. In this way, stresses for the three load cases could be compared to the same allowable values.

** One-half of the span between adjacent columns was used to calculate tributary areas (NBC, 1975, Commentary G).

The connections in shear buildings and moment frame buildings were assumed to develop the full capacities of members framing into a joint and to be rigid (unless noted otherwise). Column bases were considered to be fix-ended.

For X-braced frames, it was assumed that the bracing members could develop their full tensile strengths based on gross area. The connections of columns were assumed to resist no moment and to be completely flexible.

It was assumed that 20 percent of the transient live load contributed to the building weights and column axial loads during earthquake motion. Thus, floor masses and axial loads were calculated for a dead plus 20 percent gravity live loading [D.L. + 0.2(L.L.)].

For purposes of design and analysis, it was assumed that each seismic load resisting frame in a building could be considered separately. Thus, it was assumed that the individual frames about each horizontal axis of a building vibrated in phase for seismic motion in a given horizontal direction. Also, it was assumed that mass was lumped at points of horizontal story translation.

It is to be noted that some of the building designs described in this chapter are not necessarily examples of good seismic design. Rather, the buildings were proportioned so that some of the more interesting aspects of seismic behavior could be studied. In particular, shear building Design 2-C and X-braced building Designs 2-G and 3-C, because of their relatively low base shear capacities, were subjected to large deformations during earthquake excitation. Also, some of the members in Designs 2-D and 2-E were overstressed under the building code loadings.

2.4 Building Descriptions

Information pertaining to the building designs studied is contained in Tables 2.2, 2.3 and 2.4, and is shown in Figs. 2.2 and 2.3. The information recorded is for the most part self-explanatory; however, a few general comments are made here for clarity. The symbol f_1 used in Fig. 2.2 denotes the fundamental frequency of vibration. The seismic design forces and the modal properties of the building designs are presented in Appendix A.

The first group of designs was for a portion of a two-story building with three bays in the assumed direction of earthquake motion and a frame spacing of 32 ft in the perpendicular direction, Fig. 2.2(a), (b) and (c). The loadings tabulated in Table 2.2 were assumed to include exterior cladding weight.

Buildings with extremely stiff and strong girders (shear buildings), Designs 2-A, 2-B and 2-C shown in Fig. 2.2(a), were designed for a base shear coefficient of 10 percent. Of course, the design stresses as percentages of the AISC allowable stresses tabulated in Table 2.4 indicated that the actual base shear coefficients were different from the design value. The values tabulated in Table 2.4 refer to the design stresses in the most highly stressed members in the structures. For buildings with extremely stiff and strong girders, the maximum stresses occurred in the base story interior columns. As would be expected, the design stresses for Design 2-A, composed of W12 x 58 sections, were much less than those for Design 2-C, composed of W8 x 24 sections.

The moment frame buildings shown in Fig. 2.2(b) also were designed for a base shear coefficient of 10 percent. In this case, the problem of design was complicated since there were many possible combinations

of column and beam sections resulting in adequate structures. Both Designs 2-D and 2-E were designed such that yielding tended to be confined to the columns. Conversely, Design 2-F was sized according to the strong column, weak beam philosophy. Design stresses in critical members are presented in Table 2.4. Design 2-D represents a well-designed building for which the design stresses in the critical column members and the critical beam members are on the same order of magnitude. The stresses are slightly less than the allowable stresses. Conversely, the critical columns of Design 2-E and the critical beams of Design 2-F are overstressed under the building code loadings.

X-bracing was used for seismic load resistance in Designs 2-G and 2-H shown in Fig. 2.2(c). For this type of structure, ignoring the second order effects, only lateral forces contribute to stress in the bracing members. As a result, the member cross-sectional areas listed correspond to member sizes required to resist the given base shear coefficient at 100 percent of the AISC allowable stress. As mentioned previously, it was assumed that the connections of columns to beams were completely flexible in these frames.

Three-story buildings comprise the final group of structures studied. The ductile moment resisting frame building design shown in Fig. 2.3 was taken, with minor changes, directly from Army, Navy and Air Force (1973) Design Example C-2. The floor loadings given in Table 2.3 and an exterior cladding weight of 4 lb/ft^2 were used to calculate the seismic weights. The roof diaphragm for this building was assumed to be perfectly flexible, and the floor diaphragms were assumed to be perfectly rigid. In the reference cited, the lateral design forces were obtained using the SEAOC

(1968) recommendations for a Zone 3 earthquake hazard. The design forces were consistent with a 5 percent base shear coefficient.

For this building only the frames along lines A, C, 1, 4 and 7 shown in Fig. 2.3 are lateral load resisting. In the East-West direction, from consideration of symmetry, 1/2 of the lateral load is resisted along each of the exterior walls (lines A and C). Each exterior wall is composed of two identical frame subassemblages which, by stiffness, attract 1/4 of the lateral load. Design 3-A shown in Fig. 2.2(d) represents such a subassemblage.

The behavior in the North-South direction is complicated because the roof diaphragm is flexible and the floor diaphragms are rigid. A rigorous dynamic analysis would require the idealization of the building as three frames in parallel (the frames along lines 1, 4 and 7, Fig. 2.3), the first- and second-story levels of all frames being constrained to vibrate with the same displacement, and the roof of each frame being allowed to vibrate independently. However, for simplicity it was assumed that the vibration of the central frame (line 4) was independent of the other frames, and 1/2 of the roof weight and 1/3 of the floor weights were tributary to it. The structural idealization in the North-South direction, Design 3-B, is shown in Fig. 2.2(d). Stresses in critical members for both Designs 3-A and 3-B under the design loadings are tabulated in Table 2.4.

Designs 3-C and 3-D shown in Fig. 2.2(e) were for the building configuration illustrated in Fig. 2.3, but it was assumed that lateral resistance was provided by X-bracing along lines A and C. The relatively large design base shear coefficients selected were in line with the requirements of modern building codes for X-braced buildings in zones of maximum earthquake hazard.

3. ANALYTIC PROCEDURES

3.1 Introduction

This chapter contains a brief description of (a) the step-by-step numerical integration (time-history) procedure used to solve the coupled equations of motion which govern the dynamic behavior of low-rise buildings, (b) the modal method as used in conjunction with inelastic response spectra, and (c) the quasi-static building code approach modified to explicitly take inelastic behavior into account. The methods described are limited to planar structures founded on a rigid base and subjected to one horizontal component of earthquake base motion. The computational techniques described were used to perform the analytical and behavioral studies discussed in Chapter 4.

In an attempt to limit computational effort it was necessary to make several simplifying assumptions. Some of the assumptions are discussed in the following sections. The use of simplified analytical models permitted the study of the fundamental parameters which control the inelastic dynamic response of low-rise buildings.

3.2 Time-History Analysis

3.2.1 Mass and Damping -- For the buildings considered in this study, it was assumed that mass was lumped at points of horizontal story translation. The resulting mass matrix was diagonal with nonzero entries only for translational degrees-of-freedom. Under this assumption, it was possible to formulate the equations of motion in terms of a set of ordinary differential equations.

Damping was assumed to be proportional to mass, and the arbitrary constant of proportionality (Appendix B, Section B.3) was adjusted so that 5 percent critical viscous damping in the first mode of vibration resulted. Since inelastic hysteretic behavior was taken into account explicitly when establishing the structural stiffness, it was felt that this relatively low value of damping was justified. The higher modes of vibration were damped less strongly than the first mode using this formulation.

3.2.2. Element Stiffness -- Flexural members were assumed to resist end rotation in an elastoplastic manner. The moment-rotation diagram shown in Fig. 3.1 represents the hysteretic behavior of a typical flexural element subjected to moment at one of its ends. Until the end moment capacity of the member is reached, the elastic resistance curve passing through the origin is followed. If the moment capacity is reached, an inelastic hinge forms and subsequent end rotation occurs without increase in end moment. If the direction of end rotation is now changed, unloading follows a curve parallel to the initial elastic curve. Subsequent loading or unloading is along the offset elastic curve until the end moment capacity of the member is again reached.

The flexural element end moment-rotation relationship used ignores any increase in moment capacity resulting from strain hardening, and any decrease in elastic stiffness caused by the Bauschinger effect.

The hysteretic story shear-displacement relationship used for X-braced frames is shown in Fig. 3.2. On first loading it is assumed that the compression brace buckles out of the way and the tension brace carries the lateral load elastically. If the lateral load is increased a sufficient

amount, the tension bar yields in an elastoplastic manner. If the direction of load is now reversed and the tension bar is unloaded, the lateral force will not experience any resistance to deformation until the system passes back through its initial configuration of zero displacement. The bar, which had formerly buckled in compression, now is in tension and carries load as described for the tension bar above. On subsequent load cycles, the tension bar begins to carry load when the displacement equals the maximum deformation in the last cycle minus the elastic recovery.

Igarashi, et al. (1973) have shown that this model predicts the dynamic behavior of steel diagonal braces well, provided the slenderness ratio is greater than $2\pi\sqrt{E/F_y}$ (or 181 for A36 steel). For the low-rise buildings considered in this study, the slenderness ratios were greater than this value.

As a story displaces relative to the story below, geometric forces are caused by gravity loads acting on column members. These secondary load-displacement (P-delta) effects must be opposed by the lateral load resisting system. The stiffness matrices for flexural and X-braced frame elements were modified to take account of P-delta effects.

The detailed derivations of element stiffness properties are given in Appendix C.

3.2.3 Method of Solution -- Once the structural properties were established, the equations of motion were assembled by conventional matrix procedures and solved using time-history analysis. In performing the time-history analyses, the response history was divided into a number of small increments in time, and the change in response during

each increment was calculated for a linear system having stiffness properties determined at the beginning of the time increment. Since structural stiffness changed with the member states of inelasticity, calculations advanced in a step-by-step manner in the time domain for a series of linear systems with changing stiffness properties.

The basic feature of the incremental time-history analysis procedure is the transformation of the ordinary differential equations of motion into a set of incremental algebraic equations. The transformation was accomplished in this study by using the expressions of Newmark (1959) with $\beta = 1/6$.

The details of the numerical procedure are found in Appendix D.

3.3 Modal Method

In the modal method calculations referred to in Chapter 4, inelastic behavior was taken into consideration by using inelastic design response spectra to obtain the modal response quantities. For a given building, the spectral ordinates used were consistent with 5 percent critical viscous damping and a constant value of the ductility factor for all modes of vibration. The elastic mode shapes and frequencies were used for both elastic and inelastic response calculations. The total response was obtained by taking the sum of the absolute values of the modal quantities.

A summary of the modal method as it was used for inelastic response calculations in this study is as follows:

(1) Obtain the frequencies and mode shapes of elastic vibration for the given building.

(2) Select the design response spectrum consistent with the

desired degree of inelastic response. The design response spectra used were inelastic maximum acceleration or yield displacement spectra.

(3) By means of the conventional procedure for elastic systems, calculate the yield (maximum) forces and the yield displacements using the modal method in conjunction with the design response spectrum.

(4) Multiply the yield displacements by the selected ductility factor to obtain the maximum inelastic displacements.

3.4 Building Code Approach

In using the quasi-static building code approach in Chapter 4, the base shear was calculated by multiplying the mass of the building by the spectral acceleration in the first mode of vibration. Inelastic behavior was taken into consideration by using inelastic response spectra to obtain the spectral accelerations.

A detailed discussion of the modal method and the building code approach is found in Appendix B.

4. RESULTS OF THE ANALYSIS

4.1 Introduction

This chapter is devoted to the discussion of the results of analytical studies on the building designs described in Chapter 2. The results of time-history behavioral studies using the digitalized El Centro earthquake record for base motion are discussed. Calculations using modal analysis in conjunction with design response spectra consistent with the El Centro base motion are compared to the results of the time-history studies. The quasi-static building code approach for obtaining the design base shear, modified to explicitly take inelastic behavior into account by use of response spectra, also is reviewed in light of the time-history calculations.

4.2 Building Behavior Determined from Time-History Calculations

Time-history analysis was carried out according to the methods described in Chapter 3. Each building design was analyzed under the following assumptions (shown schematically in Fig. 4.1):

(1) Elastic - The structural members were assumed to respond in a linearly elastic manner under all displacements.

(2) Inelastic - Yielding was assumed to occur (a) when the plastic moment capacities of beam members were exceeded, (b) when the reduced plastic moment capacities of column members were exceeded, and (c) when the story yield displacements of X-braced frames were exceeded.

(3) Inelastic + PΔ - Yielding was assumed to occur, and column and X-braced frame stiffnesses were reduced to take geometric effects resulting from gravity axial loads into account. The influence of gravity axial loads on the response, referred to as P-delta effects in this study,

was physically modelled by links (false members) subjected to axial force. The links subjected to axial force shown in Fig. 4.1(c) depend on the column members or the X-braced frame for stability under lateral story displacement. The abbreviation PΔ, standing for the influence of gravity axial loads on the response, is used only when the inelastic + PΔ analysis case is referred to in the text.

For the three cases listed above, it was assumed that only lateral loads contributed to the first order member forces. An additional analytical assumption was made for some of the moment frame building designs:

(4) Inelastic + FEF - Yielding was assumed to occur and gravity loads were assumed to be present on the beam members during seismic motion. At the beginning of the time-history analysis, fixed end forces and moments were applied as equivalent joint loads to account for gravity loads acting on the beam members. The gravity loads acting were calculated from a dead plus 20 percent gravity live loading [D.L. + 0.2(L.L.)]. The abbreviation FEF, standing for fixed end forces and moments, is used only when the inelastic + FEF analysis case is referred to in the text.

In Section 4.2.3 story shears, and in Section 4.2.4 story displacements and drifts, are sometimes referred to as "design" quantities. The design quantities were obtained from the earthquake loadings used to proportion the buildings in Chapter 2.

In the following sections, the most important results of the time-history calculations are discussed. In cases where the results of the inelastic + PΔ analysis and the inelastic + FEF analysis were nearly the same as those for the inelastic analysis, only the results of the

inelastic analysis are discussed. The detailed numerical data are presented in Appendix F.

4.2.1 Overview of Results -- This section contains a brief overview of the significant trends observed from the time-history response calculations. The intent is to familiarize the reader with the manner in which the three types of buildings considered in this study (shear buildings, moment frames, and X-braced frames) behaved generally during the El Centro base motion. The structural configurations of the buildings studied are shown in Fig. 2.2.

The first observations involve those structures proportioned with fairly uniform story shear strengths over the building heights. The structures in this category were the shear building designs, the moment frame buildings designed so that yielding was forced into the columns, and the X-braced building designs. For these buildings it was found that the first story tended to be the weak link in the seismic load resistant system, and as a result, inelastic deformations were concentrated in the base story. The upper portions of these buildings remained elastic or responded in only a slightly inelastic manner.

By contrast, for the moment frame buildings proportioned with weak beams and strong columns, yielding was distributed fairly uniformly throughout the beams of all stories. It was found that the presence of gravity loads on the beam members of these buildings had a marked influence on the location of inelastic hinges during seismic motion.

The story shears attracted during earthquake motion depended on the location and magnitude of inelastic behavior within the buildings. For

buildings with yielding concentrated in the bottom stories (shear buildings, moment frame buildings designed so that yielding was forced into the columns, and X-braced buildings), the inelastic analysis case shears were fairly uniformly distributed over the building heights and were reduced from the elastic analysis case shears. The reductions were largest in the first stories.

Conversely, for the moment frame buildings designed with strong columns, the inelastic story shears observed were only slightly reduced from, and had the same distribution as, the elastic shears. The response of these buildings under the El Centro base motion was nearly elastic on an overall scale.

When the deformations that occurred under the elastic analysis case were compared to the inelastic analysis case deformations for buildings with inelastic response concentrated in the base story (shear buildings, moment frame buildings designed so that yielding was forced into the columns, and X-braced buildings), it was observed that yielding tended to concentrate the deformations in the base story and reduce the deformations in the upper portions of the building. For the shear buildings and moment frame buildings designed so that yielding was forced into the columns, the inelastic deformations were equal to or slightly less than the deformations for the elastic case. The inelastic deformations of the X-braced buildings were often significantly larger than the elastic deformations.

For moment frames proportioned with strong columns and weak beams, the elastic and inelastic deformations were for all practical purposes the same.

It is the purpose of the following four sections to evaluate in detail the time-history response of some low-rise steel buildings subjected to earthquake base motion. Particular emphasis is placed on the application of the results to the design of low-rise buildings.

4.2.2 Inelastic Response -- The locations where inelastic behavior tends to be concentrated within a structure during seismic motion, the magnitude of inelastic response, and the capacity of members to resist inelastic deformations are of interest to design engineers. Unfortunately, it is often difficult to determine how a building responds in the inelastic range without resorting to complicated time-history calculations. In this section the locations of inelastic response and the magnitudes of inelastic deformations of some low-rise steel buildings are determined from time-history calculations.

On reaching their plastic moment capacities, the flexural members making up shear buildings and moment frame structures form inelastic hinges. The maximum inelastic hinge rotations and the locations of inelastic hinges observed during the earthquake base motion are illustrated in Fig. 4.2 for the buildings studied. It can be seen that the inelastic hinge rotations were concentrated in the first-story columns for the two-story shear buildings, Designs 2-A, 2-B and 2-C. This might have been anticipated since the maximum response usually occurs in the first-story for shear-beam systems in the high or medium frequency ranges during seismic motion.

Similarly, for moment frame Designs 2-D, 2-E and 3-A (buildings proportioned so that yielding was forced into the columns), the maximum

inelastic hinge rotations were found to be at the tops and bottoms of the first-story columns.

The response of moment frame buildings designed such that yielding is forced into the beams is strongly influenced by gravity loads acting on beam members. In Fig. 4.3 bending moment diagrams for a beam element under gravity load and increasing lateral load are compared to those for a beam element subjected only to increasing lateral load. For the combined loading case, yielding first occurs at the end of the beam where the moments resulting from the two types of loading are of the same sign. On subsequent increase in lateral load, yielding occurs either in the interior or the opposite end of the yielded beam, depending on the magnitude of the gravity loads and the beam moment capacity. Conversely, for the lateral load only case, yielding is restricted to the beam ends.

Moment frame building Designs 2-F and 3-B were designed according to the strong column, weak beam philosophy. It was observed that inelastic response occurred in the beams of building Design 2-F (Fig. 4.2) for the inelastic + FEF case; no yielding occurred in any of the members of Design 2-F for the inelastic analysis case. In this study the magnitudes of moments resulting from lateral loads were not large enough to cause two inelastic hinges to form in any of the beams at any one time during the response history. For Design 3-B yielding occurred for both the inelastic and inelastic + FEF analysis cases. Again, most of the beam members under the inelastic + FEF case could have resisted more lateral load than was caused by the El Centro base motion. As a matter of practical interest, building Designs 2-F and 3-B had a margin of reserve strength that was not available for the moment frame buildings proportioned so that yielding

was concentrated in the columns. Also, the inelastic action was more uniformly distributed throughout the frames for Designs 2-F and 3-B than it was for the designs with yielding concentrated in the columns.

The cumulative hinge rotations, defined as the sum of the absolute values of all the inelastic rotations occurring at a given hinge location during dynamic motion, are of interest. As can be seen from the schematic representation in Fig. 4.4, the ratio of the cumulative to maximum hinge rotation serves as an indication of the amount of inelastic load reversal or cyclic response that has occurred at a given hinge location. For the buildings considered in this study, the normalized cumulative hinge rotations were small numbers, in general less than about 6, suggesting that significant inelastic load reversal made up a relatively small portion of the total response history. The cumulative rotations, normalized by the corresponding maximum hinge rotations, are presented in Appendix F (Figs. F.1, F.3 and F.4(b)) for the moment frame and shear building designs considered.

Popov and Bertero (1973) have presented a simple formula for estimating the available inelastic hinge rotation capacity, θ_h, that an inelastic region of beam can develop during its critical loading after it has been subjected to several cycles of load reversal. The expression has been developed from consideration of the results of cyclic tests on a number of cantilever steel beam specimens. The suggested formula is

$$\theta_h = a \frac{\phi_{av}}{\phi_p} \phi_p^* \qquad (4.1)$$

in which ϕ_{av}/ϕ_p is the normalized hinge curvature capacity selected from experimental results and ϕ_p^* is the plastic curvature used in design.

The quantity ϕ_{av} denotes the average curvature in the inelastic zone during the critical loading, and $\phi_p (= M_p/EI)$ denotes the plastic curvature of the given section. The length of the inelastic hinge, a, is estimated from knowledge of the shape of the moment diagram and the strain hardening characteristics of the material.

In Table 4.1 the maximum hinge rotations observed in the columns of some of the buildings considered in this study are compared to the maximum hinge rotation capacities calculated using Eq. (4.1). In performing the calculations, it was assumed that Eq. (4.1) is applicable to lightly loaded columns and that $\phi_p^* = M_p/EI$. In order to estimate the hinge length, it was assumed that the columns were bent in antisymmetric double curvature and that the ratio of maximum end moment to the plastic moment capacity was 1.15. A reasonable value of the quantity ϕ_{av}/ϕ_p was estimated to be 7.5.* These numbers were selected so that conservative estimates to the hinge rotation capacities were obtained. It can be seen that the maximum inelastic hinge rotations observed during the time-history calculations were less than the rotation capacities in all cases.

The inelastic behavior of X-braced buildings is measured in terms of story ductility factors calculated by dividing the maximum relative story displacements by the yield relative story displacements. It can be seen from Table 4.2 that the maximum inelastic response occurred in the first-story for the two- and three-story building Designs 2-G, 2-H, 3-C and 3-D. (In Table 4.2 a ductility of less than one denotes elastic response.)

---

* The normalized hinge curvature capacity was estimated from the data recorded in Table 3 of the article by Popov and Bertero.

For the low-rise buildings studied, the following observations about the locations of inelastic response and the magnitudes of inelastic deformations can be made:

(1) The maximum inelastic response was concentrated in the base story for all designs except moment frames with weak beams. Such behavior is thought to be typical of many types of low-rise buildings of practical proportions, provided the fundamental frequency of vibration is in the high or medium frequency range of the elastic response spectra.

(2) For moment frames proportioned such that yielding was forced into the beams, yielding was spread throughout the buildings in a fairly uniform manner and gravity loads acting on beam members had an important influence on the locations of inelastic regions within the structures.

(3) The inelastic hinge rotations observed for the shear buildings and the moment frame buildings with inelastic deformations concentrated in the columns were smaller than the limit capacities estimated by the procedure of Popov and Bertero.

4.2.3 Story Shear -- In proportioning a building to resist seismic motion, member sizes are usually selected to resist specified story shears. It is of interest, therefore, to discuss the shear distributions observed for the building designs during the El Centro base motion. As would be expected, the shear distributions depended on the inelastic response.

The story shears attracted by the buildings, normalized by the total building weights, are shown in Fig. 4.5. The normalized shears designated as "design" represent the shears used to proportion the buildings in Chapter 2. The most notable feature of the story shear diagrams for shear

building Designs 2-A, 2-B and 2-C is that the distributions for the elastic and inelastic cases were of different shapes. Upon yielding in the base stories, the shear distributions became more uniform over the building heights. Moreover, even though the second stories responded elastically for the inelastic analysis case, the second-story shears were reduced from those observed for the elastic case.

The behavior of moment frames proportioned so that yielding was concentrated in the first-story columns, Designs 2-D, 2-E and 3-A, was similar to that observed for the shear buildings.

Conversely, even though yielding occurred in the beam members of moment frame Designs 2-F and 3-B, the story shears for the inelastic + FEF analysis case were not significantly different than the elastic values. On an overall scale the response of these frames was nearly elastic.

For X-braced building Designs 2-G, 2-H, 3-C and 3-D, the inelastic story shears were much smaller than the elastic shears. The inelastic shear distributions were relatively uniform over the building heights and, in fact, for Designs 2-G, 3-C and 3-D both the first and second stories reached their yield capacities. The behavior in yielding was, of course, similar to the other designs with inelastic response concentrated in the first story.

The story shears for the yielding buildings plotted in the figure can be compared to the design values. It is clear that the shear buildings and the moment frame buildings had base shear capacities far exceeding the design values. Of course, this was to be expected since some of the members in many of these designs were stressed below the AISC (1969) allowable values, and an effort was made to use common section sizes throughout. In addition, during the earthquake motion the instantaneous live load was

assumed to be less than the design live load. For these buildings member strength that was assumed to be needed to resist gravity load in design was, in fact, available to resist lateral load.

On the other hand, only lateral load contributes to the first order stresses in X-braced frames, and the nature of X-bracing members is such that they can be sized close to the intended design strengths. Therefore, the story shears for the X-braced frames were near the design values.

From these studies on some two- and three-story steel buildings, the following observations about the story shear distributions during the El Centro base motion can be made:

(1) The inelastic story shear response for shear building, moment frame, and X-braced building designs was similar when yielding was concentrated in the first story in that the distribution of the story shears over the building heights tended to become fairly uniform. As a result, the elastic and inelastic story shear distributions were not of the same shape.

(2) Moment frame buildings designed so that yielding was forced into the beams tended to have larger story shear capacities than moment frames designed so that yielding was concentrated in the columns. (For low-rise moment frames it is often difficult to force yielding into the beams without using artifically large column sizes.) The response of the moment frames with strong columns and weak beams was nearly elastic.

(3) X-braced frames, because of their lack of redundancy and the dependence of their member sizing on lateral load only, can be proportioned such that their base shear capacities are close to the intended design shears.

4.2.4 Displacement and Drift -- The designer endeavors to proportion a building so that deformations during seismic motion are not excessive. In general, the deformations that occur if the structure remains elastic during the design earthquake can be estimated using simple analytical procedures. Conversely, it is often difficult to obtain estimates of the deformations that occur if the structure responds inelastically. It is the purpose of this section to compare the inelastic deformations of some low-rise steel buildings to the elastic deformations. The inelastic deformations are also compared to the deformations under the design loading.

The maximum lateral story displacements relative to the ground observed during the El Centro base motion are shown in Fig. 4.6 for the building designs studied. Story drifts, defined as the maximum lateral deflections between consecutive floors divided by the corresponding story heights, are also presented in Fig. 4.6. The two types of plots illustrate slightly different information since the maximum displacements and drifts did not necessarily occur at the same instant during the time-history calculations. The displacements and drifts designated as "design" represent the deformations calculated under the full earthquake loading (i.e., not including the 0.75 load reduction factor) used for the design of the buildings in Chapter 2.

It can be seen that the maximum deformations occurred in the first stories for the two-story shear building Designs 2-A, 2-B and 2-C. The inelastic analysis case deformations were less than those for the elastic analysis case, particularly in the second stories.

For moment frame Designs 2-D, 2-E and 3-A, once yielding occurred in the first-story columns, the deformations in the upper stories were reduced from those observed for the elastic case. The first-story deformations

were about the same magnitude for the elastic and inelastic analysis assumptions. The deformed shapes of these designs were similar to those for the shear building designs described above, especially after yielding occurred.

By contrast, the behavior of moment frame building Designs 2-F and 3-B was such that the upper portions of the buildings were more flexible than the first story. For these buildings yielding was concentrated in the beams, and the deformed shapes on yielding were similar to the elastic analysis case deformed shapes. The deformed shapes observed for these buildings indicated that the lack of significant (shear reducing) yielding in the first stories permitted forces to be carried up the building frames.

The response of the X-braced buildings, Designs 2-G, 2-H, 3-C and 3-D, was similar to that for the shear buildings under the elastic analysis assumption. However, on yielding, especially for the lower strength Designs 2-G and 3-C, the first-story deformations were greater than the elastic deformations. As before, when yielding was concentrated in the first story the drifts in the upper portions of the structures were reduced.

For seismic design purposes it is often assumed that the maximum displacements are the same whether the system responds elastically or in an inelastic manner. Exhaustive studies on single-degree-of-freedom oscillators with various types of resistances have indicated that this assumption may be conservative, unconservative, or approximately correct, depending on the frequency of vibration and the nature of the resistance function.

The elastic displacements serve as slightly conservative approximations of the inelastic displacements for the shear buildings, and as reasonable

approximations for the moment frame buildings. However, when inelastic deformations were largest in the first stories, the elastic and inelastic deformed shapes were of different form. Yielding in the base story concentrated the response in the base story and reduced the response in the upper portions of the building.

On the other hand, the elastic displacements serve as unconservative estimates of the inelastic displacements for X-braced buildings. This might have been anticipated since there can be times during the response history when X-braces, as modelled in this study, offer no resistance to deformation.

A comparison between the maximum inelastic and the design story drifts is given in Table 4.3. It can be seen that the inelastic drifts during earthquake motion were from about 4 to 10 times the design values. The inelastic drifts of the lower strength X-braced frame Designs 2-G and 3-C and the relatively weak shear building Design 2-C are over 2 percent; the inelastic drifts for all other designs are under 1.5 percent. The maximum inelastic drift occurred in the first story for all designs except moment frame Designs 2-F and 3-B; frames 2-F and 3-B were proportioned so that yielding was forced into the beams.

The following observations regarding deformation response can be made from the results of the studies on the low-rise buildings considered in this investigation:

(1) The elastic and inelastic displacements and drifts were on the same order of magnitude for the shear building and moment frame building designs. This could have been anticipated from the results of studies on single-degree-of-freedom elastoplastic systems in the frequency ranges of

the fundamental frequencies of these buildings.

(2) For X-braced buildings, particularly for low base shear capacities, inelastic deformations were larger than elastic deformations. The reduced hysteretic energy absorptive capacity of X-braced frames on load reversal is believed to be responsible for this trend. In order to avoid the possibility of excessive deformations during seismic excitation, it is recommended that X-braced frames be proportioned in a conservative manner.

(3) When yielding occurred in the bottom story of a building, the deformation response was concentrated in the first story and the response in the upper portions of the building was reduced. For buildings with this type of response, the first story was the critical link of the seismic load resistant system.

4.2.5 P-delta Effects -- The influence of P-delta effects (gravity axial load effects) on the response of low-rise buildings is generally believed to be of secondary importance. Nevertheless, under some circumstances P-delta loads can modify dynamic behavior. It is the purpose of this section to evaluate the influence of P-delta effects on the response of the buildings considered in this study.

The differences between the first story displacements under the inelastic and the inelastic + PΔ analysis cases are tabulated in Table 4.4 for the buildings considered. Displacements were for the most part increased by P-delta forces, but the increases were in general small.

The influence of P-delta forces tended to be most important for flexible buildings or buildings of low base shear resistances. For example, shear building Design 2-C was much more flexible and of smaller first story shear capacity than was Design 2-A. The increase in displacement

due to P-delta loads was 18.9 percent for Design 2-C, but the increase was only 0.1 percent for Design 2-A. The same trends apply when moment frame Design 2-E is compared to Design 2-D and when X-braced frame Design 2-G is compared to Design 2-H. (The base shear resistances of the buildings can be assessed from the plots of Fig. 4.5 for the inelastic analysis case.)

These studies suggest that P-delta effects can be ignored for well-designed low-rise buildings of reasonably high strengths and stiffnesses.

4.3 Modal Method and Building Code Calculations

The intent of this section is to evaluate the use of less complicated procedures for estimating the response of low-rise buildings to earthquakes. The less complicated procedures considered are (a) the modal method used in conjunction with inelastic response spectra and (b) the quasi-static building code approach modified to explicitly take inelastic behavior into account. The response quantities obtained using these procedures are compared to the response quantities calculated using the time-history method of analysis.

In order to facilitate comparisons between the less complicated methods of analysis and time-history analysis, the response spectra used for the modal method and building code calculations were consistent with the largest story ductility observed for the given building from the time-history analysis. The techniques used to estimate ductility factors for the different types of buildings considered are discussed in Section 4.3.1.

Elastoplastic response spectra were used for the modal method and building code calculations pertaining to shear buildings and moment frames. For X-braced frames modified inelastic response spectra were developed

using the techniques discussed in Section 4.3.1.

The results of the modal method and building code calculations are presented in Section 4.3.2.*

4.3.1 Story Shear-Deformation Relationships -- The response spectra that are generally available for use in design calculations have been derived from consideration of the dynamic response of elastoplastic systems and therefore strictly apply only to buildings with elastoplastic story shear-deformation relationships. For the designs considered, the story shear-deformation relationships were not purely elastoplastic by virtue of the different yielding mechanisms involved during deformation. Consequently, it was necessary to estimate equivalent elastoplastic story ductility factors or to modify the elastoplastic design response spectra for use in spectral calculations. The procedures used to estimate ductilities and to modify the elastoplastic response spectra are described in the following paragraphs.

The story ductility factors for the buildings were calculated using the expression

$$\mu = \frac{u_m}{u_y} \tag{4.2}$$

in which u_m is the maximum relative story displacement and u_y is the story yield displacement.

---

* The modal properties for the building designs studied are tabulated in Appendix A (Tables A.3 and A.4), and the elastoplastic response spectra used for calculations are shown in Fig. 2.1(b). The details of the modal analysis and the quasi-static building code procedures are discussed in Chapter 3.

Story Yield Displacements. Under the assumptions made in this study, the shear-deformation relationships for the individual column members in the shear buildings were elastoplastic. However, the story shear-deformation relationships were not in general elastoplastic since the individual columns of a story sometimes yielded at different levels of deformation. The yield displacement of a column can be calculated using the expression

$$u_y = \frac{M_{pc} h^2}{6EI} \tag{4.3}$$

in which the symbol h denotes the story height. Equation (4.3) follows from consideration of the slope-deflection equations for a flexural member of moment capacity M_{pc} under relative end displacement with no end rotation (fixed-fixed case). The equivalent elastoplastic story ductility can be calculated using Eq. (4.2) under the assumption that the story yield displacement is equal to the average of the yield displacements calculated for all columns in a story.

The shear-deformation relationship for a story in a moment frame building in which yielding at the top and bottom of all column occurs can be represented graphically by the solid line curve in Fig. 4.7. Point "a" represents the story shear at which the first column in the story reaches its moment capacity, and point "b" represents the shear at which all columns in the story have formed inelastic hinges at their tops and bottoms. Unfortunately, the initial story stiffness, k, and the shape of the resistance curve between points "a" and "b" cannot be determined easily. However, a reasonable estimate of k can

be made by dividing the story shear by the relative story displacement under lateral loading proportional to the first mode shape.

In order to use Eq. (4.2) to estimate the equivalent elastoplastic story ductility, some estimate of the yield displacement must be made. The following three approximate procedures gave quite similar estimates of the yield displacements for building Designs 2-D, 2-E and 3-A:

(1) Extrapolate the initial resistance curve "oa" linearly to a horizontal line drawn at the ordinate representing the maximum story shear, Q, and use the displacement corresponding to point "c" as the yield value.

(2) Equate the areas under the estimated curve "oab" and an equivalent elastoplastic curve "odb", and use the displacement corresponding to point "d" as the yield value.

(3) With knowledge of the inelastic hinge rotations occurring in zones of inelastic response, sum the energy dissipated by inelastic hinge rotation, $M_{pc}\,\alpha_m$, over all the columns in a story. By equating this energy to the inelastic energy dissipated by an equivalent elastoplastic oscillator, $Q(u_m - u_y)$, one obtains

$$u_y = u_m - \frac{\Sigma M_{pc}\alpha_m}{Q} \tag{4.4}$$

as an expression for the yield displacement. The symbol α_m in Eq. (4.4) denotes the maximum inelastic (plastic) hinge rotation.

In establishing the yield displacements for building Designs 2-D, 2-E and 3-A, preference was given to the third approach.

The problem of obtaining estimates of the story shear-deformation relationships for moment frames with yielding beams is difficult. Because building Designs 2-F and 3-B considered in this study responded to the

El Centro base motion in a nearly elastic manner, the problem was not specifically addressed in this report.

The lateral yield displacement of a story in an X-braced frame with bracing in one bay can be calculated in a straightforward manner using the expression

$$u_y = \frac{F_y L_b}{E} \left(\frac{L_b}{L}\right) \tag{4.5}$$

in which the symbols L_b and L represent the brace length and the horizontal projection of the brace length. Equation (4.5) follows from consideration of the elongation of a tension brace as it resists lateral story deflection. Once the story yield displacement is obtained, Eq. (4.2) can be used to calculate the story ductility factor.

For reference purposes, the first-story yield displacements obtained using the procedures described in this section are presented in Table 4.5 for some of the building designs.

X-braced Frame Response Spectra. The displacements of X-braced buildings during seismic motion, because of the reduced hysteretic energy absorptive capacity of X-braced frames, are usually more than those for an associated elastoplastic building of the same elastic stiffnesses and initial yield strengths. Consequently, elastoplastic spectra could not be used for spectral calculations pertaining to X-braced buildings. In this study modified design response spectra were constructed for single-degree-of-freedom oscillators having force-deformation relationships of the type described previously for X-braced frames. The spectra shown in Fig. 4.8 give (approximately) the initial story yield displacement

required to limit the maximum deformation of an oscillator to a specified ductility.

The yield level design response spectra were constructed from the design spectrum for elastic systems in the following manner (see Fig. 4.8).

Yield Level Spectral Ordinate at Control Point	=	Elastic Spectral Ordinate at Control Point	x	Multiplication Factor
a'		a		$1/\mu$
b'		b		$1/\mu$
c'		c		$2/\mu$
d'		d		$1/\sqrt{\mu - 1}$

The construction procedure is illustrated in Fig. 4.8 for the case where $\mu = 4$.

The yield level spectra constructed for X-braced systems are in accordance with the design rules proposed by Veletsos (1969) in the low and medium frequency ranges of the elastic design response spectrum. Insufficient data are available at present (1977) to determine the shape of the yield level spectra in the high frequency range. As a result, in the high frequency range the yield level spectra for X-braced systems shown in Fig. 4.8 are at best approximate. Bazán and Rosenblueth (1974) and Sun et al. (1973) have proposed slightly different procedures for estimating the response of X-braced single-degree-of-freedom systems.

4.3.2 Results of Modal Method and Building Code Calculations -- The response quantities obtained using the modal method of analysis are presented in Table 4.6 and the base shears obtained using the building code procedure are tabulated in Table 4.7. The response quantities from the modal method and the building code calculations are normalized

by the corresponding time-history response quantities. The ductilities given in the tables were calculated using the procedures described in Section 4.3.1. It was found that the maximum ductility factors were attained in the base stories for all buildings except Designs 2-F and 3-B. Therefore, the ductilities tabulated are consistent with the first-story deformations observed during time-history calculations. For convenience the ductilities were rounded off to even multiples. Since the time-history response of Designs 2-A, 2-F and 3-B was for all practical purposes elastic, only elastic quantities are presented in the tables for these buildings.

The agreement between modal and time-history analysis for the elastic case, Table 4.6(a), was very good for all building designs. The modal response values were never more than 30 percent over or 13 percent under the time-history values.

The results of inelastic modal calculations are compared to those from time-history analysis (inelastic analysis case) in Table 4.6(b). For the shear building Designs 2-B and 2-C, the moment frame Designs 2-D, 2-E and 3-A, and the lower strength X-braced building Designs 2-G and 3-C, reasonable estimates of the first-story displacements and shears were obtained using the modal method of analysis. In general, in the upper portions of the buildings the story shears were underestimated and the displacements were overestimated. The modal method gave response quantities that were almost always larger than the time-history response quantities for the higher strength X-braced frame Designs 2-H and 3-D. (It is likely that the procedure used to obtain design response spectra for X-braced buildings tends to be conservative for systems with relatively high base shear strengths.)

The fact that the response in the upper portions of the buildings was not well predicted by the modal method might have been anticipated. In using the modal method, it was tacitly assumed that the elastic and inelastic deformed shapes were of the same form and that the elastic and inelastic story shear distributions were of the same form. However, inelastic behavior was concentrated in the first stories for these designs, and this caused the inelastic deformed shapes and shear distributions to differ from those for the elastic case.

It can be seen from Table 4.7(a) that the building code approach provided good estimates of the elastic base shears. The shears were never more than 27 percent over or 15 percent under the time-history values. The building code approach gave values which were almost identical to the modal analysis first-story shears, but with much less computational effort (compare Table 4.7(a) to Table 4.6(a), "first-story shear").

The building code approach, as can be seen from Table 4.7(b), also gave reasonable estimates of the inelastic base shears. Again, the base shears obtained using the building code approach were nearly the same as those obtained using the modal method.

> Example. As an example of the procedure used to obtain the entries to Tables 4.6(b) and 4.7(b), consider the following calculations for moment frame Design 2-D.
>
> The first step in the procedure is to estimate the first-story ductility factor from the results of the time-history analysis for the inelastic case by means of Eqs. (4.2) and (4.4). The reduced plastic moment capacities of the columns are calculated using the expression

$$M_{pc} = 1.18\left(1 - \frac{P}{P_y}\right) M_p \leq M_p$$

Thus, for the exterior base columns

$$M_{pc} = 1.18\left(1 - \frac{46.1k}{529k}\right) 2610 \text{ in.k} = 2810 \text{ in.k} \leq 2610 \text{ in.k}$$

and for the interior base columns

$$M_{pc} = 1.18\left(1 - \frac{92.2k}{529k}\right) 2610 \text{ in.k} = 2540 \text{ in.k} \leq 2610 \text{ in.k}$$

The base story shear capacity is found by assuming all columns in the story (bent in double curvature) develop hinges at their tops and bottoms. By summation of moments

$$Q = \frac{2 \times 2610 \text{ in.k}}{144 \text{ in.}} + \frac{2 \times 2540 \text{ in.k}}{144 \text{ in.}} + \frac{2 \times 2540 \text{ in.k}}{144 \text{ in.}} + \frac{2 \times 2610 \text{ in.k}}{144 \text{ in.}}$$

$$= 143k$$

The maximum inelastic hinge rotations obtained from Fig. 4.2(b) are

exterior base column	interior base column
$\alpha_m = 22.2 \times 10^{-5}$ rad, top	$\alpha_m = 318 \times 10^{-5}$ rad, top
$\alpha_m = 538 \times 10^{-5}$ rad, bottom	$\alpha_m = 551 \times 10^{-5}$ rad, bottom

The maximum first-story displacement for the inelastic analysis case from Table F.4 or Fig. 4.6 is $u_m = 1.54$ in. The first-story yield displacement estimated by means of Eq. (4.4) is

$$u_y = 1.54 \text{ in.} - \frac{2[(22.2+538)2610 \text{ in.k} + (318+551)2540 \text{ in.k}] \times 10^{-5}}{143k}$$

$$= 1.0 \text{ in.}$$

The elastoplastic first-story ductility can finally be obtained using Eq. (4.2)

$$\mu = 1.54 \text{ in.}/1.0 \text{ in.} = 1.54 \text{ , use } 1.5$$

The next step is to obtain the quantities used for the modal method calculations. From Table A.1, the total weight

of the building is W = 276.5 k and the masses of the first and second stories are $m_1 = 0.477$ k-sec^2/in. and $m_2 = 0.239$ k-sec^2/in. The elastic frequencies of vibration obtained from Table A.3(a) are

$f_1 = 1.99$ cps $\qquad \omega_1 = 2\pi f_1 = 12.5$ rad/sec

$f_2 = 4.92$ cps $\qquad \omega_2 = 2\pi f_2 = 30.9$ rad/sec

The spectral yield displacements and accelerations obtained from Fig. 2.1(b) for the $\mu = 1.5$ case are

$D_1 = 1.32$ in. $\qquad A_1 = 206$ in./sec^2

$D_2 = 0.237$ in. $\qquad A_2 = 226$ in./sec^2

The inelastic response quantities can be estimated by means of the modal method using the following procedure. (The elastic mode shapes used are obtained from Table A.4(a).)

Story Number, i	0	1	2
(a) mode shapes, $\tilde{\phi}_i^{(n)}$			
(1)		0.714	1.312
(2)		0.286	-0.312
(b) modal accelerations, $\tilde{\phi}_i^{(n)} A_n$, in./sec^2			
(1)		147	270
(2)		64.6	-70.5
(c) modal forces, $\tilde{\phi}_i^{(n)} m_i A_n$, k			
(1)		70.1	64.5
(2)		30.8	-16.9
(d) modal story shears, k			
(1)	135	64.5	
(2)	13.9	-16.9	
$\sum_{n=1}^{N} \lvert$(modal story shears)$_n\rvert$	149	81.4	
(e) modal yield displacements, $\tilde{\phi}_i^{(n)} D_n$, in.			
(1)		0.942	1.73
(2)		0.0678	-0.0739
$\sum_{n=1}^{N} \lvert\tilde{\phi}_i^{(n)} D_n\rvert$		1.01	1.80
(f) maximum displacements, $\mu \sum_{n=1}^{N} \lvert\tilde{\phi}_i^{(n)} D_{(n)}\rvert$, in.		1.52	2.70

Also, the base shear can be estimated using the quasi-static building code approach. The building code base shear is calculated from the expression $A_1 \sum_{i=1}^{N} m_i$ where N is the number of stories.

$$\text{code base shear} = (206 \text{ in./sec}^2)(0.477 \text{ k-sec}^2/\text{in.} + 0.239 \text{ k-sec}^2/\text{in.})$$
$$= 147 \text{ k}$$

If the response quantities calculated above are normalized by the corresponding time-history response quantities from Table F.4 or Figs. 4.5 and 4.6 for the inelastic analysis case, the entries to Tables 4.6(b) and 4.7(b) for Design 2-D are obtained.

From the studies recorded in this report on some low-rise steel buildings, the following observations can be made pertaining to the use of the modal method and the quasi-static building code procedure to predict response quantities:

(1) The modal method used in conjunction with inelastic design spectra gave reasonable estimates of the inelastic forces and displacements during seismic motion. However, inaccuracies arose because the elastic mode shapes and frequencies used in calculations sometimes did not represent well the actual inelastic response. Also, it was difficult to apply the technique when story shear-deformation relationships could not be easily defined.

(2) The quasi-static building code method used together with inelastic response spectra provided a simple and reasonably accurate procedure for estimating the base shears of low-rise buildings.

(3) For buildings in which yielding was most extensive in the bottom story, it was found that the ductility used in inelastic spectral

calculations should correspond to the first story ductility of the building.

(4) Both the modal method and the building code approach gave good estimates of the elastic response quantities.

5. DESIGN APPLICATIONS

5.1 Introduction

The intent of this chapter is to review the results of the studies made as a part of this investigation in the light of practical applications to the design of low-rise steel buildings. To this end the behavior of the low-rise buildings considered in this study when subjected to the El Centro base motion, and the behavior of simple spring-mass systems subjected to base excitation are briefly reviewed in Section 5.2. The studies on buildings were limited to planar two- and three-story structures subjected to one component of ground motion. In Section 5.3 the three procedures that were used in this study for seismic analysis are evaluated. In Section 5.4 a procedure for obtaining seismic deformations and seismic design forces is described. Finally, in Section 5.5 several comments concerning factors that should be considered in the design of low-rise steel buildings are made.

5.2 Behavior of Low-Rise Buildings and Simple Systems

The studies recorded in this report were directed in part towards determining the behavior of low-rise steel buildings subjected to seismic ground motion. This section serves to summarize some of the more important findings of the time-history studies presented in Appendix E on simple elastoplastic shear-beam (spring-mass) systems and studies presented in Chapter 4 on low-rise steel shear buildings, moment frames, and X-braced frames.

Simple Systems. From studies on simple shear-beam (spring-mass) systems with proportions comparable to low-rise buildings, it appears that in the frequency ranges of interest the maximum response will usually

occur in the base story. This suggests developing a design criteria, at least for certain types of low-rise buildings, which assumes the base story is the critical link in the seismic load resisting system.

Shear Buildings. The response of buildings with very stiff and strong girders (shear buildings) was similar to the response of simple systems in that the base story was the critical link in the seismic load resisting system. When the shear buildings considered in this study were subjected to the El Centro base motion, zones of inelastic response formed only in the base story columns. The deformations calculated for linearly elastic response were on the same order of magnitude as the deformations obtained from inelastic response calculations.

Moment Frame Buildings. Moment frame buildings can be proportioned for two different types of behavior: the inelastic response can be forced into the beams or it can be forced into the columns. For the moment frame buildings considered that were proportioned so yielding occurred in the columns, the inelastic response was similar to the response of shear buildings; that is, zones of inelastic response generally formed at the tops and bottoms of the base story columns. For one of the buildings considered, zones of inelastic response also formed at the bottoms of the second-story columns, but the magnitudes of the inelastic rotations were small when compared to the inelastic rotations occurring in the base story columns.

For the moment frame buildings designed so inelastic response was forced into the beams, inelastic hinges were generally uniformly distributed throughout the beams of all stories. The buildings proportioned with weak beams and strong columns had an apparent margin of reserve strength that

the buildings proportioned so that yielding was concentrated in the columns did not have. On an overall scale the weak beam, strong column moment frames considered responded in a nearly elastic manner to the El Centro base motion.

In proportioning low-rise steel moment frame buildings in the manner prescribed in modern building codes and specifications, it will often be found that yielding will be confined to the columns during seismic base motion. In order to force yielding into the beams and still satisfy the code and specification requirements for gravity loads acting on beam members, it often will be necessary to arbitrarily increase the sizes of column sections above the sizes required on the basis of stress calculations.

For the moment frame buildings, the deformations obtained from elastic response calculations were on the same order of magnitude as the deformations obtained from inelastic response calculations.

X-braced Buildings. When the X-braced buildings considered were subjected to base motion, the largest inelastic deformations occurred in the bottom story. For some of the buildings considered, a relatively small amount of yielding also occurred in the second-story bracing members. The deformations obtained from inelastic response calculations were usually larger than the deformations obtained from elastic response calculations. Further, the inelastic deformations were often excessive due to the low hysteretic energy absorptive capacity of the X-braced frames employed in this study.

In order to avoid excessive deformations during seismic motion, it is recommended that X-braced buildings be designed with relatively

high base shear coefficients, V/W. For example, the X-braced buildings considered in this study behaved well when subjected to the El Centro base motion provided the base shear coefficient was about 25 percent. Obviously, if the compression bracing could resist some of the lateral force, or secondary structural systems could be counted on to provide lateral resistance, the coefficient could be reduced somewhat.

Comments. Except in the case of moment frame buildings designed so that the inelastic response was forced into the beams, the maximum inelastic response of all buildings occurred in the base story. Thus, for many of the buildings the base story was the critical link in the seismic load resisting system. The relationship between the maximum deformations obtained from inelastic response calculations and the deformations obtained from elastic response calculations varied with the building type. However, in most cases the relationship between elastic and inelastic deformations for a building could have been anticipated from consideration of the corresponding relationship for a single-degree-of-freedom system responding with the same frequency as the fundamental frequency of the building.

5.3 Discussion of the Methods of Analysis Used

A major objective of this study was to evaluate the use of some of the different analytical techniques available for determining the deformations and forces in buildings during earthquakes. The three methods considered in this study were, in order of the most to the least complex, time-history analysis, the modal method used in conjunction with inelastic response spectra, and the quasi-static

building code approach modified to explicitly take inelastic behavior into account.

Time-History Analysis. Time-history analysis is, in general, the procedure that allows the analyst to obtain the most detailed information about the inelastic response of buildings during a particular seismic ground motion. Unfortunately, time-history calculations are too tedious, complicated, and time consuming to be justified for use in the design of any but very special or unusual low-rise buildings. The time-history method of analysis has the added disadvantage that a large number of earthquake base motions should be used for calculations to at least partially take account of the statistical nature of earthquake ground motion.

Modal Method. The modal method used in conjunction with inelastic response spectra can be employed to obtain estimates to the inelastic response of buildings. Provided a certain amount of judgment is used, and the response characteristics of the type of the building under study are considered, reasonably good estimates of response quantities can be obtained. The use of the modal method is thought to be particularly appropriate for systems responding with small inelastic deformations (low ductilities).

Building Code Approach. The simplest procedure, and the procedure that is most familiar to design engineers, is the quasi-static building code approach. In using the building code approach, the design base shear is estimated by multiplying the mass of the building times the inelastic response spectrum ordinate in the first mode of vibration. This procedure seems to be particularly appropriate for structures in

the high and medium frequency ranges of the elastic design response spectrum, provided response is primarily in the first mode. Therefore, the procedure is suited to low-rise buildings. Once the base shear is estimated, the distribution of forces over the building and the deformations under the forces can be estimated by procedures similar to those recommended in modern building codes (NBC, 1975; SEAOC, 1975; UBC, 1976; ATC, 1977).

Comments. The quasi-static building code procedure is thought to be the most appropriate procedure for use in the design of the majority of low-rise steel buildings. In using the procedure, it is tacitly assumed that the response of a building is similar to the response of a single-degree-of-freedom system subjected to the same design base motion and having a resistance system similar to the building under construction. For many of the buildings considered in this study, the first story was the critical link in the seismic load resisting system. Consequently, the first story ductility was the appropriate ductility for use in spectral calculations.

5.4 Recommended Design Procedure

The purpose of this section is to formulate simple recommendations which can be applied by engineers to the design of low-rise buildings. The intent is to formulate a quasi-static procedure that is familiar to design engineers, but that explicitly takes inelastic behavior into account. In the following section a quasi-static design procedure that is in principle similar to the ATC (1977) approach is described. The application of the procedure to low-rise buildings of the types considered in this study is discussed.

Procedure. The suggested design procedure for a regular low-rise building may be summarized as follows:

(1) Construct yield design response spectra for different levels of elastic and inelastic response that are consistent with the earthquake hazard and building type. It is recommended that design response spectra for elastoplastic systems (see for example Newmark and Hall, 1973 and 1976) be used for moment frame buildings with yielding concentrated in the columns and shear buildings.

At present (1977) simple rules for developing design response spectra for X-braced systems are not available; however, the recommendations of Veletsos (1969), Sun et al. (1973) or Bazán and Rosenblueth (1974) can be used, at least in some frequency ranges, to establish the general shape of the design response spectra (see also Section 4.3.1). Also, accepted procedures are not available at present for constructing design response spectra that are applicable to moment frame buildings with inelastic response occurring in the beams.

(2) Estimate the fundamental frequency of vibration and obtain the design base shear using the quasi-static building code approach. The base shear is obtained by multiplying the mass of the building times the response spectrum ordinate in the first mode of vibration. The design spectrum used should be consistent with the degree of inelastic response or ductility desired.

(3) Obtain the lateral yield forces by assuming some distribution of the base shear over the height of the building, and proportion the building to resist the yield lateral forces.

In calculating the lateral yield forces, it is recommended that a triangular distribution of acceleration in the structure from zero at the base to a maximum at the top (as recommended by current building codes), or a distribution of acceleration proportional to the first mode shape be used. The inertial forces associated with the assumed distribution of acceleration are the lateral yield forces. The assumed value of acceleration at the top of the structure is adjusted so that the total distributed lateral forces add up to the design base shear.

(4) Obtain the yield displacements. The yield displacements are the displacements that occur when the design (yield) lateral forces are applied to the structure and the structure responds in a linearly elastic manner.

(5) Multiply the yield (elastic) displacements by the selected ductility factor to obtain the estimated maximum displacements.

(6) Estimate the actual base shear capacity of the building now proportioned* and estimate the actual fundamental frequency of vibration, for example by means of Rayleigh's method. The base shear capacity and fundamental frequency of vibration should be commensurate with the values assumed above for design.

(7) Determine whether or not the building can accommodate the maximum displacements associated with the design base motion while maintaining its strength and without being subjected to undue structural or nonstructural damage. If the building cannot accommodate the maximum displacements, return to Step (1).

---

* For low-rise steel moment frame buildings, the base shear capacity can usually be assessed in a straightforward manner by consideration of the possible plastic collapse mechanisms that can occur as the static lateral load is increased.

Example. As an example of the design procedure, consider the following calculations for moment frame Design 2-D. The structural configuration for Design 2-D is shown in Fig. 2.2(b).

(1) The elastoplastic design response spectra shown in Fig. 2.1(b) are used for calculations.

(2) The estimated fundamental frequency, f_1, and the selected design ductility, μ, are

$$f_1 = 1.99 \text{ cps}$$

$$\mu = 1.5$$

(In this case the actual value of the fundamental frequency is known from previous calculations, see Fig. 2.2(b).) The spectral yield acceleration is obtained from the design response spectrum for $\mu = 1.5$. Thus

$$A_1 = 206 \text{ in./sec}^2$$

Finally, the design base shear is calculated using the expression $V = A_1 \sum_{i=1}^{N} m_i$ in which the masses of the first and second stories obtained from Table A.1 are $m_1 = 0.477$ k-sec^2/in. and $m_2 = 0.239$ k-sec^2/in., and N is the number of stories. Thus

$$V = (206 \text{ in./sec}^2)(0.477 \text{ k-sec}^2/\text{in.} + 0.239 \text{ k-sec}^2/\text{in.})$$
$$= 147 \text{ k}$$

(3) The lateral yield forces are obtained by assuming a triangular distribution of acceleration over the building height. From the calculations presented in Table A.1,

$$F_1 = 0.5 \text{ V} = 73.5 \text{ k}$$
$$F_2 = 0.5 \text{ V} = 73.5 \text{ k}$$

The members can now be proportioned to resist the ultimate loading. In most instances it can be assumed that the ultimate loading is made up of the yield lateral forces, the dead load, and the portion of the gravity live load judged to be present during earthquake excitation. (In many cases it will not be necessary to proportion the building in this step since

preliminary member sizes already will have been selected on the basis of gravity or gravity plus wind loadings.) It will be assumed without checking that Design 2-D is proportioned adequately.

(4) The yield displacements are calculated.

$$\begin{Bmatrix} v_1 \\ v_2 \end{Bmatrix}_{yield} = \underbrace{\begin{bmatrix} 0.639 & 0.771 \\ 0.771 & 1.857 \end{bmatrix}}_{\text{flexibility matrix}} \times 10^{-2} \frac{\text{in.}}{\text{k}} \begin{Bmatrix} F_1 \\ F_2 \end{Bmatrix} \text{k} = \begin{Bmatrix} 1.04 \\ 1.93 \end{Bmatrix} \text{in.}$$

(5) The maximum displacements are calculated.

$$\begin{Bmatrix} v_1 \\ v_2 \end{Bmatrix}_{max} = \mu \begin{Bmatrix} v_1 \\ v_2 \end{Bmatrix}_{yield} = \begin{Bmatrix} 1.56 \\ 2.90 \end{Bmatrix} \text{in.}$$

(6) The actual base shear capacity, Q, of the building under increasing lateral load and a dead plus 20 percent gravity live loading is now estimated. The [D.L. + 0.2(L.L.)] and the moment capacities of the members are shown in the figure below. (The moment capacities of the base story columns have been calculated previously in the example presented in Section 4.3.2.)

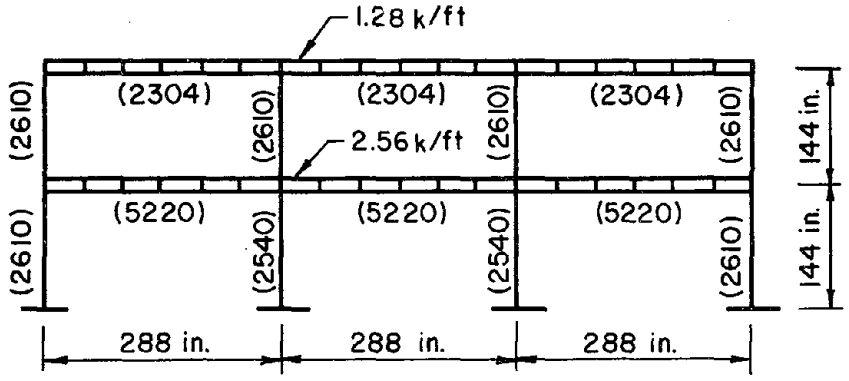

Under the assumption that the distribution of lateral forces over the building height arises from the inertial forces caused by a triangular distribution of acceleration, it can be shown that the following two collapse mechanisms are among the possible mechanisms.

Mechanism I

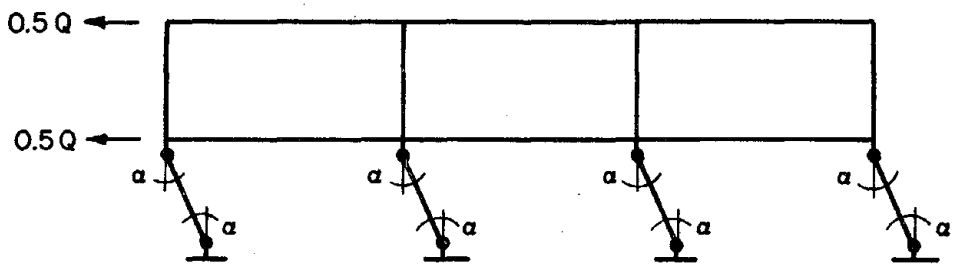

External Work + Internal Work = 0

$(0.5Q + 0.5Q)\ 144\ \text{in.}\ \alpha - (4 \times 2610 + 4 \times 2540)\ \text{in.k}\ \alpha = 0$

$\therefore\ Q = 143\ \text{k}$

Mechanism II

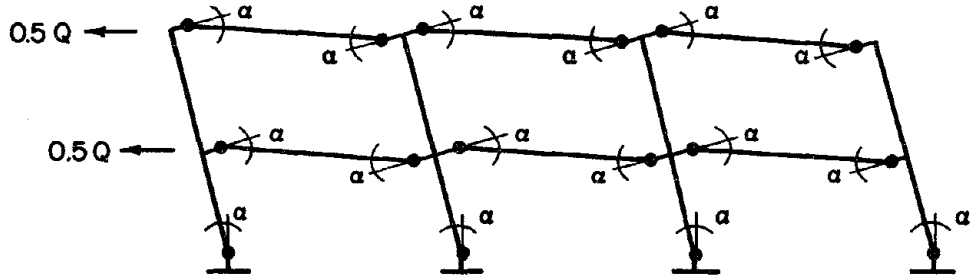

External Work + Internal Work = 0

$(0.5Q \times 144 + 0.5Q \times 288)\ \text{in.}\ \alpha - (2 \times 2610 + 2 \times 2540 + 6 \times 5220 + 6 \times 2304)\ \text{in.k}\ \alpha = 0$

$\therefore\ Q = 257\ \text{k}$

From all the possible modes of failure, Mechanism I gives the lowest base shear capacity. Therefore

$$Q = 143\ \text{k}$$

If it is assumed that all inelastic hinges form at the instant during seismic motion when the yield displacement of the first story is reached, the maximum inelastic hinge rotations can be estimated from consideration of Mechanism I. Thus

$$\alpha_m = \frac{\text{inelastic story displacement}}{\text{story height}} = \frac{1.56\ \text{in.} - 1.04\ \text{in.}}{144\ \text{in.}} = 0.00361\ \text{rad}$$

The elastic fundamental frequency of vibration can be estimated by means of Rayleigh's method,

$$f_1 \simeq \frac{1}{2\pi}\sqrt{\left(\sum_{i=1}^{N} F_i v_i\right) \div \left(\sum_{i=1}^{N} m_i v_i^2\right)}$$

Since the elastic frequency is to be obtained, the yield displacements are used for calculations. Thus

$$f_1 \simeq \frac{1}{2\pi}\sqrt{\frac{(73.5\ \text{k})(1.04\ \text{in.}) + (73.5\ \text{k})(1.93\ \text{in.})}{(0.477\ \text{k-sec}^2/\text{in.})(1.04\ \text{in.})^2 + (0.239\ \text{k-sec}^2/\text{in.})(1.93\ \text{in.})^2}}$$

$$\simeq 2.0\ \text{cps}$$

The values of the base shear capacity and fundamental frequency estimated in this step are commensurate with the values assumed for design in Step (2).

(7) The design for a ductility of 1.5 is complete provided the building can accommodate the maximum displacements, inelastic deformations, and so forth.

The response quantities calculated in this example can be compared to the response quantities obtained from time-history analysis and the response quantities obtained from modal analysis. The time-history response quantities (inelastic analysis case) are shown in Fig. 4.2 and tabulated in Table F.4, and the modal analysis response quantities are calculated in the example presented in Section 4.3.2.

5.5 Design Considerations

The conventional approach to the earthquake resistant design of structures requires that inelastic deformations be relied upon to dissipate energy during seismic ground motion. It is therefore necessary that structures be designed to deform in a ductile manner throughout the cylic response.

In proportioning a low-rise building to resist earthquake base excitation, due consideration should be given to the overall structural performance of the lateral load carrying system, including not only primary

and secondary structural systems, but also nonstructural items. Secondary structural and nonstructural items such as stairs, exterior walls, partition walls, and floor systems can have a significant influence on the response. Also, when assessing the available ultimate deformation capacity of a building system, it should be remembered that damage to nonstructural items is often much more expensive to repair than structural damage.

With these factors in mind, a good start to the earthquake resistant design procedure can be made by proportioning the structure to resist gravity and wind loads. The adequacy of the design can then be checked using the recommendations of the seismic provisions in modern building codes, and the recommendations given in this study.

Strength versus Flexibility. The design engineer endeavors to proportion his building such that it responds to earthquake base motion without being subjected to excessive deformations. On the other hand, he does not want to make the building so strong that it attracts very large inertial forces. Thus, the designer attempts to strike a balance between strength and flexibility.

Redundancy. In an effort to minimize the likelihood of a major structural failure, the prudent designer will, if possible, include redundancy in his design. In the event that failure of an element or a portion of the structure occurs, second lines of defense are then available.

Redundancy can be built into a design by separating the lateral load resisting system into a number of structural cells or units so that the weakening of one unit will not endanger the overall structural integrity of the building system. Further, the structure should be detailed in such a way that secondary structural members and systems (floor systems, secondary

framing connections, and so forth) can resist a certain amount of lateral load and add to damping in the system, especially for significant levels of deformation. Redundancy also can be included in the design by combining more than one type of structural system to resist lateral load, provided the different types of structural systems are compatible with each other and provided the strength of the redundant system is maintained under deformation.

Design for Reserve Strength. In order for structures to reach and sustain their strength under inelastic deformations, the connections between structural members must be carefully detailed. It is usually preferable to make a connection stronger than the members framing into it, thus forcing the inelastic deformations into the members. In proportioning a connection, due account should be taken of strain hardening effects that occur in the members under inelastic deformations.

The load carrying capacity of flexural members under cyclic deformations can be reduced significantly or lost if local buckling or a fracture occurs. Thus, the width to thickness ratios of flexural members should satisfy the requirements for plastically designed sections. Also, the fracture toughness of materials and fabricated elements (including X-bracing members) should be selected to ensure that the resistance (strength and deformation capability) will be maintained under the design temperatures.

In the case of the primary structural system, the designer must evaluate the effective resistance offered by all load carrying members. Careful attention is required to ensure that beams, for example, cannot fail by lateral torsional buckling. For architectural reasons it may not be possible to brace column members against lateral torsional buckling.

Unfortunately, simplified procedures for evaluating the strength-deformation capacities of unbraced steel columns subjected to thrust and end moment are not yet available.

For several of the moment frame buildings considered in this study, it was observed that yielding tended to be concentrated in the base story columns. It is thought that this type of behavior is typical of many low-rise steel moment frame buildings of practical proportions. Because the failure of columns is usually considered to be more severe than the failure of beams, it is recommended that buildings in which yielding tends to be concentrated in the columns be designed for relatively low ductilities, say less than about 2 or 3.

Well-proportioned low-rise buildings, including shear buildings, moment frames, and X-braced frames, should preferably have story shear strengths that decrease slightly as the story number increases. There seems to be little justification for deliberately designing buildings with a weak or "soft" base story, or buildings with large strength discontinuities between stories.

Low-rise buildings as a class are often irregular in form and cannot be modelled simply for purposes of analysis. Nevertheless, the prudent designer will attempt to proportion a well-balanced system of comparable structural properties in the orthogonal horizontal directions. Redundancies should be included in the design if possible, and designs that result in large torsional forces or motions should be avoided. The members and frames of well-designed structures should be connected and tied together in a manner that allows for the satisfactory overall performance of the structure during seismic ground excitation; provision also should be made for overturning and torsional effects at each elevation and the base.

REFERENCES

1. Aktan, A.E., D.A. Pecknold and M.A. Sozen, 1974, "R/C Column Earthquake Response in Two Dimensions", Proc. ASCE, 100 (ST10), pp. 1999-2015.

2. American Institute of Steel Construction, 1969, Specification for the Design, Fabrication and Erection of Structural Steel for Buildings, including Supplements 1, 2 and 3, New York, New York.

3. Anderson, J.C. and R.P. Gupta, 1972, "Earthquake Resistant Design of Unbraced Frames", Proc. ASCE, 98 (ST11), pp. 2523-2539.

4. Applied Technology Council, 1977, Final Review Draft of Recommended Comprehensive Seismic Design Provisions for Buildings, Palo Alto, California.

5. Army, Navy and Air Force, 1973, "Seismic Design for Buildings", Tri Service, TM 5-809-10, NAV FAC P-355, AFM 88-3, Chapter 13, Washington, D.C., pp. C-39 to C-47.

6. Arnold, P., P.F. Adams and L.-W. Lu, 1968, "Strength and Behavior of an Inelastic Hybrid Frame", Proc. ASCE, 94 (ST1), pp. 243-266.

7. Bazán, E. and E. Rosenblueth, 1974, "Seismic Response of One-Story X-Braced Frames", Proc. ASCE, 100 (ST2), Technical Note, pp. 489-493.

8. Carpenter, L.D. and L.-W. Lu, 1973, "Reversed and Repeated Load Tests of Full-Scale Steel Frames", AISC Steel Research for Construction, Bulletin No. 24.

9. Clough, R.W. and K.L. Benuska, 1967, "Nonlinear Earthquake Behavior of Tall Buildings", Proc. ASCE, 93 (EM3), pp. 129-146.

10. Clough, R.W. and J. Penzien, 1975, Dynamics of Structures, McGraw-Hill, Inc., New York, New York.

11. Clough, R.W., K.L. Benuska and E.L. Wilson, 1965, "Inelastic Earthquake Response of Tall Buildings", Proc. Third World Conference on Earthquake Engineering, Auckland and Wellington, New Zealand, Vol. II, pp. 68-69.

12. Galambos, T.V., 1968, Structural Members and Frames, Prentice-Hall, Inc., Englewood Cliffs, New Jersey.

13. Giberson, M.F., 1969, "Two Nonlinear Beams with Definitions of Ductility", Proc. ASCE, 95 (ST2), pp. 137-157.

14. Goel, S.C. and R.D. Hanson, 1972, "Seismic Behavior of Multistory Braced Steel Frames", AISC Steel Research for Construction, Bulletin No. 22.

15. Hanson, R.D., 1975, "Characteristics of Steel Members and Connections", Proc. U.S. National Conference on Earthquake Engineering, Ann Arbor, Michigan, pp. 255-267.

16. Igarashi, S., K. Inoue, M. Asano and K. Ogawa, 1973, "Restoring Force Characteristics of Steel Diagonal Bracings", Proc. Fifth World Conference on Earthquake Engineering, Rome, Italy, Pamphlet 270.

17. Luyties, W.H., S.A. Anagnostopoulos and J.M. Biggs, 1976, "Studies on the Inelastic Dynamic Analysis and Design of Multi-Story Frames", Publication Number R76-29, Department of Civil Engineering, Massachusetts Institute of Technology, Cambridge, Massachusetts.

18. Melin, J.W., 1976, private communication.

19. National Building Code of Canada 1975, including Commentaries on Part 4, Associate Committee on the National Building Code, National Research Council of Canada, Ottawa, Canada.

20. Newmark, N.M., 1959, "A Method of Computation for Structural Dynamics", Proc. ASCE, 85 (EM3), 67-94.

21. Newmark, N.M., 1968, "Earthquake-resistant Building Design", in Structural Engineering Handbook, edited by E.H. Gaylord and C.N. Gaylord, McGraw-Hill, Inc., New York, New York, pp. 3-1 to 3-30.

22. Newmark, N.M. and W.J. Hall, 1973, "Procedures and Criteria for Earthquake Resistant Design", National Bureau of Standards, Gaithersburg, Maryland, Building Science Series No. 46, Vol. I, pp. 209-236.

23. Newmark, N.M. and W.J. Hall, 1976, "Vibration of Structures Induced by Ground Motion", in Shock and Vibration Handbook, edited by C.M. Harris and C.E. Crede, McGraw-Hill, Inc., New York, New York, Second edition, pp. 29-1 to 29-19.

24. Newmark, N.M. and E. Rosenblueth, 1971, Fundamentals of Earthquake Engineering, Prentice-Hall, Inc., Englewood Cliffs, New Jersey.

25. Newmark, N.M., W.H. Walker, A.S. Veletsos and R.J. Mosborg, 1965, "Design Procedures for Shock Isolation Systems of Underground Protective Structures: Response of Two-Degree-of-Freedom Elastic and Inelastic Systems", Report RTD, TDR 63-3096, Vol. IV, Air Force Weapons Laboratory, Albuquerque, New Mexico.

26. Penzien, J., 1960, "Elasto-Plastic Response of Idealized Multi-Story Structures Subjected to a Strong Motion Earthquake", Proc. Second World Conference on Earthquake Engineering, Tokyo and Kyoto, Japan, Vol. II, pp. 739-760.

27. Popov, E.P. and V.V. Bertero, 1973, "Cyclic Loading of Steel Beams and Connections", Proc. ASCE, 99 (ST6), pp. 1189-1204.

28. Przemieniecki, J.S., 1968, Theory of Matrix Structural Analysis, McGraw-Hill, Inc., New York, New York.

29. Shibata, A. and M.A. Sozen, 1976, "Substitute-Structure Method for Seismic Design in R/C", Proc. ASCE, 102 (ST1), pp. 1-18.

30. Structural Engineers Association of California, 1975, Recommended Lateral Force Requirements and Commentary, San Francisco, California.

31. Sun, C.-K., G.V. Berg and R.D. Hanson, 1973, "Gravity Effect on Single-Degree Inelastic System", Proc. ASCE, 99 (EM1), pp. 183-200.

32. Tang, D.T., 1975, "Earthquake Simulator Study of a Steel Frame Structure, Vol. II: Analytical Results", Report No. EERC 75-36, Earthquake Engineering Research Center, College of Engineering, University of California, Berkeley, California.

33. Timoshenko, S., D.H. Young and W. Weaver, 1974, Vibration Problems in Engineering, John Wiley & Sons, Inc., New York, New York, Fourth edition.

34. Uniform Building Code 1973 Edition, International Conference of Building Officials, Whittier, California.

35. Uniform Building Code 1976 Edition, International Conference of Building Officials, Whittier, California.

36. Veletsos, A.S., 1969, "Maximum Deformations of Certain Nonlinear Systems", Proc. Fourth World Conference on Earthquake Engineering, Santiago, Chile, Vol. II, pp. 155-170.

37. Veletsos, A.S. and W.P. Vann, 1971, "Response of Ground-Excited Elastoplastic Systems", Proc. ASCE, 97 (ST4), pp. 1257-1281.

38. Veletsos, A.S., N.M. Newmark and C.V. Chelapati, 1965, "Deformation Spectra for Elastic and Elastoplastic Systems Subjected to Ground Shock and Earthquake Motions", Proc. Third World Conference on Earthquake Engineering, Auckland and Wellington, New Zealand, Vol. II, pp. 663-682.

39. Zienkiewicz, O.C., 1971, The Finite Element Method in Engineering Science, McGraw-Hill, Inc., London, England.

TABLE 2.1 LIMITING BASE SHEAR COEFFICIENTS, V/W

Building Code	Ductile Moment Frame	X-braced Frame
UBC (1973)[1]	0.067	0.15
NBC (1975)[2]	0.056	0.10
SEAOC (1975)[1]	0.094	0.18
UBC (1976)[1]	0.094	0.18
ATC (1977)[3]	0.14	0.22

[1]Based on allowable stress, 33 percent increase allowed for (D.L. + L.L. + E.Q.).

[2]Based on allowable stress, multiply (D.L. + L.L. + E.Q.) by a load combination probability factor of 0.75.

[3]Based on yield stress.

TABLE 2.2 LOADING FOR TWO-STORY BUILDINGS

Loading	First Floor (lb/ft^2)	Second Floor (Roof) (lb/ft^2)
D.L.	70	36
L.L.	50	20
D.L. + 0.2(L.L.)	80	40

TABLE 2.3 LOADING FOR THREE-STORY BUILDINGS

Loading	First and Second Floor (lb/ft^2)	Third Floor (Roof) (lb/ft^2)
D.L.	74.5	35.7*
L.L.	50	-
D.L. + 0.2(L.L.)	84.5	35.7*

* Includes 10 lb/ft^2 to account for the weight of second floor partitions tributary to third floor mass.

TABLE 2.4 MAXIMUM DESIGN STRESSES IN CRITICAL MEMBERS, IN PERCENT OF ALLOWABLE

Design	Design Base Shear Coefficient, V/W	Columns[1]	Beams[2]
2-A	0.10	50	-
2-B	0.10	85	-
2-C	0.10	170	-
2-D	0.10	70	85-90
2-E	0.10	100-110	90
2-F	0.10	50	130-135
3-A	0.05	50	30
3-B	0.05	30	55-85

[1]Calculated assuming F_b = 22 ksi and F_a = axial stress that would be permitted in the plane of bending.

[2]Calculated assuming F_b = 24 ksi.

TABLE 4.1 COMPARISON BETWEEN MAXIMUM HINGE ROTATIONS AND HINGE ROTATION CAPACITIES

Design	Description	Column Location	Maximum[1] Rotation (rad)	Rotation[2] Capacity, θ_h (rad)
2-A	shear building	interior, first floor	0.00046	0.0154
2-B	shear building	interior, first floor	0.00720	0.0189
2-C	shear building	interior, first floor	0.0141	0.0237
2-D	moment frame	interior, first floor	0.00551	0.0155
2-E	moment frame	interior, first floor	0.00603	0.0230
3-A	moment frame	first floor	0.00995	0.0123

[1] From the results of time-history calculations for the inelastic analysis case.

[2] Calculated using Eq. (4.1), an expression developed by Popov and Bertero (1973).

TABLE 4.2 DUCTILITY FACTORS FOR X-BRACED BUILDING DESIGNS, INELASTIC ANALYSIS CASE

Design	Design Base Shear Coefficient, V/W	First Story	Second Story	Third Story
2-G	0.157	7.91	1.04	-
2-H	0.266	3.69	0.706	-
3-C	0.158	5.58	1.82	0.720
3-D	0.253	3.30	1.09	0.612

TABLE 4.3 COMPARISON BETWEEN MAXIMUM INELASTIC AND DESIGN STORY DRIFTS

Design	Story of Maximum Drift	Design Drift (%)	Inelastic Drift (%)	Inelastic Drift / Design Drift
(a) Two-Story Shear Buildings				
2-A	1	0.0833	0.570	6.84
2-B	1	0.190	1.31	6.89
2-C	1	0.482	2.02	4.19
(b) Two-Story Moment Frames				
2-D	1	0.135	1.07	7.93
2-E	1	0.311	1.33	4.28
2-F	2	0.118	0.920*	7.80
(c) Two-Story X-braced Frames				
2-G	1	0.240	2.37	9.88
2-H	1	0.240	1.11	4.63
(d) Three-Story Moment Frames				
3-A	1	0.150	1.41	9.40
3-B	3	0.131	1.22*	9.31
(e) Three-Story X-braced Frames				
3-C	1	0.312	2.18	6.99
3-D	1	0.312	1.29	4.13

* Inelastic + FEF analysis case.

TABLE 4.4 CHANGES IN INELASTIC FIRST-STORY DISPLACEMENTS DUE TO P-DELTA EFFECTS

Design	Description	$\frac{(\text{Inelastic} + P\Delta) - (\text{Inelastic})}{(\text{Inelastic})} \cdot 100$ (%)
2-A	shear building	0.1
2-B	shear building	2.6
2-C	shear building	18.9
2-D	moment frame	1.3
2-E	moment frame	7.9
2-F	moment frame	1.7
2-G	X-braced frame	13.2
2-H	X-braced frame	-6.9
3-A	moment frame	4.3
3-B	moment frame	3.0
3-C	X-braced frame	2.8
3-D	X-braced frame	0.0

TABLE 4.5 ESTIMATED FIRST-STORY YIELD DISPLACEMENTS

Design	Description	u_y (in.)
2-B	shear building	0.89
2-C	shear building	1.0
2-D	moment frame	1.0
2-E	moment frame	1.2
2-G	X-braced frame	0.432*
2-H	X-braced frame	0.432*
3-A	moment frame	0.98
3-C	X-braced frame	0.515*
3-D	X-braced frame	0.515*

* The yield displacements for X-braced building designs are exact quantities.

TABLE 4.6 RESPONSE QUANTITIES OBTAINED USING THE MODAL METHOD NORMALIZED BY THE CORRESPONDING TIME-HISTORY RESPONSE QUANTITIES

Design	2-A	2-B	2-C	2-D	2-E	2-F	2-G	2-H
(a) elastic								
second-story shear	1.21	0.97	0.95	1.01	1.27	1.05	1.01	1.25
first-story shear	1.13	0.90	0.87	0.99	1.26	1.25	0.90	1.12
second-story displ.	1.21	0.89	0.87	0.90	1.25	1.03	0.90	1.18
first-story displ.	1.13	0.91	0.87	0.96	1.26	1.16	0.90	1.12
(b) inelastic								
ductility	-	2	3	1.5	1.5	-	8	4
second-story shear	-	0.71	0.72	0.86	1.11	-	0.52	0.96
first-story shear	-	1.11	1.08	1.04	1.35	-	1.03	1.43
second-story displ.	-	1.28	1.38	1.10	1.54	-	1.33	1.91
first-story displ.	-	1.04	1.11	0.99	1.29	-	1.04	1.54

Design	3-A	3-B	3-C	3-D
(a) elastic (continued)				
third-story shear	1.25	1.26	1.06	1.13
second-story shear	0.99	1.28	0.95	0.97
first-story shear	1.02	1.30	1.06	0.98
third-story displ.	0.95	1.16	0.92	0.93
second-story displ.	0.90	1.23	0.91	0.90
first-story displ.	0.97	1.29	1.06	0.98
(b) inelastic (continued)				
ductility	2	-	6	3
third-story shear	0.90	-	0.54	0.90
second-story shear	0.76	-	0.82	1.30
first-story shear	1.05	-	1.05	1.72
third-story displ.	1.42	-	1.51	2.06
second-story displ.	1.26	-	1.35	1.96
first-story displ.	1.01	-	1.14	1.56

TABLE 4.7 BASE SHEARS OBTAINED USING THE BUILDING CODE APPROACH NORMALIZED BY THE TIME-HISTORY BASE SHEARS

Design	2-A	2-B	2-C	2-D	2-E	2-F	2-G	2-H
(a) elastic								
base shear	1.13	0.90	0.85	0.98	1.23	1.27	0.90	1.12
(b) inelastic								
ductility	-	2	3	1.5	1.5	-	8	4
base shear	-	1.10	1.04	1.03	1.31	-	1.01	1.43

Design	3-A	3-B	3-C	3-D
(a) elastic (continued)				
base shear	0.89	1.20	1.04	0.98
(b) inelastic (continued)				
ductility	2	-	6	3
base shear	0.87	-	0.99	1.71

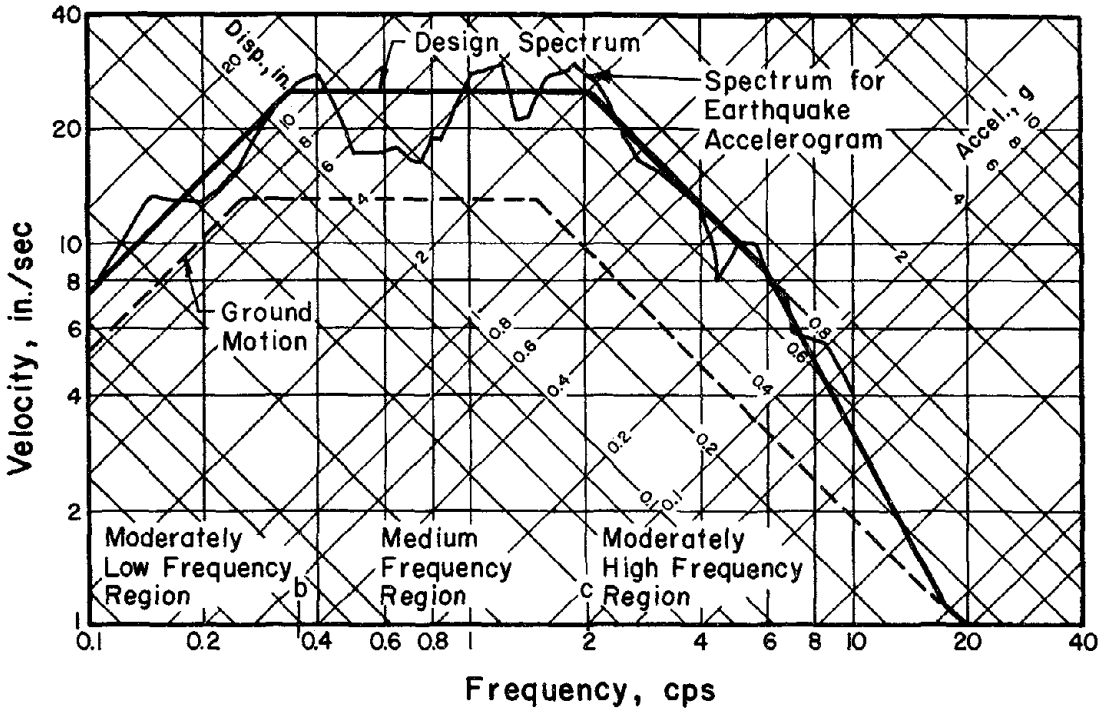

(a) Elastic Spectra

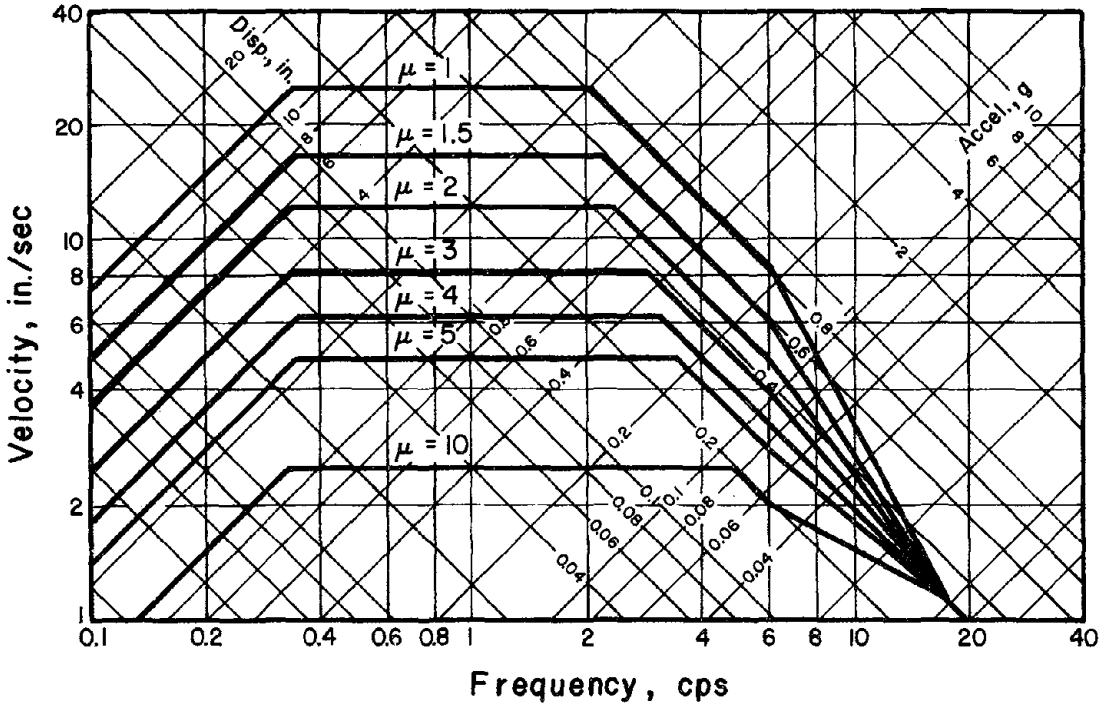

(b) Elastoplastic Design Spectra

FIG. 2.1 RESPONSE SPECTRA, EL CENTRO 1940 NS, 5 PERCENT CRITICAL DAMPING

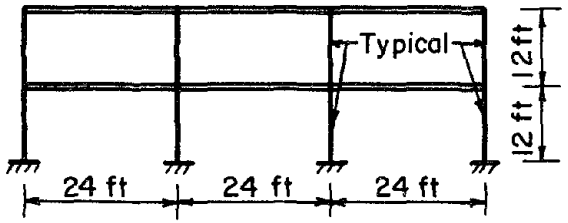

Design	Column Size	f_1 (cps)
2-A	W12x58	2.67
2-B	W10x39	1.78
2-C	W8x24	1.11

Designs 2-A, 2-B, and 2-C

(a) Two-Story Shear Buildings

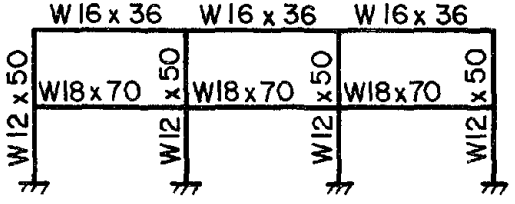

Design 2-D, f_1 = 1.99 cps

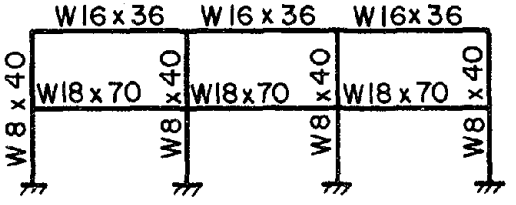

Design 2-E, f_1 = 1.35 cps

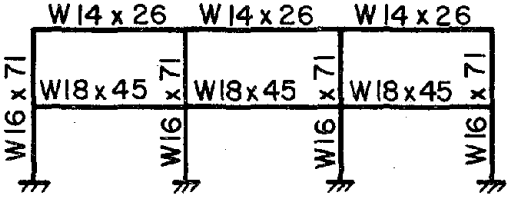

Design 2-F, f_1 = 2.27 cps

(b) Two-Story Moment Frames

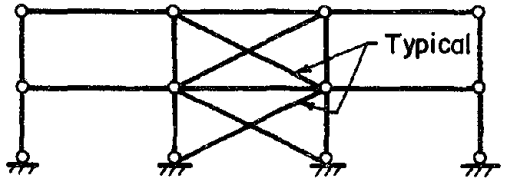

Design	$\frac{V}{W}$	Brace Area ($in.^2$)	f_1 (cps)
2-G	0.157	1.69	1.98
2-H	0.266	2.86	2.58

Designs 2-G and 2-H

(c) Two-Story X-Braced Frames

FIG. 2.2 BUILDING DESIGNS

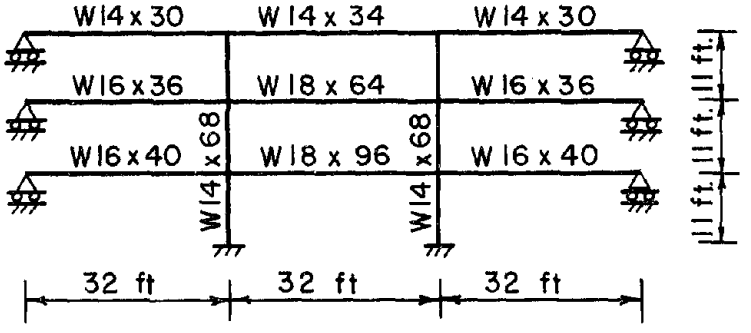

Design 3-A, f_1 = 1.10 cps

(d) Three-Story Moment Frames

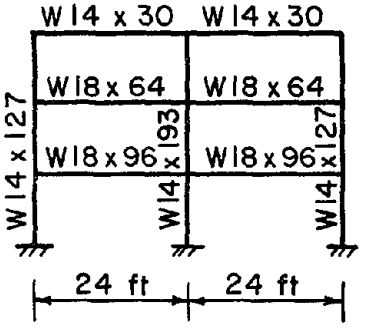

Design 3-B, f_1 = 1.39 cps

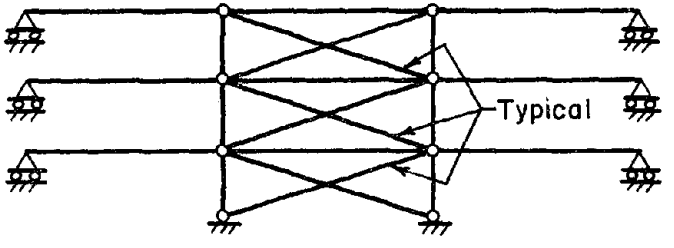

Designs 3-C and 3-D

(e) Three-Story X-Braced Frames

Design	$\frac{V}{W}$	Brace Area ($in.^2$)	f_1 (cps)
3-C	0.158	2.86	1.59
3-D	0.253	4.59	2.02

FIG. 2.2 (CONTINUED)

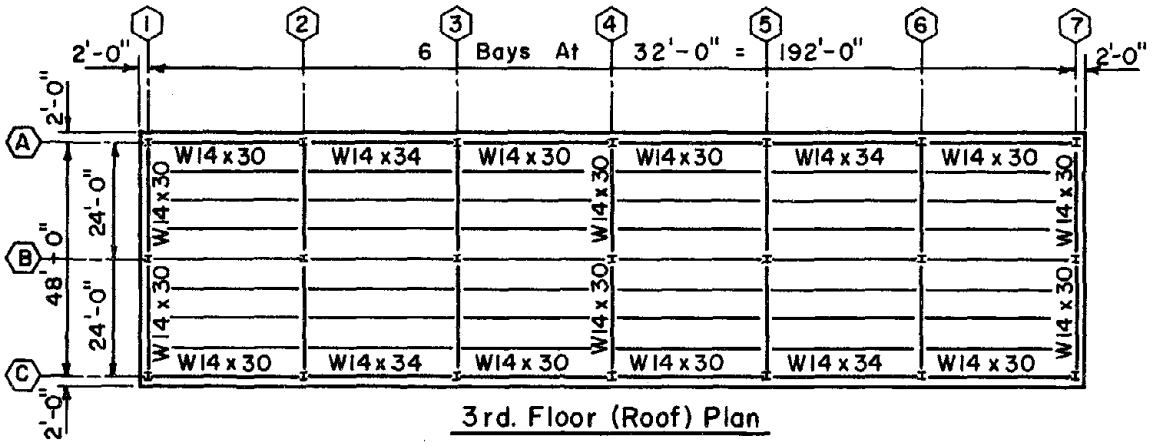

3rd. Floor (Roof) Plan

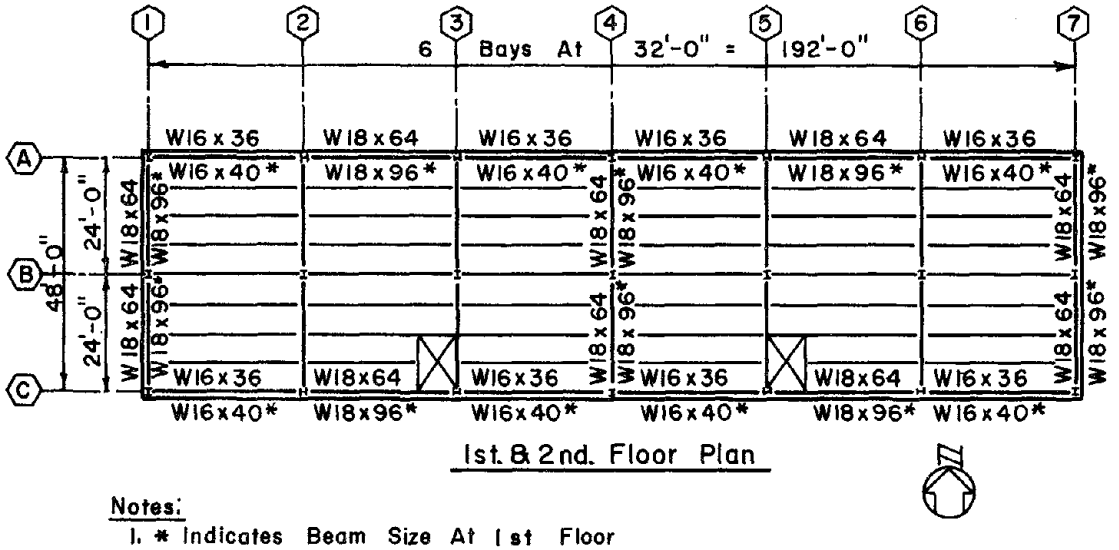

1st & 2nd. Floor Plan

Notes:

1. * Indicates Beam Size At 1st Floor
2. Floor and Roof Construction and Beams Not Called Out

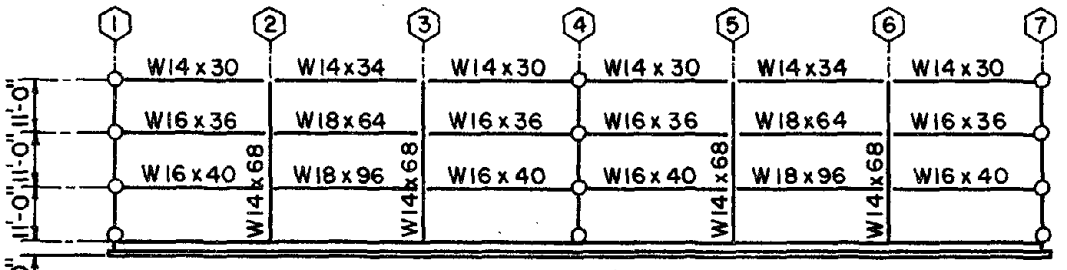

South Elevation (North Elev. Sim. Opp. Hand)

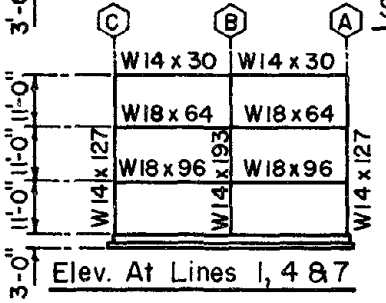

Elev. At Lines 1, 4 & 7

Note: Except Those Indicated o, All Connections of Beams and Girders To Columns Shown on Elevations Shall Develop The Flexural Capacity of The Beam. Others Are Standard Framing Connections.

FIG. 2.3 STRUCTURAL PLANS AND ELEVATIONS, THREE-STORY MOMENT FRAME BUILDING (AFTER ARMY, NAVY AND AIR FORCE, 1973)

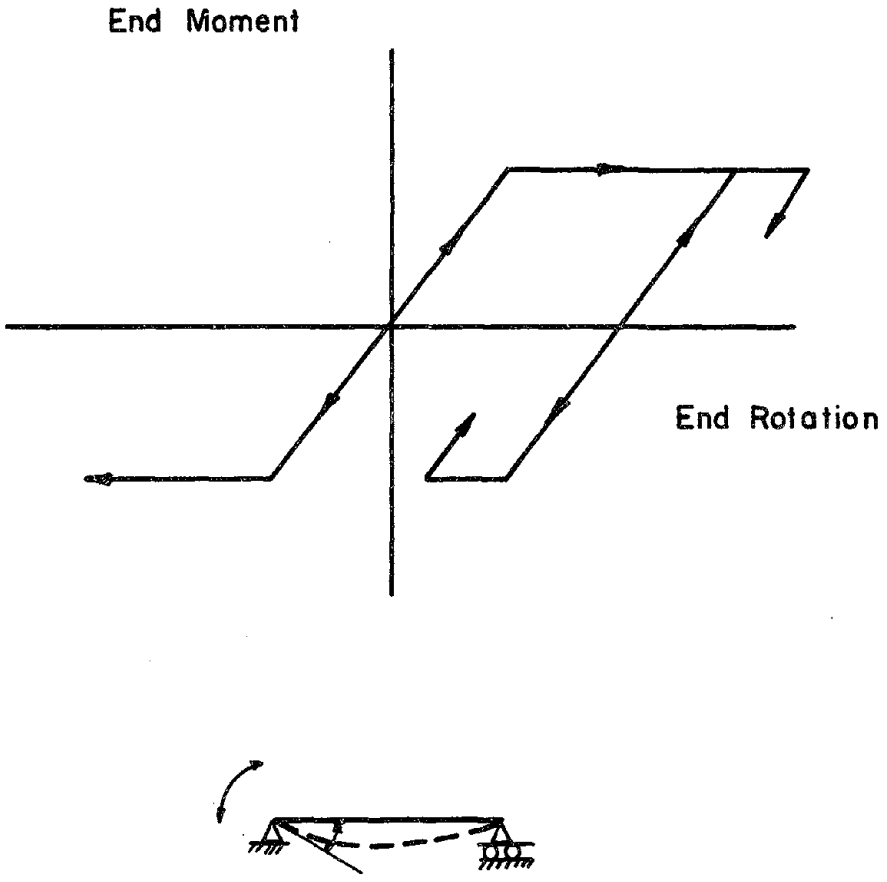

FIG. 3.1 FLEXURAL ELEMENT END MOMENT-ROTATION RELATIONSHIP

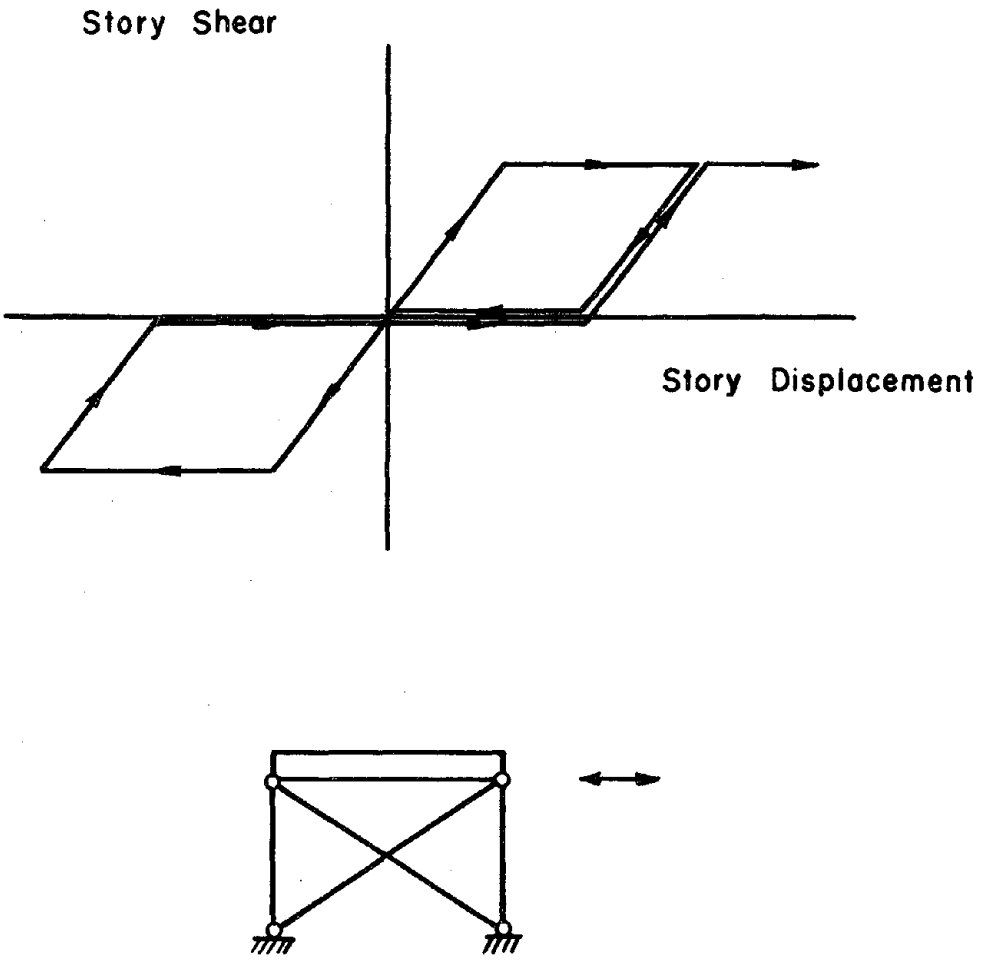

FIG. 3.2 X-BRACE ELEMENT STORY SHEAR-DISPLACEMENT RELATIONSHIP (AFTER NEWMARK AND ROSENBLUETH, 1971)

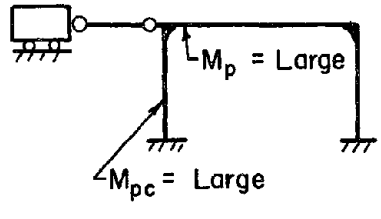

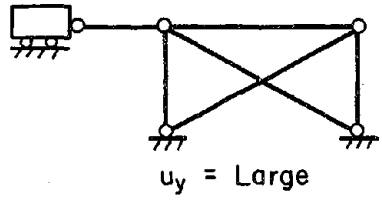

(a) Elastic

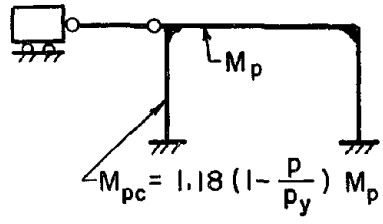

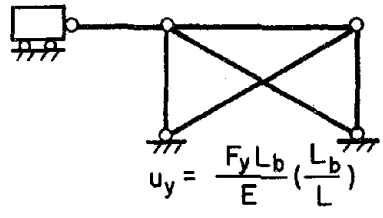

(b) Inelastic

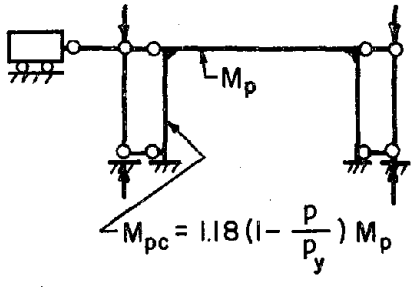

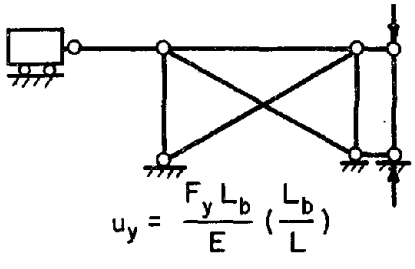

(c) Inelastic + PΔ

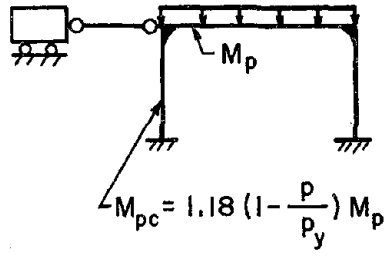

(d) Inelastic + FEF

FIG. 4.1 SCHEMATIC REPRESENTATION OF ANALYSIS CASES

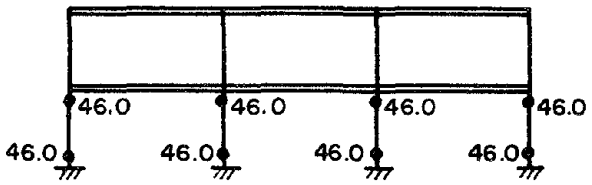

Design 2-A, Inelastic

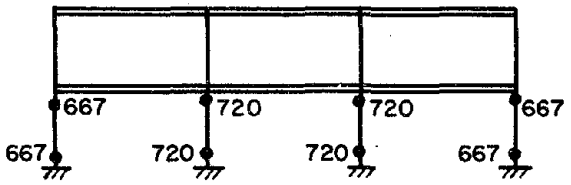

Design 2-B, Inelastic

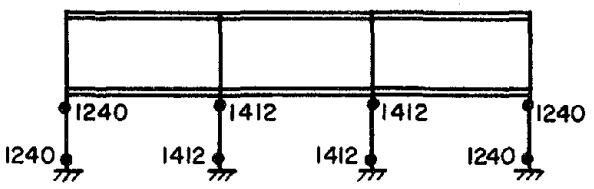

Design 2-C, Inelastic

(a) Two-Story Shear Buildings

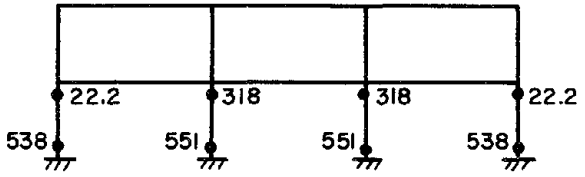

Design 2-D, Inelastic

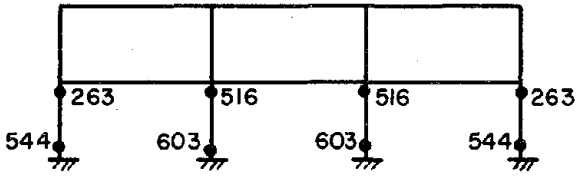

Design 2-E, Inelastic

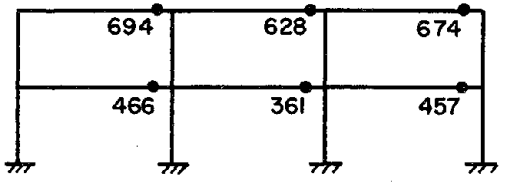

Design 2-F, Inelastic + FEF

(b) Two-Story Moment Frame Buildings

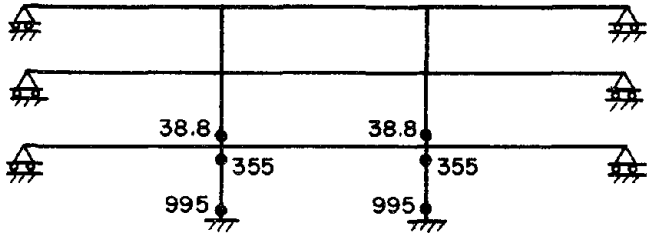

Design 3-A, Inelastic

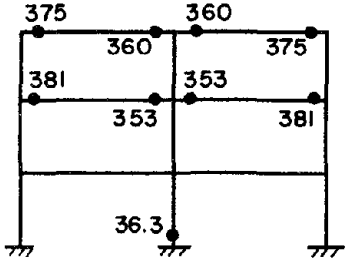

Design 3-B, Inelastic

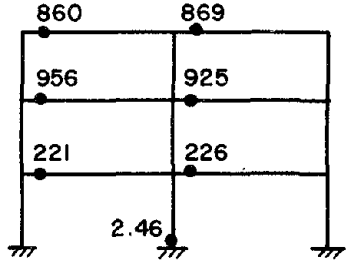

Design 3-B, Inelastic + FEF

(c) Three-Story Moment Frame Buildings

FIG. 4.2 MAXIMUM HINGE ROTATIONS, 10^{-5} Rad

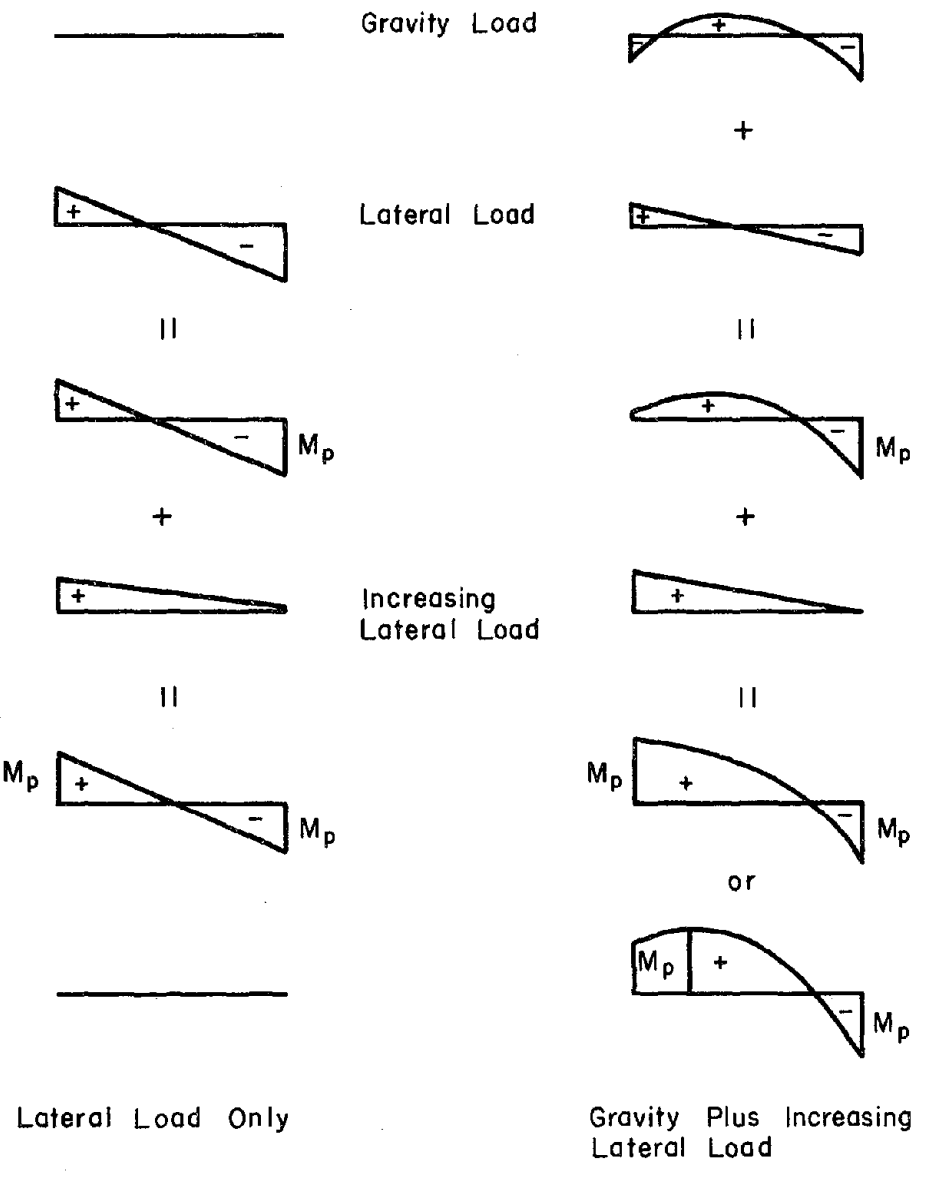

FIG. 4.3 THE EFFECT OF GRAVITY LOAD ON YIELDING BEAM MEMBERS

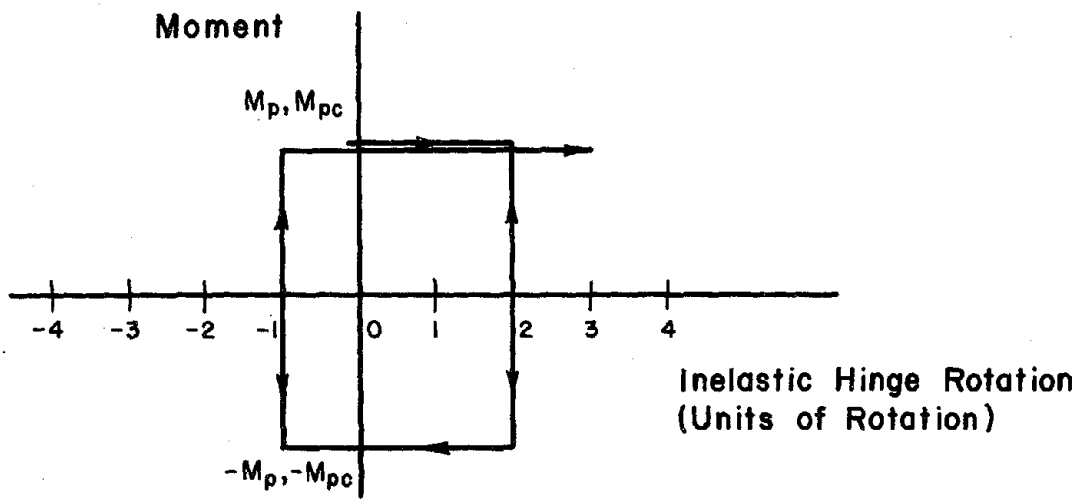

Maximum Rotation = 3 Units
Cumulative Rotation = $2 + |-3| + 4 = 9$ Units
Cumulative / Maximum Rotation = $9/3 = 3$

FIG. 4.4 NORMALIZED CUMULATIVE HINGE ROTATION

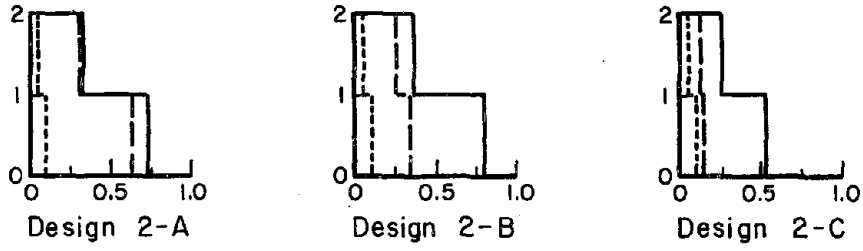

(a) Two-Story Shear Buildings

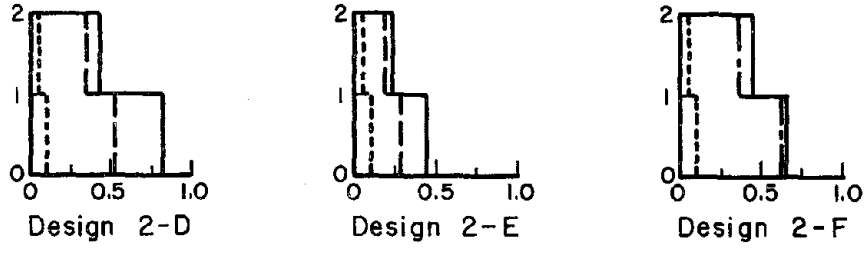

(b) Two-Story Moment Frames

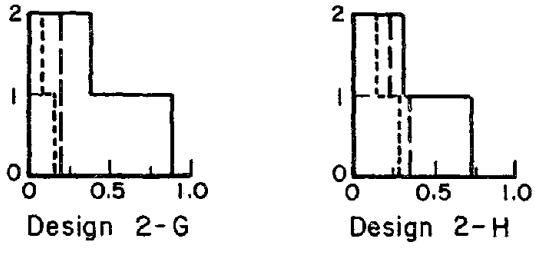

(c) Two-Story X-Braced Frames

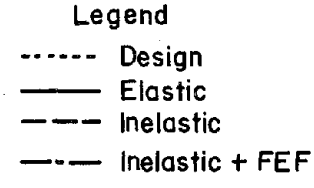

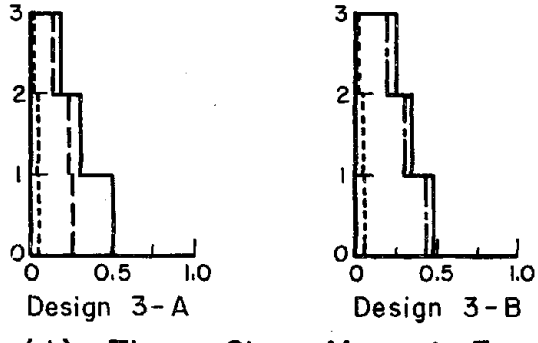

(d) Three-Story Moment Frames

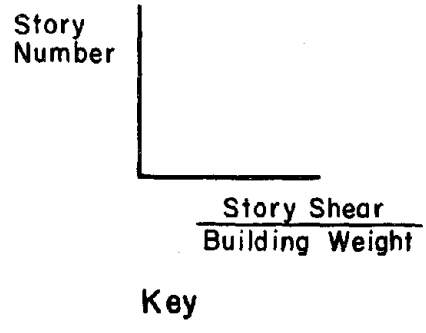

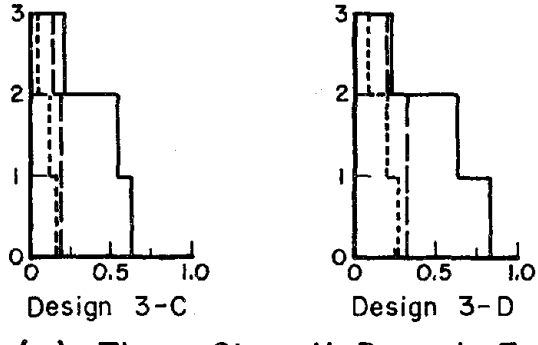

(e) Three-Story X-Braced Frames

FIG. 4.5 STORY SHEAR COEFFICIENTS

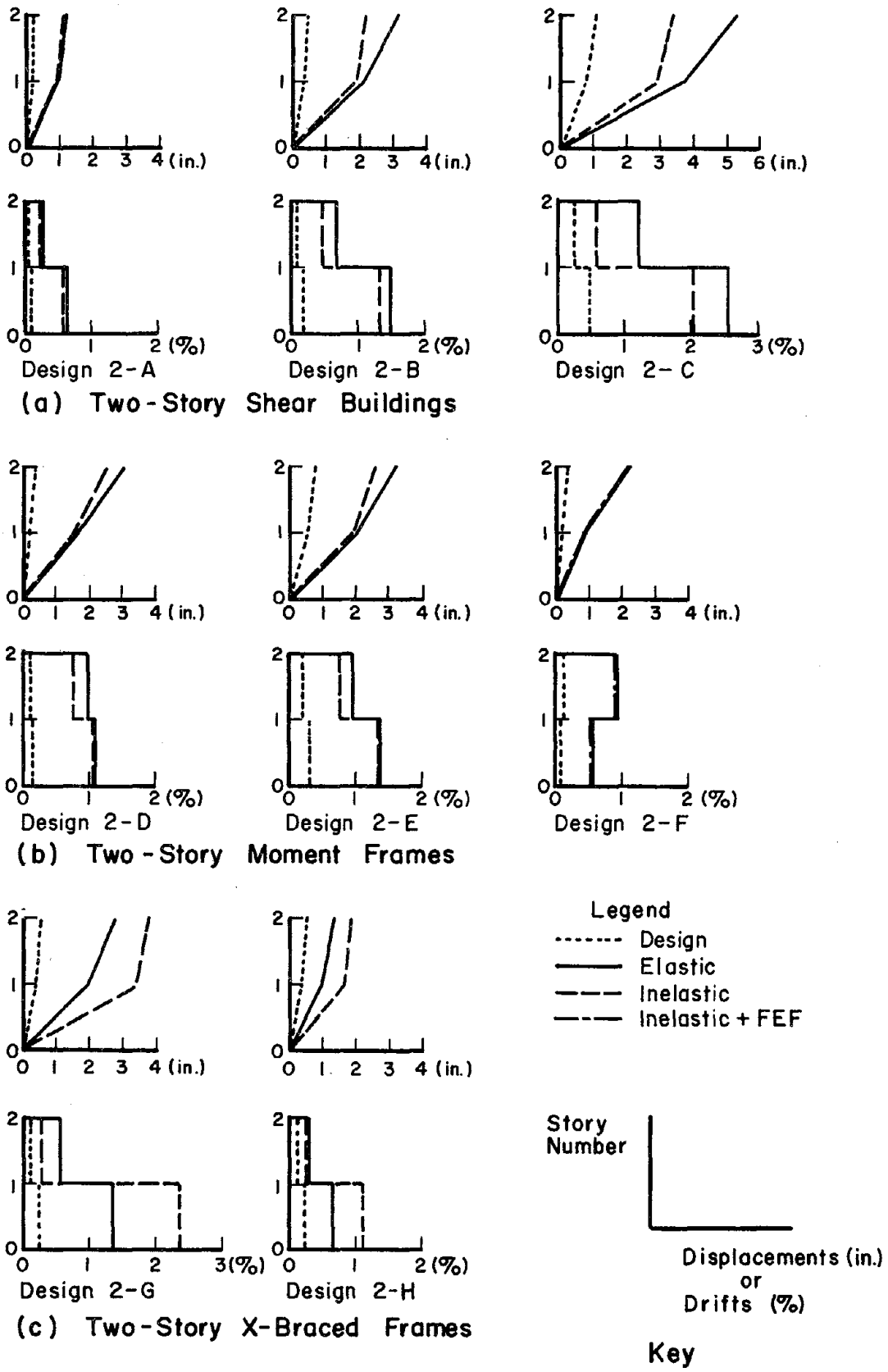

FIG. 4.6 STORY DISPLACEMENTS AND DRIFTS

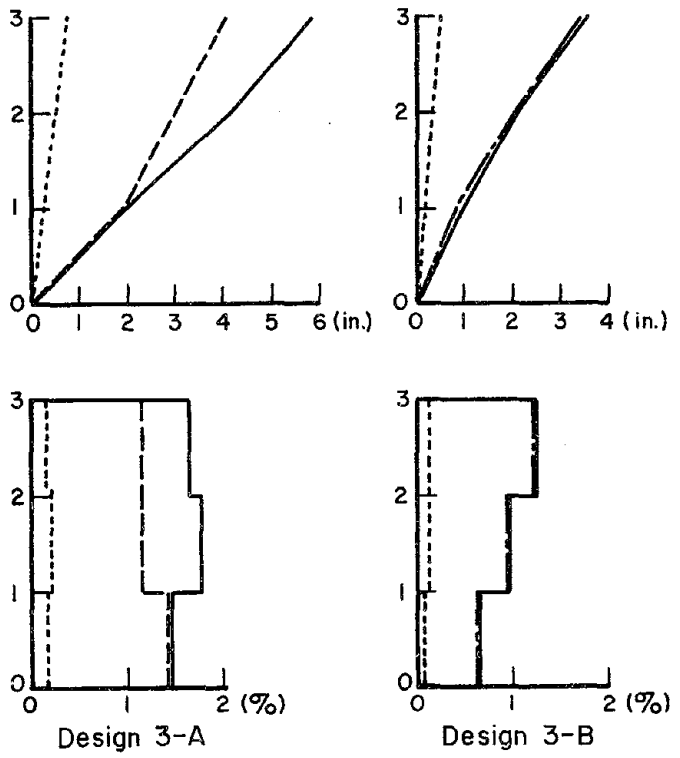

(d) Three-Story Moment Frames

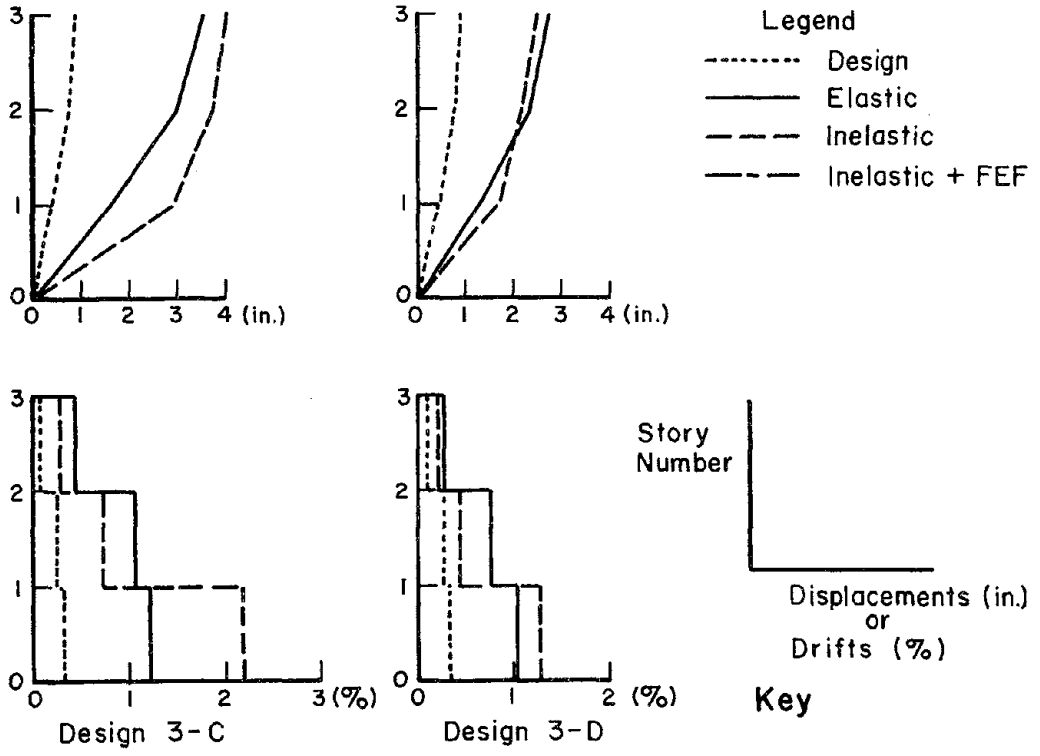

(e) Three-Story X-Braced Frames

FIG. 4.6 (CONTINUED)

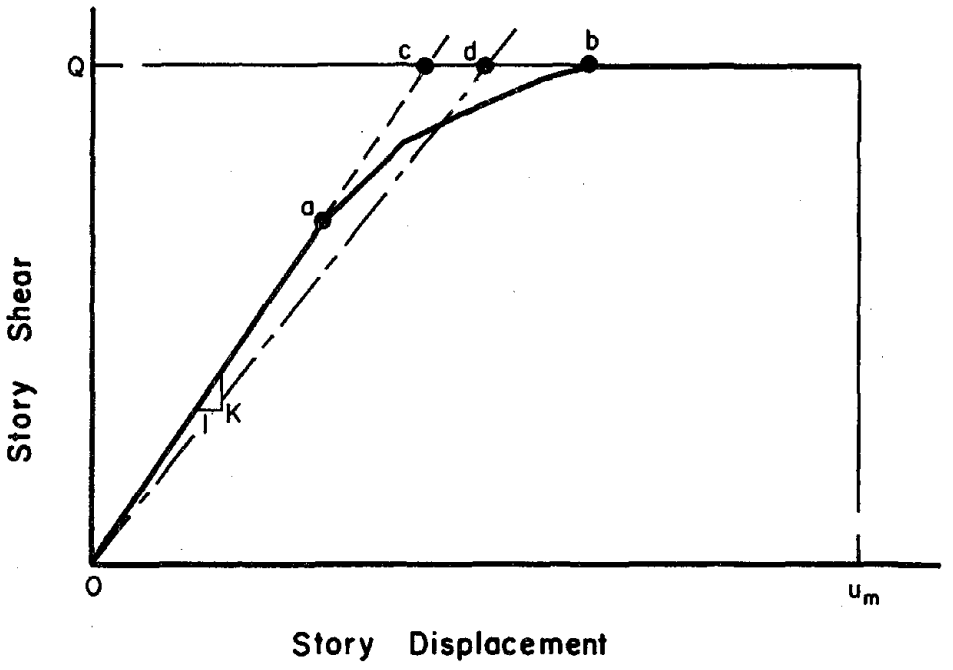

FIG. 4.7 STORY SHEAR-DISPLACEMENT RELATIONSHIP FOR A STORY FORMING A SIDESWAY MECHANISM

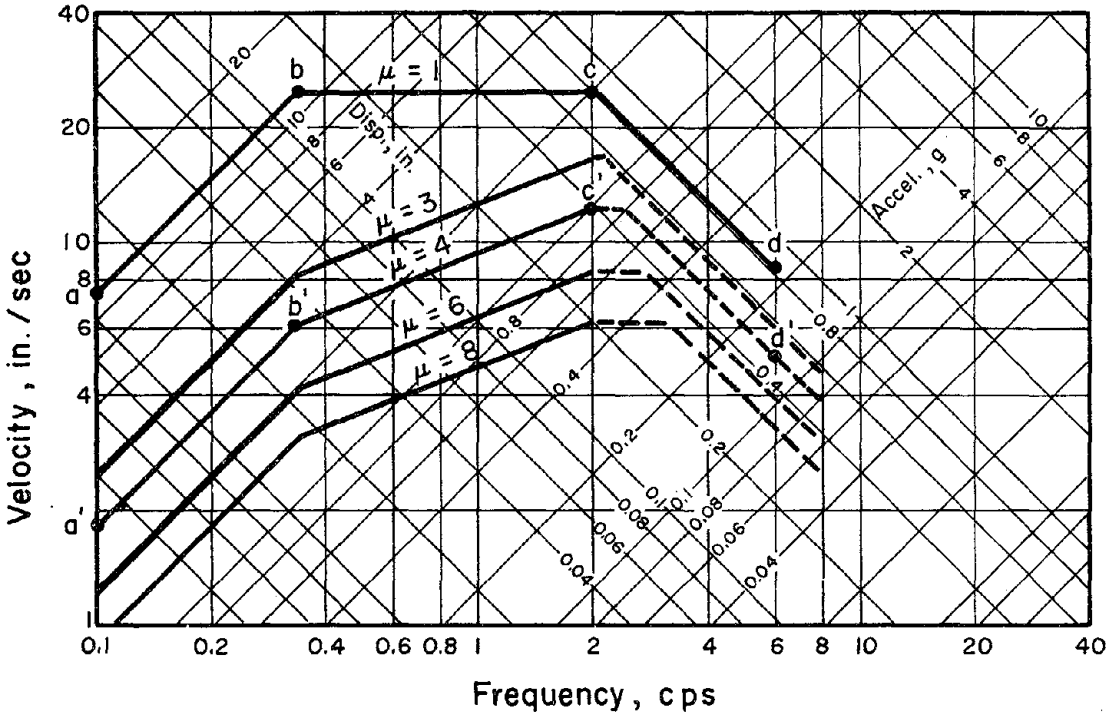

FIG. 4.8 DESIGN RESPONSE SPECTRA FOR X-BRACED SYSTEMS, EL CENTRO 1940 NS, 5 PERCENT CRITICAL DAMPING

APPENDIX A. SEISMIC DESIGN FORCES AND MODAL PROPERTIES

This appendix contains (a) in Tables A.1 and A.2, the seismic design forces used to proportion the two- and three-story building designs and (b) in Tables A.3 and A.4, the elastic frequencies of vibration and mode shapes for the building designs. The information contained in this appendix is supplementary to the data presented in Chapter 2 pertaining to the building designs considered in this study.

TABLE A.1 SEISMIC DESIGN FORCES FOR TWO-STORY BUILDINGS

Floor	w_x (k)	h_x (ft)	$w_x h_x$ (kft)	$\frac{F_x}{V}$
2	92.16	24	2212	0.5
1	184.3	12	2212	0.5
Σ	276.5		4424	1.0

TABLE A.2 SEISMIC DESIGN FORCES FOR THREE-STORY BUILDINGS

Floor	Floor Weight (k)	Cladding Weight (k)	w_x (k)	h_x (ft)	$w_x h_x$ (kft)	$\frac{F_x}{V}$
3	364	10.6	375	33	12,375	0.319
2	779	21.1	800	22	17,600	0.454
1	779	21.1	800	11	8,800	0.227
Σ			1975		38,775	1.000

TABLE A.3 NATURAL FREQUENCIES OF ELASTIC VIBRATION

(a) Two-Story Buildings

Design	2-A	2-B	2-C	2-D	2-E	2-F	2-G	2-H
f_1(cps)	2.67	1.78	1.11	1.99	1.35	2.27	1.98	2.58
f_2/f_1	2.41	2.41	2.41	2.47	2.41	2.88	2.41	2.41

(b) Three-Story Buildings

Design	3-A	3-B	3-C	3-D
f_1(cps)	1.10	1.39	1.59	2.02
f_2/f_1	2.83	3.04	2.73	2.73
f_3/f_1	4.93	6.23	3.73	3.73

TABLE A.4 ELASTIC MODE SHAPES

(a) Two-Story Buildings

Design		2-A	2-B	2-C	2-D	2-E	2-F	2-G	2-H
Mode	Story								
1	2	1.207	1.207	1.207	1.312	1.265	1.361	1.207	1.207
	1	0.854	0.854	0.854	0.714	0.787	0.569	0.854	0.854
2	2	-0.207	-0.207	-0.207	-0.312	-0.265	-0.361	-0.207	-0.207
	1	0.146	0.146	0.146	0.286	0.213	0.431	0.146	0.146

(b) Three-Story Buildings

Design		3-A	3-B	3-C	3-D
Mode	Story				
1	3	1.411	1.371	1.243	1.243
	2	0.968	0.825	1.084	1.084
	1	0.408	0.308	0.628	0.628
2	3	-0.558	-0.466	-0.333	-0.333
	2	0.226	0.391	-0.014	-0.014
	1	0.368	0.410	0.333	0.333
3	3	0.147	0.095	0.090	0.090
	2	-0.194	-0.216	-0.070	-0.070
	1	0.224	0.282	0.039	0.039

APPENDIX B. MODAL ANALYSIS AND APPROXIMATE PROCEDURES

B.1 Introduction

This appendix contains (a) a review of the mode-superposition procedure as used in conjunction with response spectra and (b) a discussion of three approximate procedures which can be used to estimate dynamic base shear. Since the modal method is well known (see for example Timoshenko, et al., 1974; Clough and Penzien, 1975), only the details pertinent to this study are repeated. The approximate procedures follow from consideration of the normal-mode method, and they have been discussed previously by Newmark and Rosenblueth (1971, pp. 468-469, 482).

B.2 Modal Method

The governing set of simultaneous differential equations of motion can be uncoupled if the normal modes of vibration are used as generalized coordinates. Each of the resulting independent differential equations can be solved as if they governed the response of single-degree-of-freedom systems. The total response can then be found by transforming back to the original set of coordinates. This procedure, known as the normal-mode method, is based on superposition and therefore strictly applies only to elastic systems. The procedure described in the following paragraphs applies to building structures founded on the ground and subjected to base motion.

The first step in the normal-mode method involves solving for the mode shapes and modal frequencies. In this study it was assumed that mass was lumped only at locations of story translation. Therefore, in order to avoid including unwanted degrees-of-freedom in the analysis, it

was convenient to find the mode shapes and frequencies using the flexibility approach. The equations of motion for free vibration using flexibility formulation are

$$[F]\lceil M\rfloor\{\ddot{v}\} + \{v\} = \{0\} \tag{B.1}$$

in which $\{v\}$ and $\lceil M\rfloor$ represent the horizontal displacements of the lumped story masses and the diagonal mass matrix, respectively. The entries to the i-th column of the flexibility matrix, [F], are the story displacements caused by a unit force applied at the i-th story. If it is assumed that each of the story masses vibrates with harmonic motion about the static equilibrium position according to the equation

$$\{v\} = \{\phi^{(n)}\} \sin(\omega_n t + \varepsilon_n) \tag{B.2}$$

then Eq. (B.1) can be reduced to the following set of algebraic equations

$$([F]\lceil M\rfloor - \frac{1}{\omega_n^2}[I])\{\phi^{(n)}\} = 0 \tag{B.3}$$

In Eq. (B.2), $\{\phi^{(n)}\}$ represents the mode shape, ω_n represents the natural circular frequency, and ε_n represents the phase angle associated with the n-th mode of vibration. In Eq. (B.3), [I] denotes the identity matrix. A nontrivial solution to the set of equations is possible only when

$$\det([F]\lceil M\rfloor - \frac{1}{\omega_n^2}[I]) = 0 \tag{B.4}$$

The natural circular frequencies of vibration are found by expanding the determinate and solving the resulting algebraic equation for the N roots $1/\omega_1^2, 1/\omega_2^2, \ldots, 1/\omega_N^2$ in which N represents the number of degrees-of-freedom. The N mode shapes are found by successively substituting the

roots into Eq. (B.3).

It can be shown that the mode shapes have the following orthogonality relationships, provided $\omega_n^2 \neq \omega_m^2$:

$$\{\phi^{(n)}\}^T \lceil M \rfloor \{\phi^{(m)}\} \begin{cases} = 0, & n \neq m \\ \neq 0, & n = m \end{cases} \tag{B.5}$$

$$\{\phi^{(n)}\}^T [S^*] \{\phi^{(m)}\} \begin{cases} = 0, & n \neq m \\ \neq 0, & n = m \end{cases} \tag{B.6}$$

in which $[S^*](= [F]^{-1})$ represents the structural stiffness matrix condensed to include only story displacements as degrees-of-freedom.

Next, the response in each mode is found. For purposes of evaluating the dynamic response in this study, it was convenient computationally to reformulate the equations of motion using the stiffness approach. If the stiffness formulation is used, the equations of motion including the effects of damping and support excitation can be written

$$\lceil M \rfloor \{\ddot{v}\} + [C]\{\dot{v}\} + [S^*]\{v\} = -\lceil M \rfloor \{1\} \ddot{x} \tag{B.7}$$

in which [C] represents the damping matrix and $\ddot{x}$ represents the ground acceleration. In Eq. (B.7), {1} denotes the unit vector. Equation (B.7) can be uncoupled into normal modes of vibration if the displacements are written in terms of the mode shapes and the generalized coordinates, q_m, as follows:

$$\{v\} = \sum_{m=1}^{N} \{v^{(m)}\} = \sum_{m=1}^{N} \{\phi^{(m)}\} q_m \tag{B.8}$$

in which $\{v^{(m)}\}$ denotes the displacement vector in the m-th mode of vibration. If Eq. (B.8) is substituted into Eq. (B.7) and the resulting expression is premultiplied by $\{\phi^{(n)}\}^T$, the equations uncouple.

In performing the algebra, the orthogonality conditions on mass and stiffness are used, and it is assumed that a corresponding orthogonality condition applies to the damping matrix. The uncoupled equation of motion obtained for the n-th mode of vibration is

$$\ddot{q}_n + 2\xi_n\omega_n\dot{q}_n + \omega_n^2 q_n = \frac{-\{\phi^{(n)}\}^T [M]\{1\}}{\{\phi^{(n)}\}^T [M]\{\phi^{(n)}\}} \ddot{x} \qquad (B.9)$$

In Eq. (B.9), ξ_n denotes the amount of critical viscous damping in the n-th mode of vibration.

The response expression for the n-th generalized coordinate can be written, using Duhamel's integral to solve Eq. (B.9), as

$$q_n = \frac{\{\phi^{(n)}\}^T [M]\{1\}}{\{\phi^{(n)}\}^T [M]\{\phi^{(n)}\}} \left(\frac{-1}{\omega_{dn}} \int_o^t \ddot{x}(\tau) e^{-\xi_n\omega_n(t-\tau)} \sin \omega_{dn} (t-\tau)\, d\tau \right) \qquad (B.10)$$

in which $\omega_{dn} = \omega_n \sqrt{1 - \xi_n^2}$. The expression in the parentheses on the right hand side of Eq. (B.10) is the same expression as would be used to calculate the displacement response of a single-degree-of-freedom system vibrating with the frequency of the n-th mode. In practice only the maximum value of the displacement is available, and it can be estimated from the response spectrum ordinate that is consistent with the given frequency of vibration and amount of damping. If the participation factor, γ_n, is defined as

$$\gamma_n = \frac{\{\phi^{(n)}\}^T [M]\{1\}}{\{\phi^{(n)}\}^T [M]\{\phi^{(n)}\}} \qquad (B.11)$$

and D_n represents the spectral displacement, then the maximum value of the n-th generalized coordinate is

$$(q_n)_{max} = \gamma_n D_n \tag{B.12}$$

By Eq. (B.8), the maximum displacements in the n-th mode are $\{v^{(n)}\}_{max} = \{\phi^{(n)}\}\gamma_n D_n$. If, for convenience, the mode shapes are normalized* so that

$$\{\tilde{\phi}^{(n)}\} = \{\phi^{(n)}\}\gamma_n \tag{B.13}$$

then the maximum displacements in the n-th mode become

$$\{v^{(n)}\}_{max} = \{\tilde{\phi}^{(n)}\}D_n \ .$$

Finally, the modal responses are combined to obtain the general solution. An upper bound to the response of the system is obtained by taking the sum of the absolute values of the modal quantities. Thus, upper bounds to the story displacements are

$$\{v\}_{max} = \sum_{n=1}^{N} |\{v^{(n)}\}_{max}| = \sum_{n=1}^{N} |\{\tilde{\phi}^{(n)}\}D_n| \tag{B.14}$$

---

* When the mode shapes are normalized in this manner, the sum of the N modal amplitudes at each mass point (degree-of-freedom) is unity, i.e., $\sum_{n=1}^{N} \{\phi^{(n)}\}\gamma_n = \sum_{n=1}^{N} \{\tilde{\phi}^{(n)}\} = \{1\}$. That this is so can be shown by calculating the participation factor required such that $\sum_{m=1}^{N} \{\phi^{(m)}\}\gamma_m = \{1\}$. If the expression $\sum_{m=1}^{N} \{\phi^{(m)}\}\gamma_m = \{1\}$ is premultiplied by $\{\phi^{(n)}\}^T[M]$ and modal orthogonality is used, $\{\phi^{(n)}\}^T[M]\{\phi^{(n)}\}\gamma_n = \{\phi^{(n)}\}^T[M]\{1\}$ results. If the resulting expression is solved for γ_n, Eq. (B.11) is obtained.

Since the maximum modal responses do not in general occur at the same time, the probable response of the system is often estimated by taking the square root of the sum of the squares of the modal quantities. Thus, the probable story displacements are

$$\{v\}_{prob} = \sqrt{\sum_{n=1}^{N} (\{v^{(n)}\}_{max})^2} = \sqrt{\sum_{n=1}^{N} (\{\hat{\phi}^{(n)}\}D_n)^2} \qquad (B.15)$$

The accelerations, inertial forces, and story shears in each mode can be obtained from the usual relationships between these quantities and the modal displacements. The maximum and probable accelerations, inertial forces, and story shears can then be obtained by combining the modes in the fashion described above for displacements.

B.3 Modal Damping

In using the modal method as described in the previous section, it is not necessary to evaluate the entries to the damping matrix. However, when using time-history calculations the damping coefficients are usually related to some percentage of critical viscous damping in each mode of vibration. In order for the damping coefficients to be related to the damping in the normal modes, the damped equations of motion must uncouple into normal modes of vibration. This requires the damping matrix to have orthogonality properties.

If it is assumed that the damping matrix is linearly proportional to the mass matrix, i.e.,

$$[C] = b[M] \qquad (B.16)$$

where b is a constant, the equations uncouple. Once b has been set, the

percentage of critical viscous damping in the n-th mode is calculated from

$$\xi_n = \frac{b}{2\omega_n} \tag{B.17}$$

When damping is prescribed in this manner, the lower modes are damped more strongly than the higher modes.

B.4 Bounds on Base Shear

The computation of lateral design forces is often split into two parts: the calculation of the base shear and the distribution of the base shear over the building height. Three bounds to the base shear may be obtained which can be justified in terms of the modal superposition procedure.

A lower bound is obtained by computing the base shear associated with the first mode. In equation form, the base shear is

$$V \geq A_1 \sum_{i=1}^{N} \tilde{\phi}_i^{(1)} m_i \tag{B.18}$$

in which m_i and A_1 refer to the lumped mass of the i-th story and the spectral acceleration in the first mode. The symbol $\tilde{\phi}_i^{(1)}$ denotes the normalized amplitude of the first mode shape at the i-th story.

Building codes recommend the base shear be calculated by multiplying the mass of the building by a coefficient that is equivalent to the spectral acceleration in the first mode. According to studies referred to by Newmark and Rosenblueth (1971), the building code approach slightly overestimates the base shear of multistory buildings when compared to the square root of the sum of the squares method of combining modal quantities, provided the ordinates of the response spectrum do not exceed those

corresponding to a constant pseudovelocity. Thus, an upper bound may be obtained from

$$V \leq A_1 \sum_{i=1}^{N} m_i \tag{B.19}$$

Equations (B.18) and (B.19) yield the same result if $\{\overset{\gamma}{\phi}^{(1)}\}^T = \{1 \quad 1 \ldots 1\}$.

An upper bound of some interest may be defined for shear-beam systems. This bound was not specifically considered in this study. The base shear is less than or equal to the first story stiffness times the spectral displacement corresponding to a single-degree-of-freedom system having the same frequency as the fundamental frequency of the system. In equation form

$$V \leq k\, D_1 \tag{B.20}$$

in which k represents the first story stiffness. Equation (B.20) is an upper bound provided the spectral displacement in the first mode is larger than the spectral displacement in any of the higher modes.*

---

* This may be shown as follows. By Eq. (B.14), $V \leq k \sum_{n=1}^{N} |\overset{\gamma}{\phi}_1{}^{(n)} D_n|$. Noting $\overset{\gamma}{\phi}_1{}^{(n)}$ are positive for all n and therefore $\sum_{n=1}^{N} |\overset{\gamma}{\phi}^{(n)}| = 1$, it follows that $V \leq k \max_n D_n$. Thus, Eq. (B.20) is true provided $D_1 \geq D_n$, $n \neq 1$.

APPENDIX C. ELEMENT STIFFNESS PROPERTIES

C.1 Introduction

In the analysis of buildings of the types considered in this report, nonlinearities arise from two sources. The first source of nonlinearity is caused by the inelastic behavior of the structural material, and this source is referred to as material nonlinearity. The second source of nonlinearity, referred to as geometric nonlinearity, arises when the deformations are large and changes in the geometry of the structure must be accounted for in the analysis. Consequently, it is convenient to separate the formulation of the stiffness properties into the formulation of material stiffness and geometric stiffness.

In this appendix member stiffness matrices to be used in establishing the structural stiffness matrix are derived. Element stiffness properties are formulated to account for (a) material nonlinearities resulting from the yielding of beams, columns, and X-braces and (b) geometric nonlinearities due to gravity loads acting on columns. The material stiffness for beam and column members is derived from consideration of a beam made up of an elastic flexural portion with rigid-plastic hinges at the ends. The material stiffness for X-braced frames represents the behavior of lateral bracing which resists only tensile forces. To account for geometric nonlinearities due to gravity loads acting on columns (P-delta effects), it is assumed that column and X-brace members support rigid, pin-ended, bar segments (false members) subjected to axial load.

The relationship between member end forces, $\{G\}$, and end displacements, $\{U\}$, can be written (Przemieniecki, 1968, pp. 383-384)

$$\{\Delta G\} = ([S_E] - [S_G])\{\Delta U\} \qquad (C.1)$$

in which $[S_E]$ and $[S_G]$ represent the material and geometric stiffnesses, respectively. The minus sign before the geometric stiffness is used in this study to account for the fact that P-delta effects tend to reduce the element stiffness. Since the material element stiffness changes as a function of the member force-displacement history, Eq. (C.1) is valid only for small changes in displacement and must be written in incremental form. A Greek delta prefix to a symbol indicates an incremental value.

C.2 Flexural Element Material Stiffness

In formulating the flexural element material stiffness, it is convenient to first establish the stiffness of a beam element which is constrained in such a way that all rigid body degrees-of-freedom are eliminated. The constrained stiffness is obtained from consideration of the slope-deflection equations for a simply supported beam, modified to take inelastic behavior into account. The complete or unconstrained stiffness is then established from the constrained stiffness by using a transformation of coordinates. When the beam member is unconstrained, rigid body displacements that do not induce strains in the beam element are possible and the corresponding stiffness matrix is singular.

The simply supported beam element shown in Fig. C.1 is made up of an elastic flexural portion with inelastic hinges at either end. If it is assumed that prior to yielding the hinges at either end are rigid, and after yielding they sustain the plastic moment capacity of the member (or reduced plastic moment capacity in the case of columns), four states of yield can be defined:

State one, the moment capacity at either end is not exceeded.

State two, the moment capacity at the left end is reached, the right end remaining elastic.

State three, the moment capacity at the right end is reached, the left end remaining elastic.

State four, the moment capacity is reached at both ends.

From consideration of the slope-deflection equations, Giberson (1969) has demonstrated that the relationship between total end rotations, $\{u\}$, and end moments, $\{g\}$, can be written in incremental form as

$$\begin{Bmatrix} \Delta g_1 \\ \Delta g_2 \end{Bmatrix} = \begin{bmatrix} k_A & k_B \\ k_B & k_C \end{bmatrix} \begin{Bmatrix} \Delta u_1 \\ \Delta u_2 \end{Bmatrix} \tag{C.2}$$

in which k_A, k_B and k_C are stiffness coefficients that depend on the state of yield. The relationship between inelastic hinge rotations, $\{\alpha\}$, and the total end rotations can be written in incremental form as

$$\{\Delta\alpha\} = [T_1]\{\Delta u\} \tag{C.3}$$

in which $[T_1]$ is a transformation matrix that also depends on the state of yield. The values of k_A, k_B and k_C and the entries to $[T_1]$ are recorded in Table C.1 for the four states of yield described above. In Fig. C.1 and Table C.1, E and I denote the modulus of elasticity and the moment of inertia of the section.

In the unconstrained coordinate system, the beam element shown in Fig. C.2 is capable of rigid body motions. The end displacements in the unconstrained coordinate system, $\{U\}$, can be related to the end rotations in the constrained coordinate system by consideration of the geometry of

the beam element under deformation. Thus

$$\{u\} = [T_2]\{U\} \tag{C.4}$$

in which

$$[T_2] = \begin{bmatrix} -1/L & 1 & 1/L & 0 \\ -1/L & 0 & 1/L & 1 \end{bmatrix} \tag{C.5}$$

If the principle of contragradience is used, the unconstrained element forces, $\{G_E\}$, can be found from

$$\{G_E\} = [T_2]^T \{g\} \tag{C.6}$$

If Eqs. (C.2) and (C.4) are substituted into Eq. (C.6) and incremental notation is used where appropriate, the following expression can be obtained for the element forces:

$$\{\Delta G_E\} = [S_E]\{\Delta U\} \tag{C.7}$$

in which the complete element material stiffness is

$$[S_E] = [T_2]^T \begin{bmatrix} k_A & k_B \\ k_B & k_C \end{bmatrix} [T_2] \tag{C.8}$$

The incremental hinge rotations can be obtained from the unconstrained displacements by writing Eq. (C.4) in incremental form and substituting into Eq. (C.3). Thus

$$\{\Delta\alpha\} = [T_1][T_2]\{\Delta U\} \tag{C.9}$$

C.3 X-brace Material Stiffness

The material stiffness for the X-brace subassemblage shown in Fig. C.3(a) is obtained by analogy to the derivation used in the previous section for the flexural element.

The stiffness in the constrained coordinate system is established from consideration of the story shear-deformation relationship for the tension brace in the subassemblage. In establishing the constrained stiffness, it is assumed that the tension brace is elastic, the compression brace resists no lateral load, and the gravity loads acting on the columns can be ignored. From consideration of equilibrium, Fig. C.3(b), Hooke's Law and compatibility, Fig. C.3(c), the horizontal story shear resisted is

$$Q = \frac{AE}{L_b}\left(\frac{L}{L_b}\right)^2 u \qquad \text{(C.10)}$$

In Eq. (C.10), A denotes the cross-sectional area of the brace and u represents the relative story displacement.

The story shear resisted by an X-brace subassemblage depends on the cyclic load history. If it is assumed that the resistance-deformation relationship described in Section 3.2.2 (see Fig. 3.2) applies, then, for displacement in the positive direction, the story shear resisted can be calculated from the following expressions:

$$u \geq u_{ps},\ u - u_{ps} - u_y < 0 \qquad Q = \frac{AE}{L_b}\left(\frac{L}{L_b}\right)^2 (u - u_{ps}) \qquad \text{(C.11a)}$$

$$u \geq u_{ps},\ u - u_{ps} - u_y \geq 0 \qquad Q = AF_y\left(\frac{L}{L_b}\right) \qquad \text{(C.11b)}$$

$$u < u_{ps} \qquad Q = 0 \qquad \text{(C.11c)}$$

in which $u_y \left(= \frac{F_y L_b}{E}\left[\frac{L_b}{L}\right]\right)$ represents the initial yield displacement and F_y denotes the yield stress of steel. The permanent set in the positive direction, u_{ps}, is equal to the maximum positive displacement minus the elastic recovery during the previous excursion into the inelastic range.

The use of Eq. (C.11) to calculate the hysteretic response of an X-brace subassemblage is illustrated by the examples shown in Fig. C.4. Conditionals similar to those listed above can be written for negative displacements.

Equations (C.11) can be written more conveniently in the incremental form

$$\Delta Q = k \cdot \Delta u \tag{C.12}$$

in which k is the constrained stiffness. Two states of yield can then be defined:

State one, the force resisted changes according to the elastic stiffness, $k = \frac{AE}{L_b}\left(\frac{L}{L_b}\right)^2$.

State two, the change in force resisted in zero, i.e., $k = 0$.

The complete or unconstrained element stiffness matrix is obtained from the constrained element stiffness by a transformation of coordinates. The relative story displacement can be calculated from the displacement in the unconstrained coordinate system, $\{U\}$, by using the transformation

$$u = \{-1 \quad 1\}\{U\} \tag{C.13}$$

If the contragredient relationship for forces is used, the X-brace material stiffness in the unconstrained coordinate system can be formulated. Thus

$$[S_E] = \begin{bmatrix} k & -k \\ -k & k \end{bmatrix} \tag{C.14}$$

C.4 Geometric Stiffness

A linear approximation of the flexural element geometric stiffness can be obtained from consideration of the physical model shown in Fig. C.5

(Clough and Penzien, 1975, pp. 167-169). The model is made of a rigid bar segment subjected to axial force N and a stabilizing flexural element. As the flexural element deflects, the rigid bar also deflects developing forces which must be resisted by the flexural element. If it is assumed that the centerlines of the bar and the flexural element coincide, summation of moments about the top and bottom ends of the rigid bar leads to the additional (shear) forces acting on the ends of the flexural element. In matrix form, the end forces due to geometric effects are

$$\{G_G\} = [S_G]\{U\} \tag{C.15}$$

in which the geometric stiffness is

$$[S_G] = \begin{bmatrix} N/h & 0 & -N/h & 0 \\ 0 & 0 & 0 & 0 \\ -N/h & 0 & N/h & 0 \\ 0 & 0 & 0 & 0 \end{bmatrix} \tag{C.16}$$

The X-brace element geometric stiffness can be obtained in a similar manner. From consideration of equilibrium of the subassemblage shown in Fig. C.3(a) under deformation, the geometric stiffness is

$$[S_G] = \begin{bmatrix} N/h & -N/h \\ -N/h & N/h \end{bmatrix} \tag{C.17}$$

in which N represents the sum of the axial loads acting on the columns of the subassemblage.

If the axial forces are positive (compressive), the geometric stiffness tends to reduce the member stiffness. Thus, the lateral story shear that can be resisted for a given relative story displacement under monotonically increasing load is reduced from that which would be resisted if gravity

loads were not present.

It should be commented that, in the derivation of the geometric element stiffnesses, it is assumed that the axial loads acting are constant. Thus, the axial forces are assumed to arise from sources that are independent of the seismic excitation.

Buildings are frequently designed so that not all columns in a story contribute to the resistance of lateral load. The P-delta forces arising from gravity loads acting on columns that do not contribute to lateral load resistance are transferred to the seismic load resisting frames by diaphragm action. The axial loads used to formulate geometric stiffness matrices must take this transfer of P-delta forces into account.

TABLE C.1 ENTRIES TO THE BEAM ELEMENT MATERIAL STIFFNESS MATRIX AND TO THE TRANSFORMATION MATRIX USED TO OBTAIN THE INELASTIC HINGE ROTATIONS

State of yield	k_A	k_B	k_C	$[T_1]$
1	$\frac{4EI}{L}$	$\frac{2EI}{L}$	$\frac{4EI}{L}$	$\begin{bmatrix} 0 & 0 \\ 0 & 0 \end{bmatrix}$
2	0	0	$\frac{3EI}{L}$	$\begin{bmatrix} 1 & 1/2 \\ 0 & 0 \end{bmatrix}$
3	$\frac{3EI}{L}$	0	0	$\begin{bmatrix} 0 & 0 \\ 1/2 & 1 \end{bmatrix}$
4	0	0	0	$\begin{bmatrix} 1 & 0 \\ 0 & 1 \end{bmatrix}$

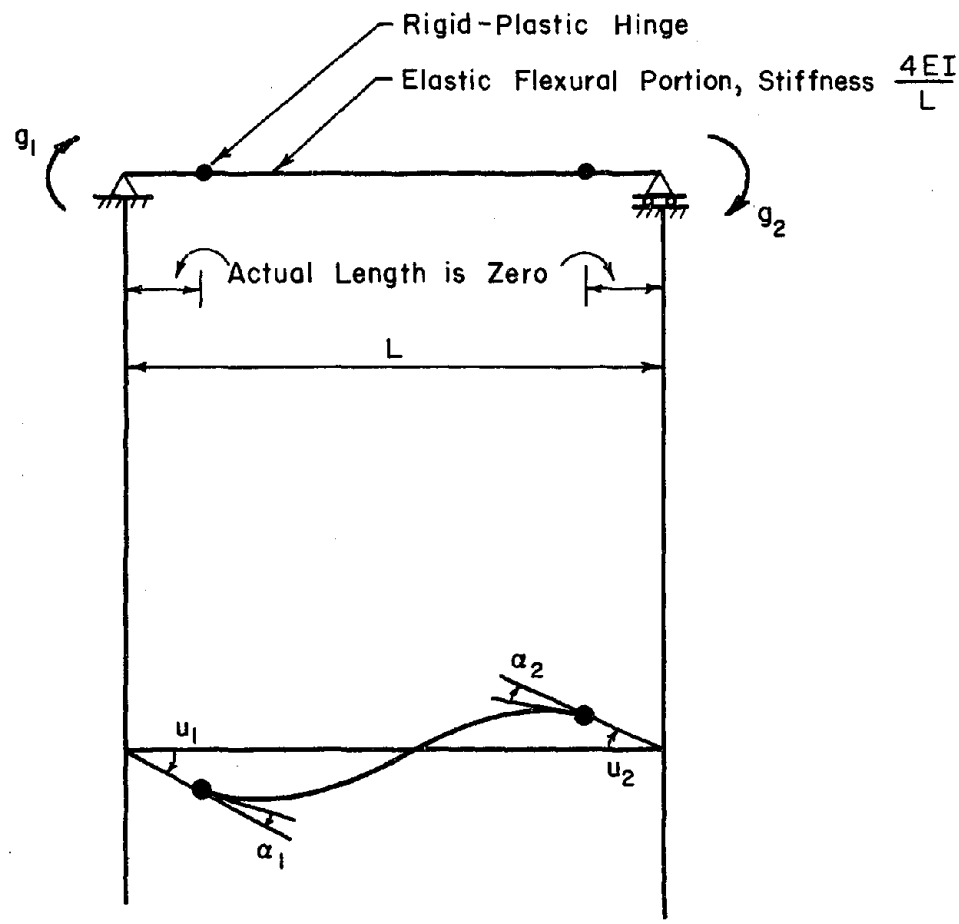

FIG. C.1 SIMPLY SUPPORTED BEAM ELEMENT

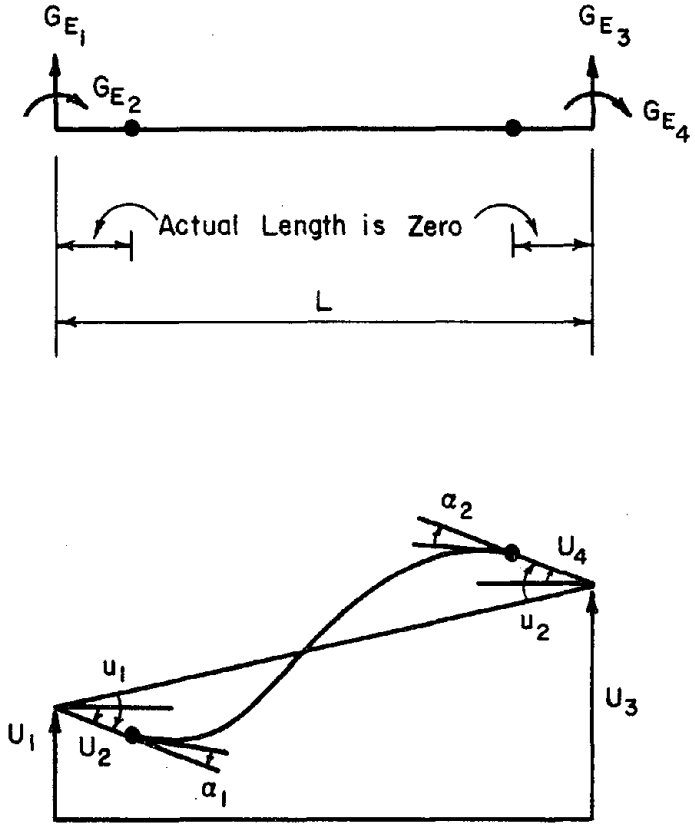

FIG. C.2 TRANSFORMATION OF COORDINATES

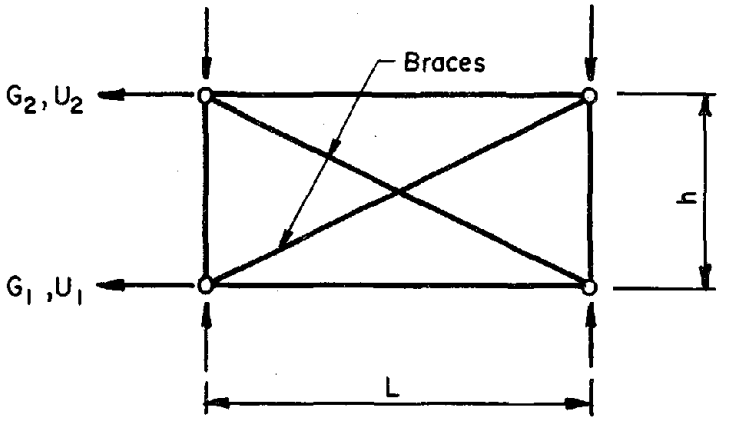

All Horizontal Beams And Vertical Columns Are Assumed To Be Rigid Links

(a) X — Brace Subassemblage

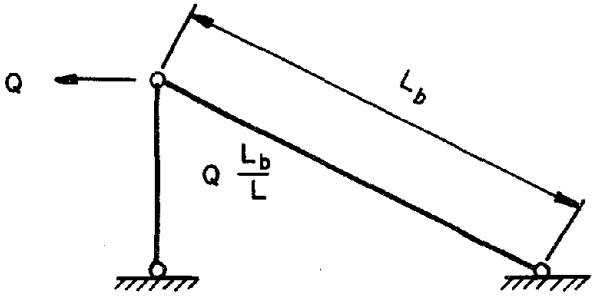

(b) Force In Tension Brace, Gravity Loads Ignored

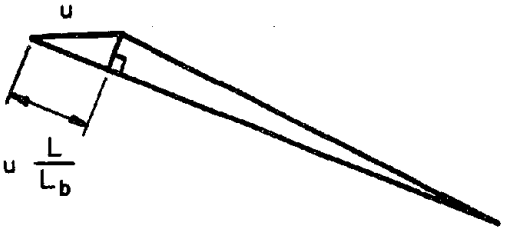

(c) Compatibility Of Displacements

FIG. C.3 X-BRACE ELEMENT

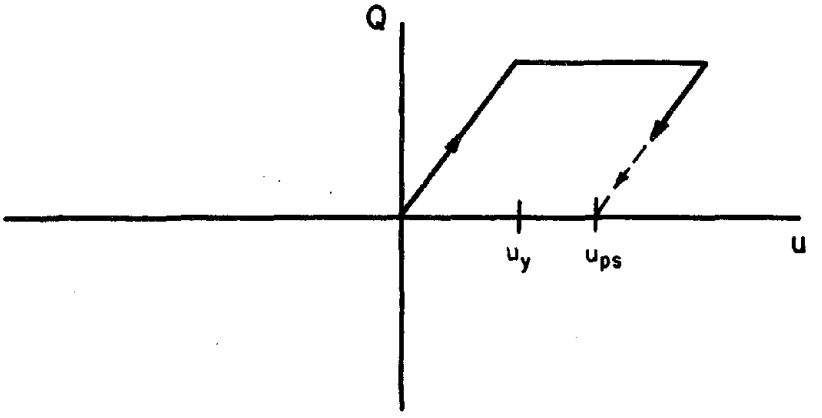

(a) $u \geq u_{ps}$, $u - u_{ps} - u_y < 0$

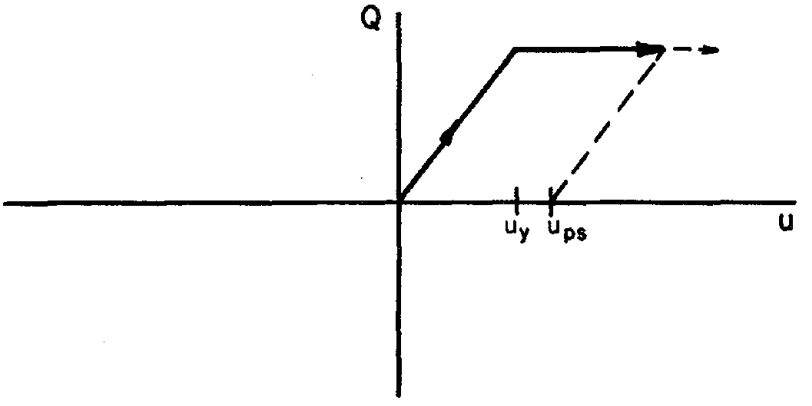

(b) $u \geq u_{ps}$, $u - u_{ps} - u_y \geq 0$

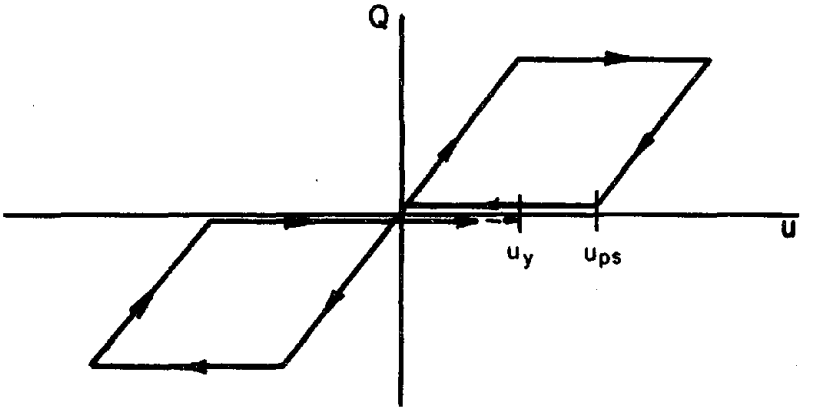

(c) $u < u_{ps}$

FIG. C.4 X-BRACE ELEMENT STORY SHEAR-DISPLACEMENT RELATIONSHIP

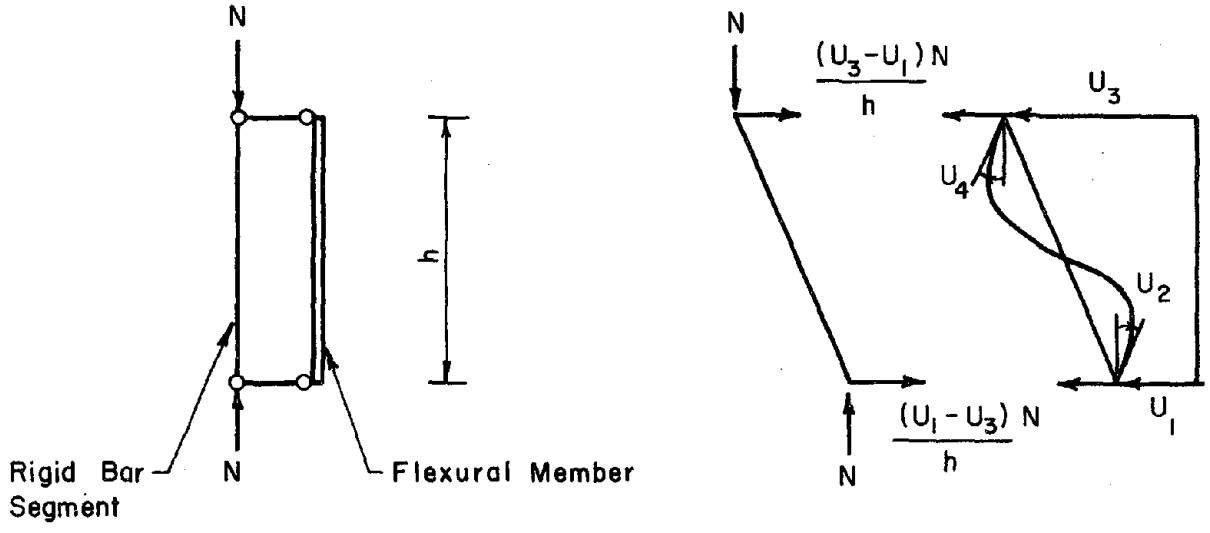

(a) Physical Model

(b) Free Body Diagram in The Deformed Configuration

FIG. C.5 PHYSICAL MODEL USED TO OBTAIN THE FLEXURAL ELEMENT GEOMETRIC STIFFNESS

APPENDIX D. INCREMENTAL NUMERICAL PROCEDURE

D.1 Introduction

This appendix contains a discussion of the step-by-step numerical integration (time-history) procedure used to solve the equations that govern the dynamic response of low-rise steel buildings. In the step-by-step procedure, the response history is divided into a number of small increments in time. The response during each increment in time is evaluated using the structural properties applicable at the beginning of the time increment. The dynamic response quantities calculated at the end of one time increment become the initial conditions for the next time increment. At the end of each time increment, the structural stiffness matrix is adjusted to account for any changes in the element stiffnesses due to yielding or hardening. Thus, the solution advances in a step-by-step manner in the time domain for a series of linear systems with changing stiffness properties.

Unless certain precautions are taken when the stiffness properties are not constant during a time increment, some error is involved in using the step-by-step numerical integration procedure. If the stiffness changes during a time increment, the forces that can actually be resisted by some members are different from the member forces calculated using the stiffness properties applicable at the beginning of the time increment. In an effort to minimize this disparity between the forces that can be resisted and the calculated forces, an iterative technique analogous to the initial stress procedure that is sometimes applied to static problems is used. Of course, it is only necessary to use the iterative procedure at the

end of time increments in which the stiffness has changed.

D.2 Equations of Motion

In order to facilitate the solution of the simultaneous differential equations of motion using the step-by-step numerical integration procedure, the equations of motion are converted into a set of simultaneous algebraic equations. This is accomplished by assuming that the structural displacements, velocities, and accelerations can be simply related to each other over small time increments.

The simultaneous differential equations of motion, assembled in incremental form, can be written as follows:

$$\begin{bmatrix} \lceil M \rfloor & \cdot \\ \cdot & \cdot \end{bmatrix} \begin{Bmatrix} \Delta\ddot{v}(t) \\ \cdot \end{Bmatrix} + \begin{bmatrix} [C] & \cdot \\ \cdot & \cdot \end{bmatrix} \begin{Bmatrix} \Delta\dot{v}(t) \\ \cdot \end{Bmatrix}$$

$$+ [S(t)] \begin{Bmatrix} \Delta v(t) \\ \Delta\theta(t) \end{Bmatrix} = - \begin{bmatrix} \lceil M \rfloor & \cdot \\ \cdot & \cdot \end{bmatrix} \{1\}\Delta\ddot{x}(t) + \{R(t)\} \qquad (D.1)$$

in which $\lceil M \rfloor$ represents the diagonal mass matrix,

$[C]$ represents the damping matrix,

$[S(t)]$ represents the tangent stiffness at time t,

$\{R(t)\}$ represents the residual load vector at time t (see Section D.3),

$\{v\}$ represents the story displacement vector,

$\{\theta\}$ represents the nodal rotation vector,

$\{1\}$ represents the unit vector,

and $\ddot{x}$ represents the ground acceleration.

A Greek delta prefix to a symbol indicates an incremental value. A superscript dot above a symbol indicates one differentiation with respect

to time. The incremental displacement quantities are associated with the time at the beginning of the time increment, t.

In order to convert Eq. (D.1) into a set of simultaneous equations, a linear variation of acceleration over a short time interval Δt is assumed. If the equations of Newmark (1959) with $\beta = 1/6$ and $\gamma = 1/2$ are used, the incremental story velocities and displacements can be written as follows:

$$\{\Delta\dot{v}(t)\} = \Delta t\{\ddot{v}(t)\} + \frac{\Delta t}{2}\{\Delta\ddot{v}(t)\} \tag{D.2}$$

$$\{\Delta v(t)\} = \Delta t\{\dot{v}(t)\} + \frac{(\Delta t)^2}{2}\{\ddot{v}(t)\} + \frac{(\Delta t)^2}{6}\{\Delta\ddot{v}(t)\} \tag{D.3}$$

At time t the velocity vector, $\{\dot{v}(t)\}$, and the acceleration vector, $\{\ddot{v}(t)\}$, are known quantities. If the incremental displacement vector is taken as the basic unknown quantity, Eqs. (D.2) and (D.3) can be solved to obtain the following expressions for the incremental velocity and acceleration vectors:

$$\{\Delta\dot{v}(t)\} = \frac{3}{\Delta t}\{\Delta v(t)\} - 3\{\dot{v}(t)\} - \frac{\Delta t}{2}\{\ddot{v}(t)\} \tag{D.4}$$

$$\{\Delta\ddot{v}(t)\} = \frac{6}{(\Delta t)^2}\{\Delta v(t)\} - \frac{6}{\Delta t}\{\dot{v}(t)\} - 3\{\ddot{v}(t)\} \tag{D.5}$$

If Eqs. (D.4) and (D.5) are substituted into Eq. (D.1) and the resulting expression is simplified, the following set of simultaneous algebraic equations is obtained

$$[A(t)]\begin{Bmatrix}\Delta v(t)\\ \\ \Delta\theta(t)\end{Bmatrix} = \{B(t)\} \tag{D.6}$$

in which

$$[A(t)] = [S(t)] + \frac{6}{(\Delta t)^2}\begin{bmatrix} [M] & \cdot \\ \cdot & \cdot \end{bmatrix} + \frac{3}{\Delta t}\begin{bmatrix} [C] & \cdot \\ \cdot & \cdot \end{bmatrix} \tag{D.7}$$

$$\{B(t)\} = \begin{bmatrix} [M] & \cdot \\ \cdot & \cdot \end{bmatrix}\left\langle \frac{6}{\Delta t}\begin{Bmatrix} \dot{v}(t) \\ \cdot \end{Bmatrix} + 3\begin{Bmatrix} \ddot{v}(t) \\ \cdot \end{Bmatrix} - \{1\}\Delta\ddot{x}(t)\right\rangle$$

$$+ \begin{bmatrix} [C] & \cdot \\ \cdot & \cdot \end{bmatrix}\left\langle 3\begin{Bmatrix} \dot{v}(t) \\ \cdot \end{Bmatrix} + \frac{\Delta t}{2}\begin{Bmatrix} \ddot{v}(t) \\ \cdot \end{Bmatrix}\right\rangle + \{R(t)\} \tag{D.8}$$

Equation (D.6) has the same form as the standard static stiffness equations and it can be solved for the incremental story displacements and rotations by Gaussian elimination. The incremental velocities and accelerations can then be found by substituting the incremental story displacements in Eqs. (D.4) and (D.5).

The structural story displacements, joint rotations, and so forth at the end of the time increment are equal to the response quantities at the beginning of the time increment plus the changes in the response quantities calculated using Eq. (D.6) and Eqs. (D.4) and (D.5). Thus

$$\begin{Bmatrix} v(t+\Delta t) \\ \theta(t+\Delta t) \end{Bmatrix} = \begin{Bmatrix} v(t) \\ \theta(t) \end{Bmatrix} + \begin{Bmatrix} \Delta v(t) \\ \Delta\theta(t) \end{Bmatrix} \tag{D.9}$$

$$\{\dot{v}(t+\Delta t)\} = \{\dot{v}(t)\} + \{\Delta\dot{v}(t)\} \tag{D.10}$$

$$\{\ddot{v}(t+\Delta t)\} = \{\ddot{v}(t)\} + \{\Delta\ddot{v}(t)\} \tag{D.11}$$

The solution procedure progresses in a step-by-step manner with the values at time $(t + \Delta t)$ calculated by Eqs. (D.9), (D.10) and (D.11) becoming the the known values at time t for the next time increment.

D.3 Initial Stress Procedure

Using the initial stress procedure (Zienkiewicz, 1971, pp. 372-373), a nonlinear problem is solved as a succession of linear problems, the nonlinearities being accounted for by additional or residual loading terms in the nodal equilibrium equations. Thus, when yielding (or hardening) occurs during a time increment, the structural stiffness changes and $[S(t)] \begin{Bmatrix} \Delta v(t) \\ \Delta\theta(t) \end{Bmatrix}$ in Eqs. (D.1) and (D.6) should be replaced by (Aktan, et al., 1974)

$$\{\Delta F(t)\} = [S(t)]\begin{Bmatrix} \Delta v(t) \\ \\ \Delta\theta(t) \end{Bmatrix} - \{\Delta P(t)\} \tag{D.12}$$

in which $\{\Delta F(t)\}$ represents the actual incremental resisting forces due to structural stiffness and $\{\Delta P(t)\}$ represents the residual forces. Incremental structural displacements and residual forces between times t and $(t + \Delta t)$ are

$$\begin{Bmatrix} \Delta v(t) \\ \Delta\theta(t) \end{Bmatrix} = \begin{Bmatrix} \Delta v(t) \\ \Delta\theta(t) \end{Bmatrix}^{o} + \begin{Bmatrix} \Delta v(t) \\ \Delta\theta(t) \end{Bmatrix}^{1} + \cdots\cdots + \begin{Bmatrix} \Delta v(t) \\ \Delta\theta(t) \end{Bmatrix}^{n} \tag{D.13}$$

$$\{\Delta P(t)\} = \{\Delta P(t)\}^{o} + \{\Delta P(t)\}^{1} + \cdots\cdots + \{\Delta P(t)\}^{n} \tag{D.14}$$

The corrections to the incremental displacements are found iteratively from

$$\left.\begin{aligned} [A(t)] \begin{Bmatrix} \Delta v(t) \\ \\ \Delta\theta(t) \end{Bmatrix}^{o} &= \{B(t)\} \\ [A(t)] \begin{Bmatrix} \Delta v(t) \\ \\ \Delta\theta(t) \end{Bmatrix}^{1} &= \{\Delta P(t)\}^{o} \\ &\vdots \\ [A(t)] \begin{Bmatrix} \Delta v(t) \\ \\ \Delta\theta(t) \end{Bmatrix}^{n} &= \{\Delta P(t)\}^{n-1} \end{aligned}\right\} \tag{D.15}$$

The tangent stiffness applicable at the beginning of the time increment is used for all cycles of iteration.

The incremental residual forces are obtained successively from consideration of the member force-deformation relationships. For the i-th iteration, the residual forces $\{\Delta P(t)\}^{i-1}$ to be applied as joint loads are assembled from the forces required to bring the member forces based on the tangent stiffness solution (the calculated forces) into coincidence with the actual forces that the members can resist under the displacements reached in the (i-1)-th iteration. The force vector $\{\Delta P(t)\}^{i-1}$ can be physically interpreted as the unbalanced residual forces left on the structure at the end of the (i-1)-th iteration.

Iteration is continued for a specified number of cycles or until $\{\Delta P(t)\}^{n}$ are smaller than a specified tolerance. Since iteration is carried out only to a tolerance, the residual forces $\{\Delta P(t)\}^{n}$ found for the last iteration cycle are added as the residual load vector, $\{R(t)\}$, during the next time increment. Before going on to the next increment in time, the structural stiffness matrix is updated to account for any changes in element stiffnesses that have occurred.

D.4 Member Residual Forces and Special Considerations

D.4.1 Member Residual Forces -- In order to formulate the residual load vectors for use in the initial stress procedure described in Section D.3, it is necessary to obtain the actual forces that can be resisted by the members under specified displacements. For X-brace elements, once the member relative displacements are known, the actual member forces can be determined from the member force-deformation relationships (Eq.(C.11)

and Fig. 3.2). The member residual forces are simply equal to the differences between the forces calculated using the tangent stiffness and the actual member forces.

No unique relationship between moment and rotation exists for flexural elements: the moment at one end of a flexural element is affected by the moment at the other end and vice versa. After each iteration of the initial stress procedure, the calculated flexural element end moments are adjusted such that the moment capacities at either end are not exceeded. An adjustment at one end is accompanied by an adjustment at the other end according to the carry-over factor applicable to the given state of yield. The carry-over factors are 1/2 for elastic far ends and 0 for inelastic far ends. The residual end moments are found from the differences between the calculated and adjusted end moments. The residual end moments may be physically interpreted as the moments to be applied to the elastic inner portion of the flexural element (of stiffness 4EI/L) in the actual deformed shape such that the actual deformed shape and the deformed shape assumed using the tangent stiffness become the same (see Fig. D.1).

The unbalanced residual forces for X-brace elements and the unbalanced residual end moments for beam elements are liquidated using the initial stress procedure.

An inelastic hinge at either end of a flexural member is free to rotate in only one direction during each excursion into the inelastic range, and if the direction of rotation changes the member becomes elastic. If it is found that a beam has unloaded (become elastic) at either end during a time increment, a special procedure is used. Rather than calculate unbalanced forces and use the iterative procedure

described in the previous section, it is convenient to return to the beginning of the time increment, modify the structural stiffness, and repeat calculations.

D.4.2 Special Considerations -- The accuracy of the numerical procedure described above depends on the size of the time increment used in calculations. Since the times when the response is evaluated do not in general correspond to the exact times of yielding or maximum deformation, certain errors can result. Melin (1976) has estimated the magnitude of these errors from studies on single-degree-of-freedom elastoplastic systems. If yielding occurs during a time increment, he concludes that the resulting errors are small provided the time increment is 1/20 to 1/40 of the elastic period of vibration. In these estimates it was assumed that the force-deformation relationship was satisfied at the end of the time increment using an iterative procedure. Melin has estimated the largest probable error in the calculation of maximum deformation to be less than 1 percent or 0.3 percent if the time increment is 1/20 or 1/40, respectively, of the elastic period of vibration.

For this study the time increment used was less than or equal to 1/20 of the elastic period of the highest mode of vibration. The earthquake base motion was assumed to be a piecewise linear function between times of known ground acceleration. In order to avoid missing abrupt changes in loading, the response was evaluated at each discontinuity in the slope of the ground acceleration history. Computations were carried out for the duration of the base motion plus a time of twice the fundamental elastic period of vibration.

D.5 Verification of the Analytical Procedures

The intent of this section is to verify the computational procedures described above by comparison of the results of some simple response calculations to the published results of other investigators. The simple structures studied were subjected to the half-cycle displacement pulse base motion shown in Fig. E.3. The structures were undamped.

The first group of studies was confined to systems composed of flexural elements with the inelastic properties described in Section C.2. The one story frame shown in Fig. D.2 has an elastoplastic resistance deformation relationship when subjected to lateral load. Its behavior during dynamic motion can be compared directly to that of an elastoplastic single-degree-of-freedom system. In Fig. D.2 the maximum displacements for a number of systems are shown as a function of the frequency parameter ft_1 where f is the elastic frequency of vibration and t_1 is a measure of the pulse duration. For both elastic and inelastic systems, the response calculated was for all practical purposes the same as that found by Veletsos and Vann (1971) for elastoplastic single-degree-of-freedom systems subjected to the same base motion.

Similarly, a flexural element under shear deflection with no end rotations has an elastoplastic force-deformation relationship. The maximum displacements of two-story shear systems are plotted in Fig. D.3 as a function of the frequency parameter f_1t_1 in which the symbol f_1 denotes the fundamental frequency of elastic vibration. The response was almost exactly the same as that found by Veletsos and Vann (1971) for elastoplastic two-degree-of-freedom systems. (There were slight discrepancies for the maximum inelastic responses of the first stories between frequency

parameters 0.2 and 0.3, see Fig. D.3(a). These discrepancies cannot be accounted for, but they may be due to the scale of plotting.)

The results of studies on X-braced single story frames with the resistance-deformation relationship described in Section C.3 are shown in Fig. D.4. Again the plots are in terms of the frequency parameter ft_1. The maximum deformations calculated by the procedures described in this appendix were for all practical purposes the same as those found by Veletsos (1969) for the same base motion.

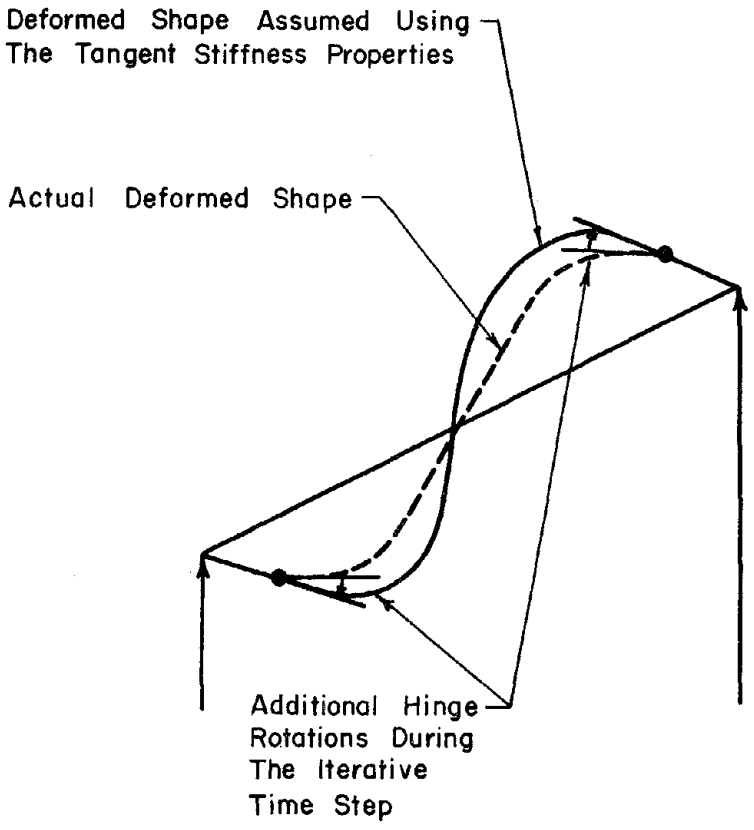

FIG. D.1 ADDITIONAL INELASTIC HINGE ROTATIONS DURING THE INITIAL STRESS PROCEDURE

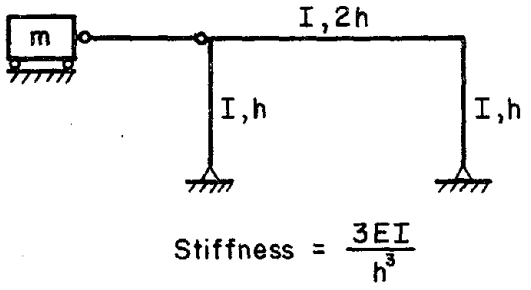

$$\text{Stiffness} = \frac{3EI}{h^3}$$

Structural Idealization

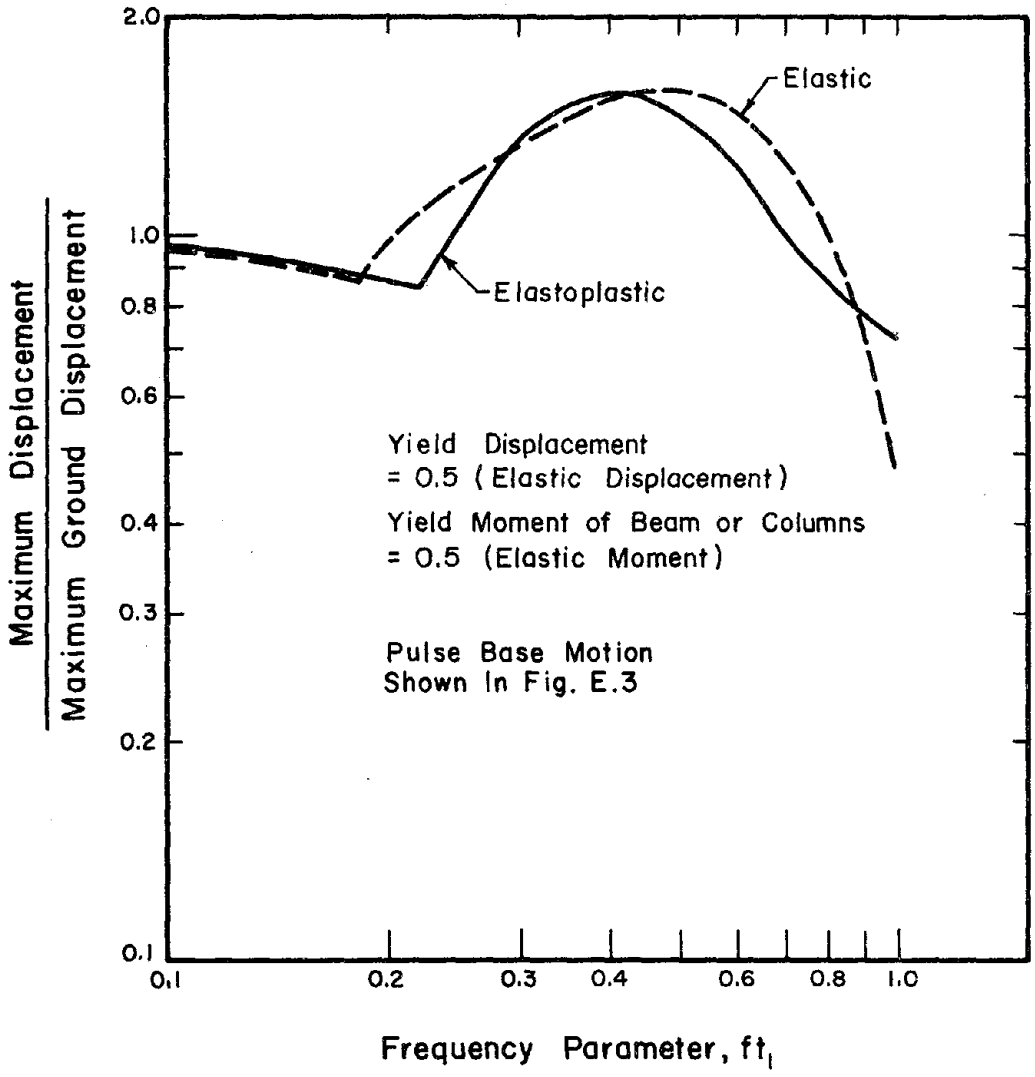

FIG. D.2 MAXIMUM RESPONSE OF SINGLE-DEGREE-OF-FREEDOM MOMENT FRAMES, PULSE BASE MOTION

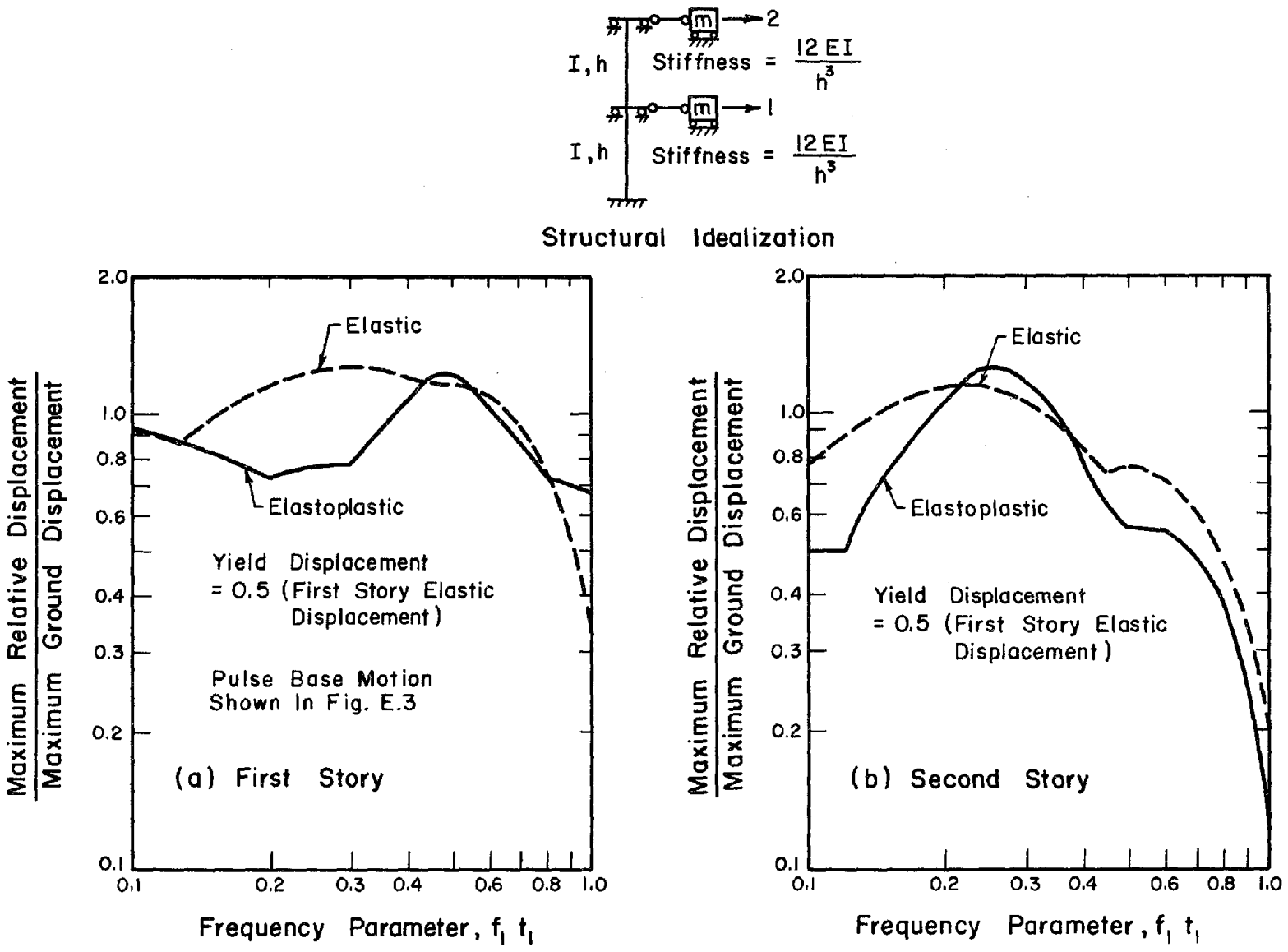

FIG. D.3 MAXIMUM RESPONSE OF TWO-DEGREE-OF-FREEDOM SHEAR SYSTEMS, PULSE BASE MOTION

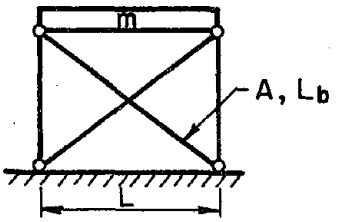

Stiffness = $\frac{AE}{L_b}\left(\frac{L}{L_b}\right)^2$

Structural Idealization

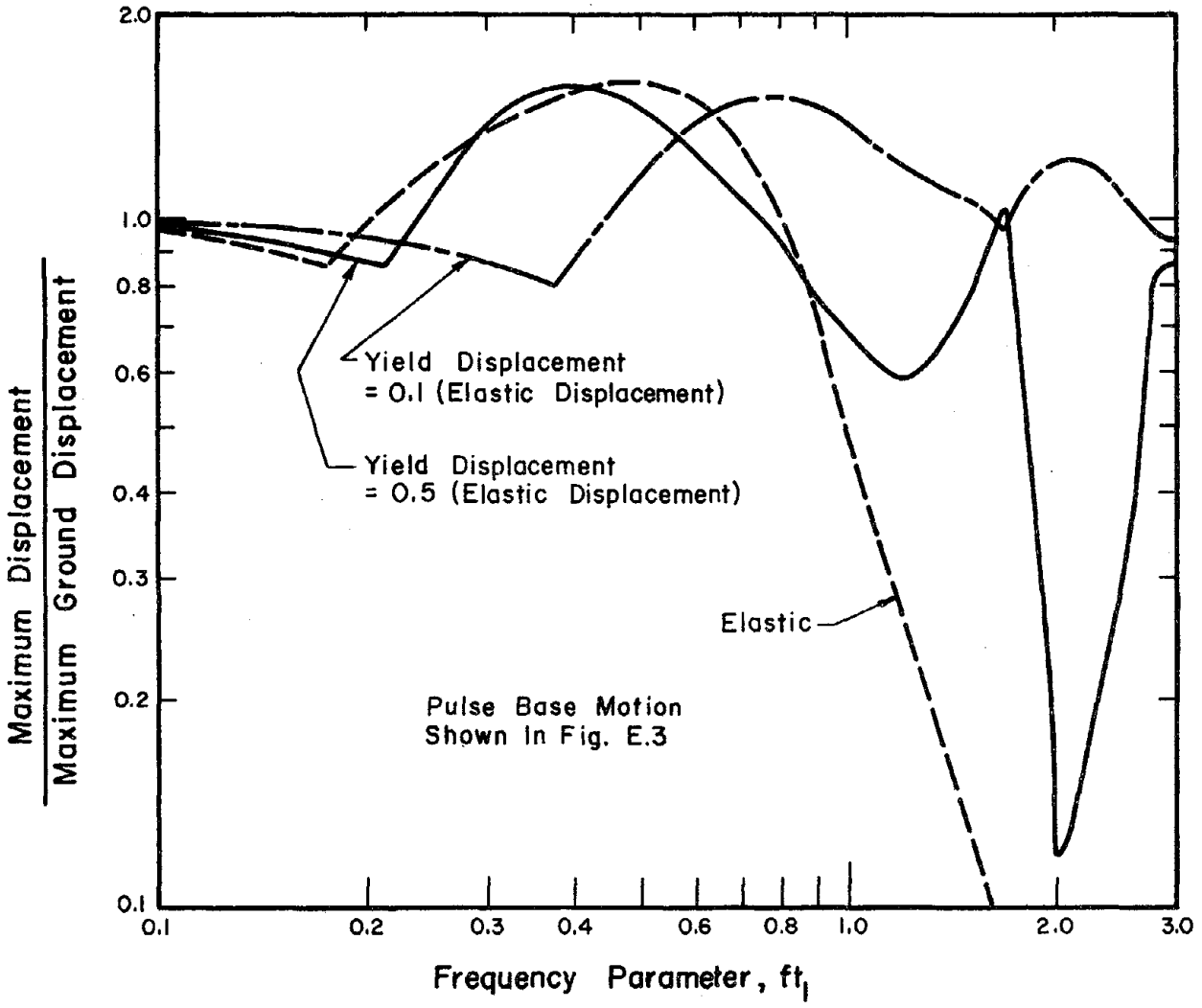

FIG. D.4 MAXIMUM RESPONSE OF SINGLE-DEGREE-OF-FREEDOM X-BRACED FRAMES, PULSE BASE MOTION

APPENDIX E. THEORETICAL STUDIES OF SIMPLE SYSTEMS

E.1 Introduction

In this chapter the results of calculations on elastoplastic two-degree-of-freedom systems subjected to pulse type base motion are summarized. The objectives of this special study were (a) to evaluate the modal procedure when applied to systems with nonuniform inelasticity, (b) to find the appropriate procedure for combining modes when applying the modal method to systems with a few degrees-of-freedom, and (c) to examine certain approximate procedures which might be used to estimate the design base shear.

The approach used in the study was to compare the results of modal method and approximate calculations to time-history solutions. The studies in part parallel earlier work by Newmark, et al. (1965), Veletsos and Vann (1971), and others. However, in this study either the base motion considered, the systems studied, or the modal and approximate procedures used for estimating inelastic response were in some way different from those used in the previous studies. It is important that such studies be pursued because the results of investigations on simple systems provide a theoretical basis on which to view the more complicated behavior of two- and three-story buildings subjected to earthquake base motion.

E.2 Systems and Base Motion Considered

Systems. The mathematical idealization for the two-degree-of-freedom systems studied is shown in Fig. E.1. The symbols f_n and $\{\tilde{\phi}^{(n)}\}$ denote the frequency and the normalized mode shape for the n-th mode of small amplitude (elastic) vibration. Mass, m, and elastic stiffness, k,

are uniform for each degree-of-freedom, and the systems are undamped.

The resistance-deformation relationship for each spring was assumed to be elastoplastic with equal yield resistances in both directions of displacement. After yielding occurred, unloading was assumed to follow a curve offset from, but parallel to, the original elastic curve. The resistance-deformation curve for the i-th spring is presented in Fig. E.2. The symbols Q_i and u_i denote the spring force and the relative displacement, respectively. The subscript "o" indicates the maximum displacement or force observed if the spring remains elastic during base motion. The ductility, μ_i, is calculated by dividing the maximum inelastic displacement, $(u_i)_m$, by the elastic component of the displacement at yield, $(u_i)_y$. The symbol $(Q_i)_y$ denotes the maximum elastoplastic spring force.

Base Motion. The half-cycle displacement pulse base motion considered is shown in Fig. E.3. The symbol t_1 denotes the duration of one-half of the base motion.

Single-Degree-of-Freedom Response Spectra. The response spectra for elastoplastic single-degree-of-freedom systems subjected to the pulse base motion are plotted in Fig. E.4. Each curve in Fig. E.4 gives the yield displacement, u_y, required to limit the maximum deformation of the spring, u_m, to a specified value of the ductility factor, μ. The spectra are plotted in terms of the quantity V_y, defined as $V_y = \omega u_y$ in which $\omega(=2\pi f)$ represents the circular frequency of elastic vibration. In some of the literature V_y is referred to as the pseudovelocity for yielding systems. The spectral values are normalized by the maximum ground velocity, v, and they are plotted in terms of the dimensionless frequency parameter ft_1 where f is the frequency of elastic vibration and t_1 is a measure of the

pulse duration. The response spectra shown in Fig. E.4 are essentially the same as those determined by Veletsos and Vann (1971) for the same base motion.

In discussing the results of the modal method and approximate calculations later in Section E.4, it is convenient to refer to the different frequency ranges of the elastic single-degree-of-freedom response spectrum, $\mu = 1$ in Fig. E.4. The transition between the moderately low and the medium frequency ranges occurs at a frequency parameter of about $ft_1 = 0.55$ (point b), and the transition between the medium and the moderately high frequency ranges occurs at a frequency parameter of about $ft_1 = 0.75$ (point c). The transition frequencies adopted in this appendix are similar to those reported by Veletsos and Vann (1971).

E.3 Time-History Calculations

It is the objective of this section to generate numerical data which can be compared to the modal and approximate calculations reported in the following section.

Method of Analysis. The time-history calculations were made using Newmark's β-Method in the well known iterative form, with $\beta = 1/6$ and $\gamma = 1/2$ (Newmark, 1959). The increment in time used for the numerical integration procedure was less than or equal to 1/20 of the elastic period of the highest mode of vibration. The response was evaluated at the end of each time increment and at the times of each discontinuity in the slope of the base acceleration history. Computations were carried out for the duration of the base motion plus a time of twice the fundamental period of elastic vibration.

One Spring Permitted to Yield. The calculated response of the two-degree-of-freedom systems where one of the springs could yield is shown in Figs. E.5 and E.6. In each case the response was determined for a number of discrete values of the dimensionless frequency parameter $f_1 t_1$ (recall that f_1 denotes the fundamental frequency of elastic vibration of a given system, and t_1 is a measure of the pulse duration). In the figures, the maximum elastic component of the response was plotted in terms of the quantity $(V_i)_o$ if the spring responded elastically, or the quantity $(V_i)_y$ if the spring responded inelastically. The quantities $(V_i)_o$ and $(V_i)_y$ are defined as $(V_i)_o = \omega_1 (u_i)_o$ and $(V_i)_y = \omega_1 (u_i)_y$ in which $\omega_1 (=2\pi f_1)$ denotes the fundamental circular frequency of elastic vibration. The displacements $(u_i)_o$ and $(u_i)_y$ are defined in Fig. E.2. It should be appreciated that the computed quantities were $(u_i)_o$ or $(u_i)_m$ where the ductility, μ_i, is given by $\mu_i = (u_1)_m / (u_i)_y$. The plots are normalized by the maximum ground velocity, v.

The response of systems for which the base spring was elastoplastic and the second spring remained elastic is given in Fig. E.5. Each curve in Fig. E.5(a) gives the yield displacement of the base spring, $(u_1)_y$, required to limit the maximum deformation of the base spring, $(u_1)_m$, to a specified ductility, μ_1. Each curve in Fig. E.5(b) gives the maximum elastic deformation of the second spring, $(u_2)_o$, under the condition that the base spring responds with the specified ductility, μ_1. The abscissa of both plots is the dimensionless frequency parameter $f_1 t_1$.

The plots in Fig. E.5 can be interpreted in the following manner. For a given value of the dimensionless frequency parameter, the quantity $(V_1)_y$ required to limit the maximum deformation of the base spring to a ductility of μ_1 can be obtained from Fig. E.5(a). For the same value of

the dimensionless frequency parameter, the quantity $(V_2)_o$ measuring the maximum elastic response of the second spring under the condition that the base spring responds with the selected base spring ductility, μ_1, can be obtained from Fig. E.5(b). The yield displacement of the base spring and the maximum elastic displacement of the second spring can then be found from the relations $(u_1) = (V_1)_y/\omega_1$ and $(u_2)_o = (V_2)_o/\omega_1$, respectively. Finally, the maximum displacement of the elastoplastic base spring can be calculated from the relation $(u_1)_m = \mu_1(u_1)_y$. Of course, the use of these plots implies that the yield displacement of the elastic second spring, if it exists, is greater than $(u_2)_o$.

Similar charts are presented in Fig. E.6 for systems in which the base spring remained elastic and the second spring was elastoplastic. Each curve in Fig. E.6(a) gives the maximum elastic deformation of the base spring, $(u_1)_o$, under the condition that the second spring responds with a specified ductility, μ_2. Each curve in Fig. E.6(b) gives the yield displacement of the second spring, $(u_2)_y$, required to limit the maximum deformation of the second spring, $(u_2)_m$, to a specified ductility, μ_2.

On the basis of the studies just described the following observations concerning the inelastic response of simple two-degree-of-freedom systems can be made. If the base spring is permitted to yield (Fig. E.5), the response of the second spring is reduced significantly, even if it remains elastic. Conversely, if the second spring is permitted to yield (Fig. E.6), the elastic response of the first spring is reduced only slightly from the response that would occur if both springs remained elastic.

It should be noted that a graphical interpolation procedure was used to construct Figs. E.4 through E.6, and the plots may contain slight inaccuracies.

Both Springs Permitted to Yield. The calculated response of two-degree-of-freedom systems where both springs could yield is shown in Fig. E.7 for systems with a frequency parameter of $f_1 t_1 = 1.0$. The graph can be used in the following manner. The maximum deformations of the springs assuming that both springs of the system respond elastically to the pulse base motion are obtained first. The maximum elastic deformations, $(u_1)_o$ and $(u_2)_o$, are given in the upper right corner of the figure. The desired design ductilities for the first and second springs of the system, μ_1 and μ_2, are selected. A point on the graph is located corresponding to the selected ductilities, noting that μ_1 is the abscissa and μ_2 is the ordinate of the plot. The quantities c_1 and c_2 corresponding to the selected ductilities can then be determined from the point on the plot by interpolation between the lines of constant c_1 and c_2. In order for the system to achieve the desired ductilities during the pulse base motion, the yield resistances of the springs must be $(u_1)_y = c_1(u_1)_o$ and $(u_2)_y = c_2(u_2)_o$. The maximum deformations of the first and second springs will then be $(u_1)_m = \mu_1(u_1)_y$ and $(u_2)_m = \mu_2(u_2)_y$.

The chart shown in Fig. E.7 demonstrates that the response of even simple systems to pulse base motion is a complicated function of the system parameters, especially when yielding is involved. Of course, figures similar to Fig. E.7 could be constructed for systems with other frequency parameters.

E.4 Modal and Approximate Calculations

It is the objective of this section to evaluate (a) the modal method for calculating spring forces and deformations, (b) the use of the first

mode base spring force as an approximation to the actual force, and (c) the quasi-static building code approach for estimating the base spring force. The approach used was to compare response quantities obtained by the three procedures to the quantities obtained in the previous section using time-history analysis. In the discussion that follows, the maximum displacement observed in the i-th spring during time-history calculations is denoted by $(u_i)_o$ if the spring remained elastic and $(u_i)_m = \mu_i (u_i)_y$ if the spring yielded. The maximum time-history spring force in the i-th spring is denoted by $(Q_i)_o = k(u_i)_o$ if the spring remained elastic and $(Q_i)_y = k(u_i)_y$ if the spring yielded.

A detailed discussion of the modal method and the approximate procedures is given in Appendix B. The discussion in Appendix B is applicable to elastic systems.

Modal Method. A summary of the modal method as used for inelastic response calculations in this appendix is as follows:

(1) Obtain the frequencies and mode shapes of elastic vibration for the given system.

(2) Select the inelastic design response spectrum that gives the elastic component of the displacement response for the desired elastoplastic ductility. (In some publications this spectrum is referred to as the inelastic maximum acceleration or yield displacement spectrum.) For the studies recorded in this section, the spectral quantities were obtained from Fig. E.4.

(3) Calculate the yield (maximum) spring forces and the yield displacements using the modal method in conjunction with the inelastic design response spectrum (as described in Appendix B for elastic systems).

(4) Multiply the yield level displacements by the design ductility factor to obtain the maximum spring deformations.

The yield (maximum) force and the maximum deformation obtained in the i-th spring are denoted by $(Q_i)_{max}$ and $(u_i)_{max}$ if the modal quantities were obtained by the sum of the absolute values of the modal quantities approach. They are denoted by $(Q_i)_{prob}$ and $(u_i)_{prob}$ if the modal quantities were combined by the square root of the sum of the squares of the modal quantities approach.

It is well to point out one inconsistency in the modal method as described above when applied to systems with nonuniform inelasticity. In particular, consider a two-degree-of-freedom system proportioned so that inelastic response occurs only in one spring. If the modal calculations conform to the ductility of the inelastic spring, the response quantities obtained for the elastic spring are inconsistent.

First Mode Approximation. The base spring force in the first mode of vibration is denoted by $(Q_1)_{1st}$. The spectral ordinates used for calculations were obtained from Fig. E.4.

Building Code Approach. In the quasi-static building code approach, the force in the base spring is approximated by multiplying the total mass of the building by the spectral acceleration, obtained from Fig. E.4, in the first mode of vibration. The building code base force is denoted by $(Q_1)_{code}$.

Both Springs Elastic. The results of calculations for the case where both springs responded elastically to the pulse base motion are presented in Table E.1. As would be expected, the sum of the absolute values of the modal quantities procedure for combining modes gave forces, $(Q_1)_{max}$ and $(Q_2)_{max}$, and deformations, $(u_1)_{max}$ and $(u_2)_{max}$, that were close to

the time-history values over a wide range of frequency parameters.* The square root of the sum of the squares of the modal quantities approach also gave forces, $(Q_1)_{prob}$ and $(Q_2)_{prob}$, and deformations, $(u_1)_{prob}$ and $(u_2)_{prob}$, that were close to the time-history response; however, in the low frequency region this procedure slightly underestimated the time-history response.

In the medium and high frequency ranges, the base spring forces in the first mode, $(Q_1)_{1st}$, were almost the same as the time-history forces. Consequently, it can be assumed that the response was primarily in the first mode in these frequency ranges.

The building code method of calculating the base spring force, $(Q_1)_{code}$, gave good estimates of the time-history spring forces in the medium and high frequency ranges.

Base Spring Permitted to Yield while Second Spring Remained Elastic. The results of calculations for the case where the base spring responded with a ductility of 3 and the second spring responded elastically are presented in Table E.2. The modal and approximate calculations were performed using the response spectrum for $\mu = 3$ shown in Fig. E.4 for both modes of vibration. Modal analysis gave results that were reasonably close to, although in general slightly under, the time-history values for the base spring forces, $(Q_1)_{max}$ and $(Q_1)_{prob}$, and base deformations, $(u_1)_{max}$ and $(u_1)_{prob}$. In the medium and high frequency ranges, the base spring forces in the first mode, $(Q_1)_{1st}$, were almost the same as the time-history values. For the medium and high frequency systems, the base spring forces estimated by the building code approximation, $(Q_1)_{code}$, were within 10

---

* The different frequency ranges of the elastic single-degree-of-freedom response spectrum are defined in Section E.2.

percent of the forces obtained by time-history analysis.

Unfortunately, the elastic second spring forces calculated by the modal method, $(Q_2)_{max}$ and $(Q_2)_{prob}$, were significantly less than the time-history values. On the other hand, the elastic deformations calculated by the modal method, $(u_2)_{max}$ and $(u_2)_{prob}$, were much larger than the time-history values. Therefore, it can be observed that the modal method, as used in this study, provided very poor estimates of the response quantities for the elastic second spring.

Example. As an example of the procedure used to obtain the entries to Table E.2, consider the following calculations for a system with m = 1.0 k-sec^2/in. and k = 103.4 k/in. For this system

f_1 = 1.0 cps $\qquad$ ω_1 = 6.283 rad/sec

f_2 = 2.618 cps $\qquad$ ω_2 = 16.45 rad/sec

Assume that the duration of one-half of the pulse base motion is t_1 = 1.0 sec and the maximum ground velocity is v = 10 in./sec. The spectral yield displacements and accelerations obtained from Fig. E.4 for elastoplastic systems with a ductility of μ = 3 are

$D_1 = 0.86(10 \text{ in./sec})/(6.283 \text{ rad/sec}) = 1.37 \text{ in.}$ $\quad A_1 = 54.1 \text{ in./sec}^2$

$D_2 = 0.25(10 \text{ in./sec})/(16.45 \text{ rad/sec}) = 0.152 \text{ in.}$ $\quad A_2 = 41.1 \text{ in./sec}^2$

in which D_1 and D_2 represent the values of u_y for the first and second modes of vibration, and $A_1 = \omega_1^2 D_1$ and $A_2 = \omega_2^2 D_2$.

The inelastic response quantities can be estimated by means of the modal method using the following procedure.

Mass Number, i	0	1	2
(a) mode shapes, $\tilde{\phi}_i^{(n)}$			
(1)		0.724	1.171
(2)		0.276	-0.171
(b) modal forces, $\tilde{\phi}_i^{(n)}$ m_i A_n, k			
(1)		39.2	63.3
(2)		11.3	-7.03

(c) modal shears, k				
(1)	103		63.3	
(2)	4.27		-7.03	
$(Q_i)_{max}$	107		70.3	
$(Q_i)_{prob}$	103		63.7	
(d) modal absolute yield displacements, $\phi_i^{(n)} D_n$, in.				
(1)		0.992		1.60
(2)		0.0420		-0.0260
(e) modal relative yield displacements, in.				
(1)	0.992		0.608	
(2)	0.0420		-0.0680	
$(u_i)_{max/\mu}$	1.03		0.676	
$(u_i)_{prob/\mu}$	0.993		0.612	
(f) total relative displacements, in.				
$(u_i)_{max}$	3.09		2.03	
$(u_i)_{prob}$	2.98		1.84	

Also, the base spring force can be estimated using the first mode approximation and the quasi-static building approach. In the building code approach, the base spring force is calculated from the expression $(Q_1)_{code} = A_1 \sum_{i=1}^{N} m_i$ where m_i is the lumped mass at the i-th degree-of-freedom and N is the number of degrees-of-freedom. Thus

$$(Q_1)_{1st} = 103 \text{ k}$$

$$(Q_1)_{code} = (54.1 \text{ in./sec}^2)(1.0 \text{ k-sec}^2/\text{in.} + 1.0 \text{ k-sec}^2/\text{in.})$$
$$= 108 \text{ k}$$

The time-history response values are obtained from Fig. E.5(a) and (b) for the spectra where $\mu_1 = 3$. Thus, $(u_1)_y = 0.70(10 \text{ in./sec})/(6.283 \text{ rad/sec}) = 1.11$ in., $(u_1)_m = 3(1.11 \text{ in.}) = 3.33$ in. and $(u_2)_o = 0.53(10 \text{ in./sec})/(6.283 \text{ rad/sec}) = 0.844$ in. Also, $(Q_1)_y = (103.4 \text{ k/in.})(1.11 \text{ in.}) = 115$ k and $(Q_2)_o = (103.4 \text{ k/in.})(0.844 \text{ in.}) = 87.3$ k.

The entries to Table E.2 can now be obtained by normalizing the response quantities calculated above using the modal method and the approximate procedures by the corresponding time-history response quantities.

Second Spring Permitted to Yield while First Spring Remained Elastic. In Table E.3 comparisons are presented for the case where the base spring responded elastically and the second spring responded with a ductility of 3. The modal method and approximate calculations were performed using the response spectrum for $\mu = 3$ in Fig. E.4. For all frequency ranges, the modal method and approximate procedures gave estimates of the elastic base spring forces, $(Q_1)_{max}$, $(Q_1)_{prob}$, $(Q_1)_{1st}$ and $(Q_1)_{code}$ that were significantly under the time-history values. The elastic base spring deformations, $(u_1)_{max}$ and $(u_1)_{prob}$, were in general overestimated by the modal calculations. In short, the estimates of the response quantities for the elastic base spring were poor.

Further, for most frequencies even the inelastic second spring forces, $(Q_2)_{max}$ and $(Q_2)_{prob}$, and the inelastic second spring deformations, $(u_2)_{max}$ and $(u_2)_{prob}$, were underestimated by the modal method calculations.

Both Springs Permitted to Yield. The comparisons are extended in Table E.4 to the case where both springs responded with a ductility of 3. Once again the modal and approximate calculations were performed using the response spectrum for $\mu = 3$ in Fig. E.4. In all cases, it can be observed that the modal and approximate calculations gave response values that were quite close to the time-history values.

Summary. From the studies on two-degree-of-freedom elastoplastic systems subjected to pulse base motion, the following observations can be made:

(1) Good estimates of the response quantities were obtained using the modal method in conjunction with response spectra for elastic systems. And for elastic systems the sum of the absolute values of the modal

quantities procedure was the most appropriate method to use to combine modes.

(2) For systems with fundamental frequencies of elastic vibration in the medium and high frequency ranges of the elastic response spectrum, the elastic response was primarily in the first mode. Consequently, the quasi-static building code approach gave good estimates of the elastic base spring force for such cases.

(3) Provided yielding was concentrated in the base spring, the modal method used in conjunction with inelastic response spectra gave reasonable estimates of the response quantities for the base spring. The response quantities in the elastic second spring were poorly predicted.

(4) Provided yielding was concentrated in the base spring, and provided the fundamental frequencies of elastic vibration of the systems fell in the medium and high frequency ranges of the elastic response spectrum, the inelastic base spring forces were predicted with reasonable accuracy using the building code approach.

(5) If yielding was concentrated in the second spring, all response quantities were poorly predicted using the modal method and approximate calculations.

(6) For the one special case studied where both springs could yield and both springs responded with the same ductility, the response quantities predicted by the modal method, by the first mode approximation, and by the building code approach were nearly the same as the time-history response quantities.

E.5 Design Applications

It is the objective of this section to discuss the application of some of the knowledge gained from the study of simple elastoplastic multi-degree-of-freedom systems to the design of low-rise steel buildings.

In order to facilitate comparisons, it is necessary to define some of the dynamic characteristics of low-rise steel buildings of the types considered in this study. The fundamental frequencies of elastic vibration of two- or three-story low-rise steel buildings are often in the range of about 1 to 8 cps. Thus, the frequencies fall in the medium or high frequency ranges of elastic design response spectra for earthquake base motion. The yield story shear capacities of low-rise steel buildings often are reasonably uniform over the heights of the structures, and the comments to follow pertain in general to this type of building.

In interpreting the theoretical studies in the light of practical applications, it is necessary to focus on the behavior of the two-degree-of-freedom simple systems in the medium and high frequency ranges when subjected to the pulse base motion. For frequency parameters in these frequency ranges, i.e., $f_1 t_1 > 0.6$, it can be seen from Fig. E.5 that the quantity $(V_1)_y$ is nearly equal to or is larger than the quantity $(V_2)_o$. This implies that, if the yield resistances of the base spring and the second spring are about equal, yielding will likely be concentrated in the base spring.

Also pertinent to this discussion are the findings of Veletsos and Vann (1971) who studied simple, uniform, elastoplastic, shear-beam systems of a few degrees-of-freedom subjected to pulse and earthquake base motion. In their studies all springs of the systems were permitted to yield.

They found that, except for a relatively narrow portion of the low frequency region of the elastic response spectrum, the maximum elastic deformation of the base spring was significantly greater than the elastic deformations in the upper portions of the system. Further, in the high frequency range and a portion of the medium frequency range, the elastic response was primarily in the first mode, with the maximum deformations of the individual springs being reached, for all practical purposes, simultaneously. Consequently, when the systems were allowed to yield, the maximum deformation occurred in a spring other than the base spring only for systems with a small ductility and only for systems with a fundamental elastic frequency of vibration in a relatively small portion of the low frequency range. Thus, in the frequency ranges of interest for low-rise buildings, the maximum deformations occurred in the base spring.

From consideration of simple systems subjected to pulse and earthquake base motion generally, it appears unlikely that a building will respond with uniform inelasticity during earthquake ground motion. In fact, the studies referred to above strongly imply that the maximum inelastic deformations will often occur in the base story. This suggests developing a design criterion for certain types of low-rise buildings which assumes the base story is the critical link in the seismic load resisting system.

In the frequency ranges of interest for low-rise steel buildings, the results of the studies recorded in this appendix indicate that the modal method or the quasi-static building code approach can be used to estimate response quantities.

TABLE E.1 COMPARISON BETWEEN MODAL AND TIME-HISTORY CALCULATIONS, BOTH SPRINGS ELASTIC

$f_1 t_1$	$(Q_1)_{max}/(Q_1)_o$	$(Q_1)_{prob}/(Q_1)_o$	$(Q_1)_{1st}/(Q_1)_o$	$(Q_1)_{code}/(Q_1)_o$	$(Q_2)_{max}/(Q_2)_o$	$(Q_2)_{prob}/(Q_2)_o$
	$(u_1)_{max}/(u_1)_o$	$(u_1)_{prob}/(u_1)_o$			$(u_2)_{max}/(u_2)_o$	$(u_2)_{prob}/(u_2)_o$
0.1	1.15	0.85	0.77	0.81	1.26	0.90
0.2	1.01	0.73	0.62	0.65	1.01	0.74
0.3	1.01	0.80	0.77	0.81	1.01	0.72
0.4	1.02	0.93	0.93	0.98	1.06	0.86
0.6	1.01	0.99	0.98	1.04	1.03	0.96
0.8	1.01	0.98	0.98	1.03	1.02	0.94
1.0	1.02	0.99	0.99	1.04	1.13	1.05
1.4	1.02	0.98	0.98	1.03	1.19	1.07
2.0	1.03	0.99	0.99	1.05	1.16	1.05
3.0	1.03	0.97	0.96	1.02	1.26	1.10

TABLE E.2 COMPARISON BETWEEN MODAL AND TIME-HISTORY CALCULATIONS, BASE SPRING ELASTOPLASTIC*

$f_1 t_1$	$(Q_1)_{max}/(Q_1)_y$	$(Q_1)_{prob}/(Q_1)_y$	$(Q_1)_{1st}/(Q_1)_y$	$(Q_1)_{code}/(Q_1)_y$	$(Q_2)_{max}/(Q_2)_o$	$(Q_2)_{prob}/(Q_2)_o$	$(u_2)_{max}/(u_2)_o$	$(U_2)_{prob}/(U_2)_o$
	$(u_1)_{max}/(u_1)_m$	$(u_1)_{prob}/(u_1)_m$						
0.1	0.99	0.78	0.74	0.79	0.78	0.56	2.34	1.68
0.2	1.39	1.00	0.81	0.85	0.79	0.59	2.37	1.77
0.3	1.23	0.91	0.79	0.84	0.65	0.47	1.95	1.41
0.4	0.94	0.82	0.81	0.86	0.49	0.38	1.47	1.14
0.6	0.90	0.86	0.86	0.90	0.51	0.45	1.53	1.35
0.8	0.91	0.88	0.88	0.93	0.53	0.49	1.59	1.47
1.0	0.93	0.90	0.90	0.94	0.81	0.73	2.41	2.18
1.4	0.97	0.92	0.92	0.97	0.81	0.72	2.43	2.16
2.0	1.08	1.01	1.01	1.07	1.13	0.97	3.39	2.91
3.0	0.99	0.93	0.93	0.98	1.02	0.88	3.06	2.64

* For the time-history calculations, the ductility of the base spring was 3 and the second spring was elastic.

TABLE E.3 COMPARISON BETWEEN MODAL AND TIME-HISTORY CALCULATIONS, SECOND SPRING ELASTOPLASTIC*

$f_1 t_1$	$(Q_1)_{max}/(Q_1)_o$	$(Q_1)_{prob}/(Q_1)_o$	$(u_1)_{max}/(u_1)_o$	$(u_1)_{prob}/(u_1)_o$	$(Q_1)_{1st}/(Q_1)_o$	$(Q_1)_{code}/(Q_1)_o$	$(Q_2)_{max}/(Q_2)_y$	$(Q_2)_{prob}/(Q_2)_y$
							$(u_2)_{max}/(u_2)_m$	$(u_2)_{prob}/(u_2)_m$
0.1	0.34	0.27	1.02	0.81	0.26	0.27	0.96	0.68
0.2	0.46	0.33	1.38	0.99	0.27	0.28	0.74	0.55
0.3	0.39	0.29	1.17	0.87	0.25	0.27	0.55	0.39
0.4	0.51	0.45	1.53	1.35	0.44	0.47	0.72	0.56
0.6	0.48	0.46	1.44	1.38	0.46	0.48	0.67	0.59
0.8	0.52	0.50	1.56	1.50	0.50	0.53	0.79	0.72
1.0	0.55	0.53	1.65	1.59	0.53	0.56	0.86	0.78
1.4	0.64	0.61	1.92	1.83	0.61	0.64	1.00	0.89
2.0	0.51	0.48	1.53	1.44	0.48	0.51	0.79	0.68
3.0	0.82	0.77	2.46	2.31	0.77	0.82	1.25	1.08

* For the time-history calculations, the base spring was elastic and the ductility of the second spring was 3.

TABLE E.4 COMPARISON BETWEEN MODAL AND TIME-HISTORY CALCULATIONS, BOTH SPRINGS ELASTOPLASTIC

$f_1 t_1$	$(Q_1)_{max}/(Q_1)_y$	$(Q_1)_{prob}/(Q_1)_y$	$(Q_1)_{1st}/(Q_1)_y$	$(Q_1)_{code}/(Q_1)_y$	$(Q_2)_{max}/(Q_2)_y$	$(Q_2)_{prob}/(Q_2)_y$
	$(u_1)_{max}/(u_1)_m$	$(u_1)_{prob}/(u_1)_m$			$(u_2)_{max}/(u_2)_m$	$(u_2)_{prob}/(u_2)_m$
1.0	1.00	0.96	0.96	1.01	1.24	1.12

* For the time-history calculations, the ductility of both springs was 3.

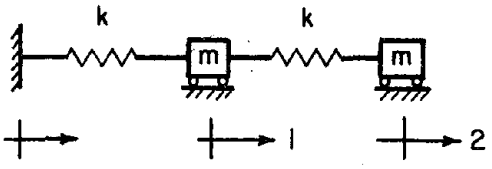

$$f_1 = 0.09836\sqrt{\frac{k}{m}} \qquad \left\{\tilde{\phi}^{(1)}\right\}^T = \left\{0.724 \quad 1.171\right\}$$

$$\frac{f_2}{f_1} = 2.618 \qquad \left\{\tilde{\phi}^{(2)}\right\}^T = \left\{0.276 \quad -0.171\right\}$$

FIG. E.1 TWO-DEGREE-OF-FREEDOM UNIFORM SHEAR-BEAM SYSTEM

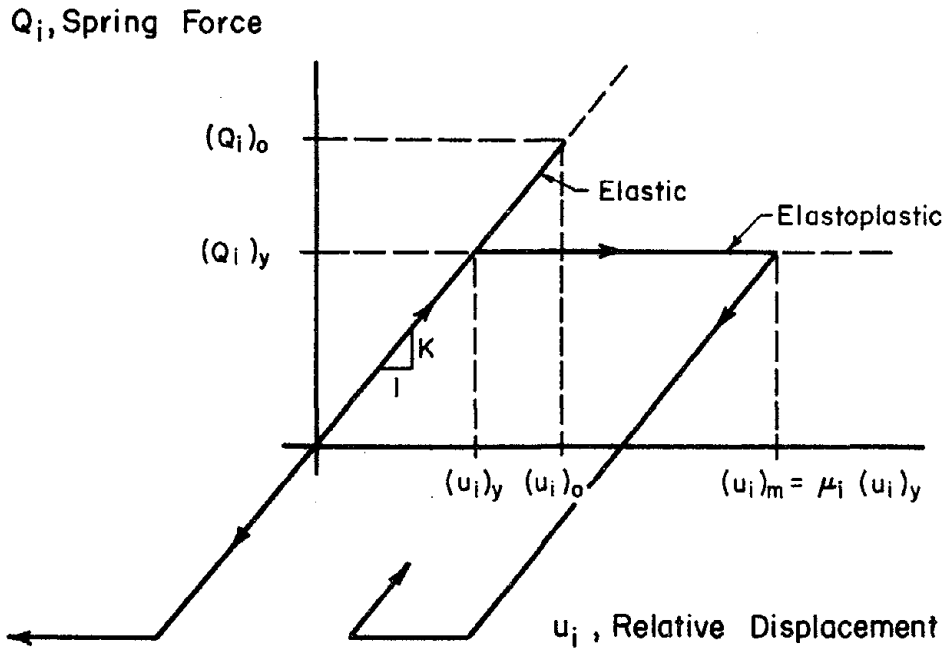

FIG. E.2 RESISTANCE-DEFORMATION RELATIONSHIP FOR A SPRING

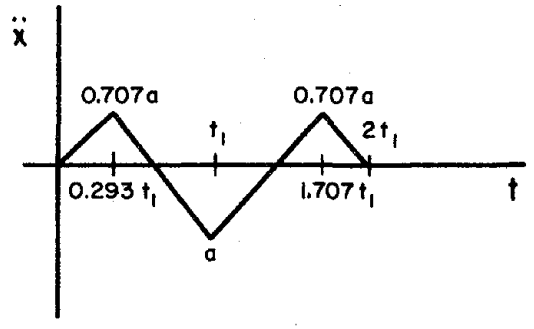

(a) Acceleration History

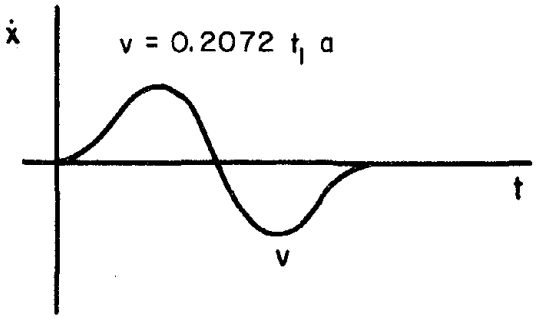

(b) Velocity History

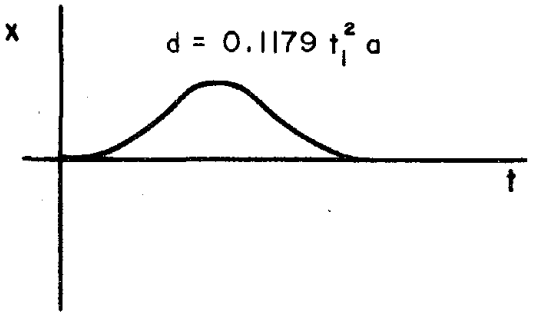

(c) Displacement History

FIG. E.3 HALF-CYCLE DISPLACEMENT PULSE
(AFTER VELETSOS AND VANN, 1971)

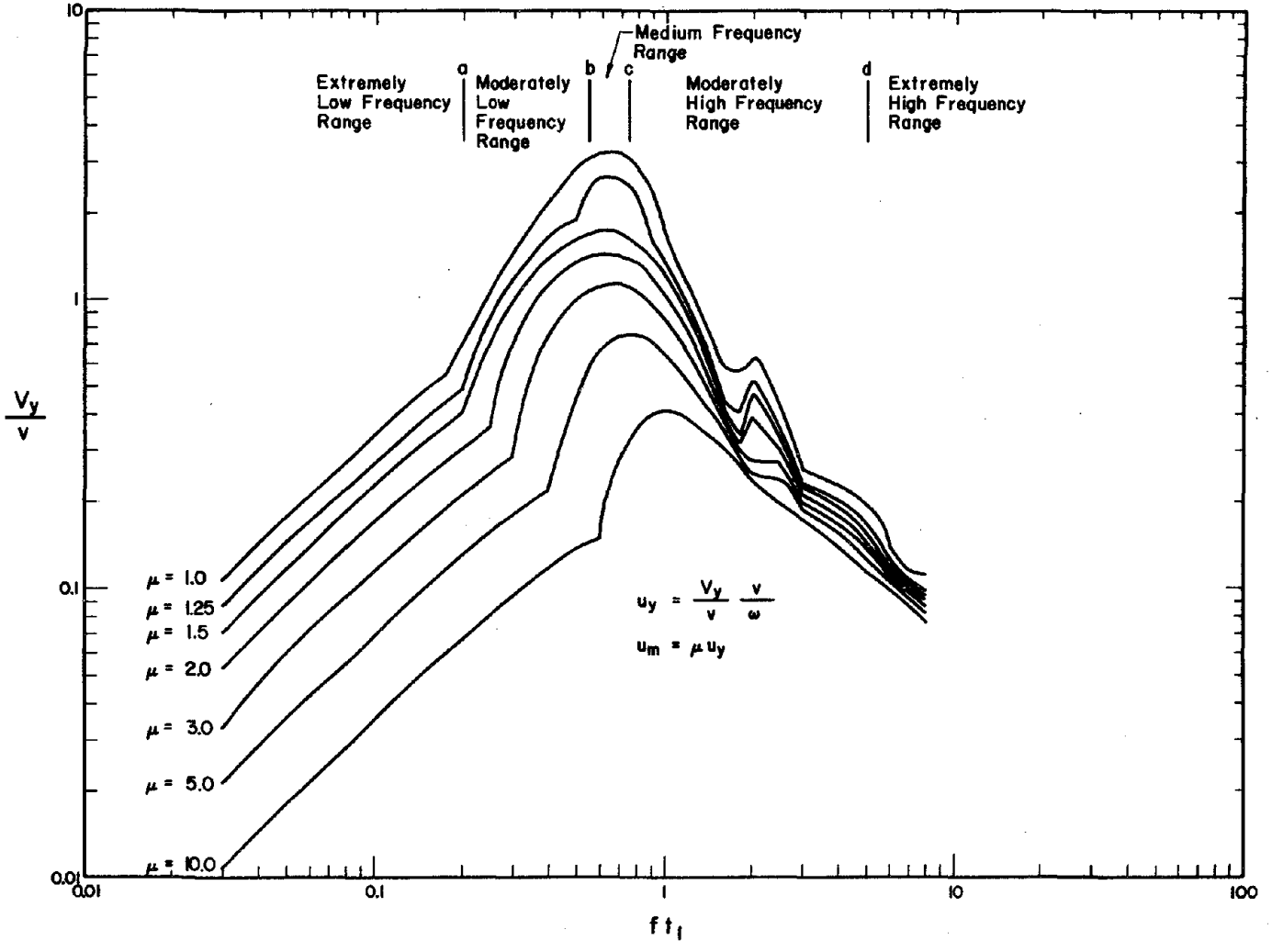

FIG. E.4 RESPONSE SPECTRA FOR UNDAMPED ELASTOPLASTIC SYSTEMS, HALF-CYCLE DISPLACEMENT PULSE

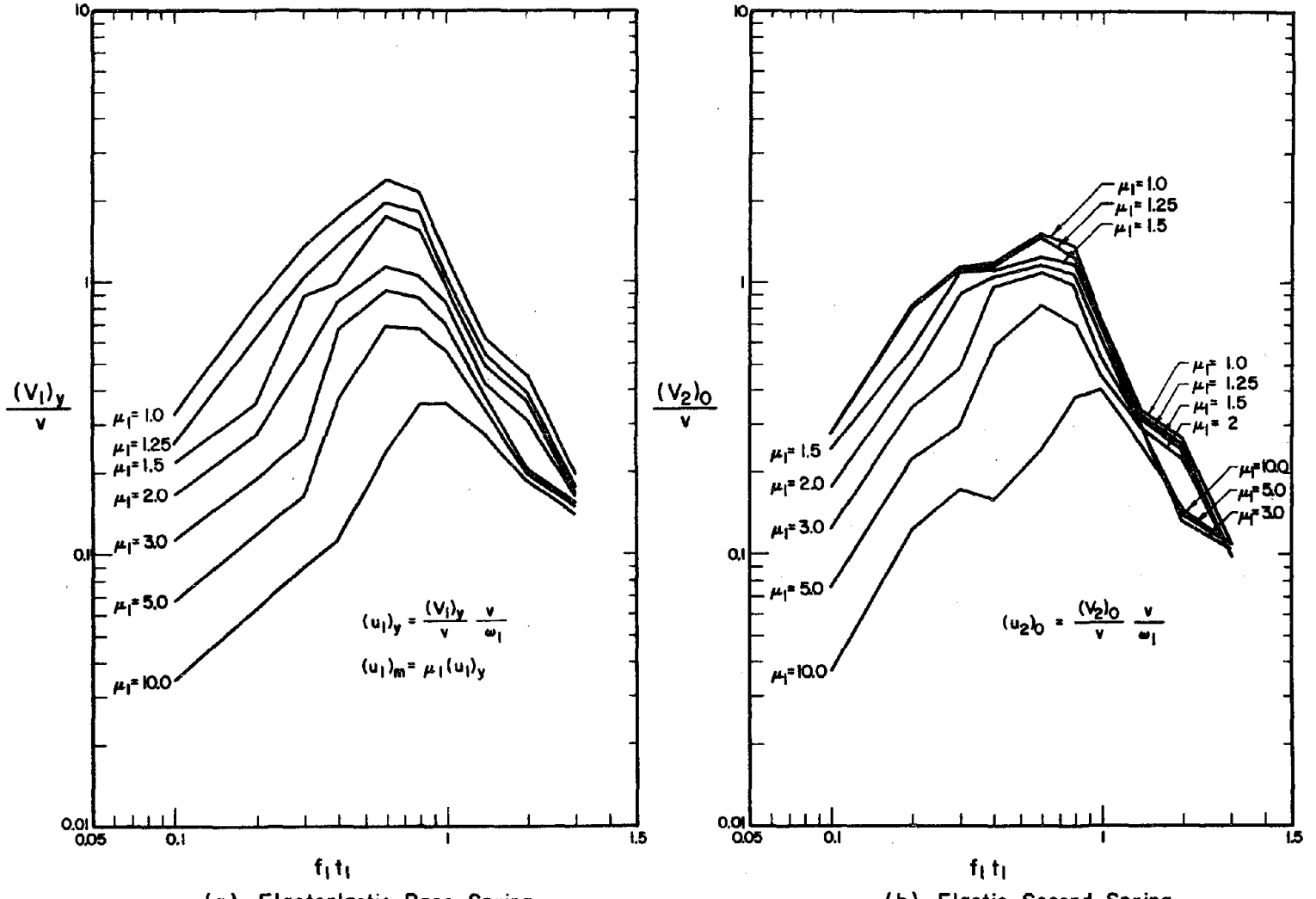

FIG. E.5 RESPONSE SPECTRA FOR TWO-DEGREE-OF-FREEDOM SYSTEMS, BASE SPRING ELASTOPLASTIC, SECOND SPRING ELASTIC, HALF-CYCLE DISPLACEMENT PULSE

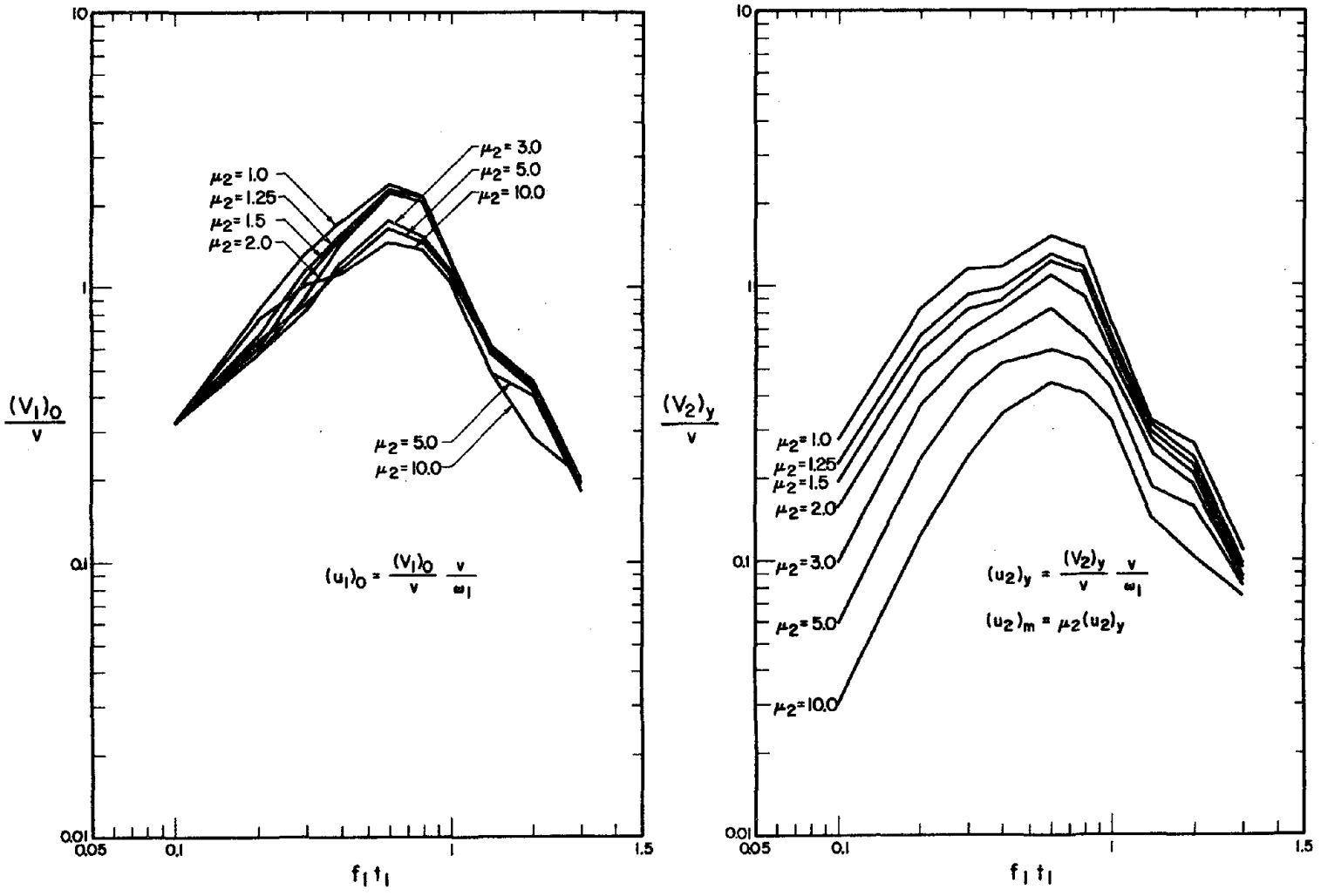

(a) Elastic Base Spring

(b) Elastoplastic Second Spring

FIG. E.6 RESPONSE SPECTRA FOR TWO-DEGREE-OF-FREEDOM SYSTEMS, BASE SPRING ELASTIC, SECOND SPRING ELASTOPLASTIC, HALF-CYCLE DISPLACEMENT PULSE

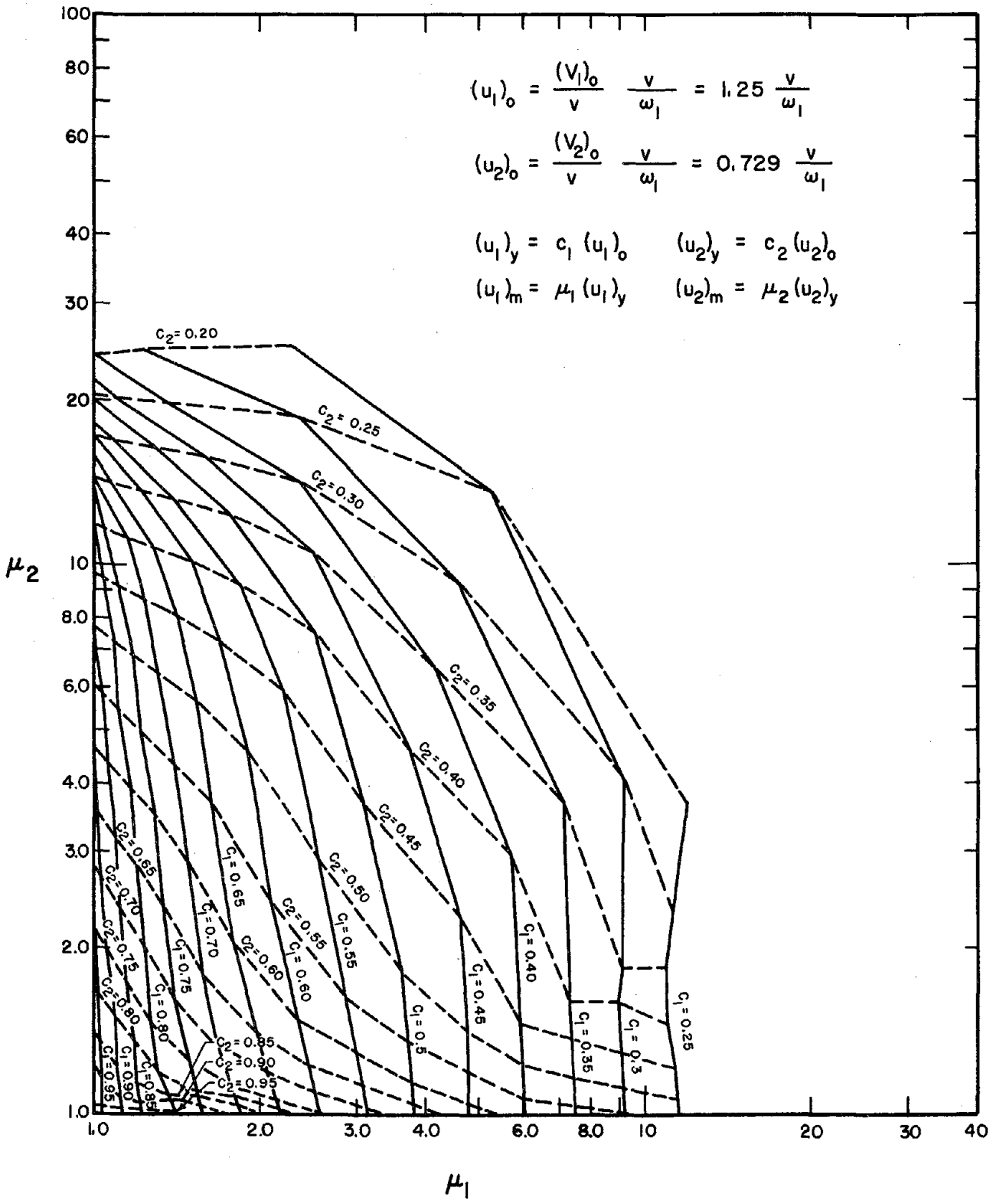

FIG. E.7 RESPONSE OF TWO-DEGREE-OF-FREEDOM SYSTEMS, BOTH SPRINGS ELASTOPLASTIC, HALF-CYCLE DISPLACEMENT PULSE, $f_1 t_1 = 1.0$

APPENDIX F. DETAILED RESULTS OF THE TIME-HISTORY CALCULATIONS

This appendix contains the detailed numerical data that were generated from the time-history analyses of the building designs considered in this study. The four time-history analysis cases considered are described in Chapter 4.

The inelastic hinge rotations for the building designs are given in Figs. F.1 through F.4. In Figs. F.2 and F.4(a), the maximum inelastic hinge rotations and the locations of the inelastic hinges on the structures during dynamic motion are presented. In Figs. F.1, F.3 and F.4(b) the cumulative hinge rotations, i.e., the sum of the absolute values of all the inelastic rotations occurring at a given hinge location during dynamic motion, are presented. The cumulative hinge rotations are normalized by the associated maximum inelastic hinge rotations. The data presented in Figs. F.1 through F.4 are supplementary to the data discussed in Section 4.2.2.

In Tables F.1 through F.12 are tabulated (a) the story shear coefficients, i.e., the story shears divided by the corresponding building weight, (b) the maximum story displacements relative to the ground, and (c) the maximum (relative) story drifts for the building designs considered. Tables F.1 through F.12 supplement the information discussed in Sections 4.2.3 and 4.2.4.

TABLE F.1 TIME-HISTORY RESPONSE QUANTITIES FOR SHEAR BUILDING DESIGN 2-A

	Elastic	Inelastic	Inelastic + PΔ
Story Shear Coefficients			
2	0.320	0.315	0.314
1	0.731	0.626	0.622
Story Displacements (in.)			
2	1.17	1.17	1.18
1	0.879	0.821	0.822
Story Drifts (%)			
2	0.268	0.264	0.263
1	0.611	0.570	0.571

TABLE F.2 TIME-HISTORY RESPONSE QUANTITIES FOR SHEAR BUILDING DESIGN 2-B

	Elastic	Inelastic	Inelastic + PΔ
Story Shear Coefficients			
2	0.355	0.251	0.252
1	0.792	0.326	0.326
Story Displacements (in.)			
2	3.11	2.18	2.20
1	2.16	1.89	1.94
Story Drifts (%)			
2	0.673	0.475	0.481
1	1.50	1.31	1.35

TABLE F.3 TIME-HISTORY RESPONSE QUANTITIES FOR SHEAR BUILDING DESIGN 2-C

	Elastic	Inelastic	Inelastic + P-Δ
Story Shear Coefficients			
2	0.250	0.118	0.111
1	0.528	0.144	0.154
Story Displacements (in.)			
2	5.21	3.31	3.90
1	3.66	2.91	3.46
Story Drifts (%)			
2	1.21	0.571	0.543
1	2.54	2.02	2.40

TABLE F.4 TIME-HISTORY RESPONSE QUANTITIES FOR MOMENT FRAME DESIGN 2-D

	Elastic	Inelastic	Inelastic + PΔ	Inelastic + FEF
Story Shear Coefficients				
2	0.430	0.344	0.340	0.343
1	0.814	0.517	0.510	0.510
Story Displacements (in.)				
2	3.01	2.46	2.48	2.45
1	1.59	1.54	1.56	1.52
Story Drifts (%)				
2	0.990	0.750	0.743	0.750
1	1.10	1.07	1.08	1.06

TABLE F.5 TIME-HISTORY RESPONSE QUANTITIES FOR MOMENT FRAME DESIGN 2-E

	Elastic	Inelastic	Inelastic + PΔ	Inelastic + FEF
Story Shear Coefficients				
2	0.237	0.184	0.187	0.185
1	0.441	0.276	0.272	0.276
Story Displacements (in.)				
2	3.12	2.54	2.70	2.63
1	1.95	1.91	2.06	1.99
Story Drifts (%)				
2	0.963	0.739	0.757	0.740
1	1.35	1.33	1.43	1.38

TABLE F.6 TIME-HISTORY RESPONSE QUANTITIES FOR MOMENT FRAME DESIGN 2-F

	Elastic	Inelastic	Inelastic + PΔ	Inelastic + FEF
Story Shear Coefficients				
2	0.445	0.445	0.445	0.351
1	0.655	0.655	0.658	0.626
Story Displacements (in.)				
2	2.14	2.14	2.16	2.12
1	0.832	0.832	0.846	0.806
Story Drifts (%)				
2	0.925	0.925	0.931	0.920
1	0.578	0.578	0.588	0.560

TABLE F.7 TIME-HISTORY RESPONSE QUANTITIES FOR X-BRACED FRAME DESIGN 2-G

	Elastic	Inelastic	Inelastic + PΔ
Story Shear Coefficients			
2	0.376	0.197	0.190
1	0.883	0.197	0.194
Story Displacements (in.)			
2	2.76	3.78	4.05
1	1.94	3.41	3.86
Story Drifts (%)			
2	0.574	0.313	0.291
1	1.35	2.37	2.68

TABLE F.8 TIME-HISTORY RESPONSE QUANTITIES FOR X-BRACED FRAME DESIGN 2-H

	Elastic	Inelastic	Inelastic + PΔ
Story Shear Coefficients			
2	0.309	0.235	0.220
1	0.738	0.333	0.330
Story Displacements (in.)			
2	1.28	1.83	1.68
1	0.956	1.59	1.48
Story Drifts (%)			
2	0.278	0.212	0.199
1	0.664	1.11	1.03

TABLE F.9 TIME-HISTORY RESPONSE QUANTITIES FOR MOMENT FRAME DESIGN 3-A

	Elastic	Inelastic	Inelastic + PΔ
Story Shear Coefficients			
3	0.184	0.137	0.134
2	0.351	0.233	0.221
1	0.499	0.253	0.241
Story Displacements (in.)			
3	5.86	3.98	4.19
2	4.14	2.98	3.10
1	1.89	1.87	1.95
Story Drifts (%)			
3	1.65	1.15	1.15
2	1.77	1.16	1.15
1	1.43	1.41	1.48

TABLE F.10 TIME-HISTORY RESPONSE QUANTITIES FOR MOMENT FRAME DESIGN 3-B

	Elastic	Inelastic	Inelastic + PΔ	Inelastic + FEF
Story Shear Coefficients				
3	0.249	0.199	0.194	0.192
2	0.331	0.301	0.304	0.299
1	0.467	0.442	0.438	0.436
Story Displacements (in.)				
3	3.54	3.62	3.61	3.45
2	2.06	2.12	2.16	2.06
1	0.840	0.832	0.857	0.805
Story Drifts (%)				
3	1.26	1.33	1.32	1.22
2	0.989	1.01	1.03	0.993
1	0.636	0.630	0.649	0.610

TABLE F.11 TIME-HISTORY RESPONSE QUANTITIES FOR X-BRACED FRAME DESIGN 3-C

	Elastic	Inelastic	Inelastic + PΔ
Story Shear Coefficients			
3	0.205	0.142	0.108
2	0.529	0.197	0.195
1	0.618	0.197	0.194
Story Displacements (in.)			
3	3.53	4.03	3.71
2	2.99	3.69	3.44
1	1.61	2.87	2.95
Story Drifts (%)			
3	0.406	0.281	0.215
2	1.05	0.711	0.614
1	1.22	2.18	2.23

TABLE F.12 TIME-HISTORY RESPONSE QUANTITIES FOR X-BRACED FRAME DESIGN 3-D

	Elastic	Inelastic	Inelastic + PΔ
Story Shear Coefficients			
3	0.226	0.194	0.167
2	0.632	0.317	0.315
1	0.827	0.317	0.313
Story Displacements (in.)			
3	2.74	2.46	2.34
2	2.37	2.17	2.17
1	1.34	1.70	1.70
Story Drifts (%)			
3	0.278	0.239	0.207
2	0.779	0.426	0.409
1	1.02	1.29	1.29

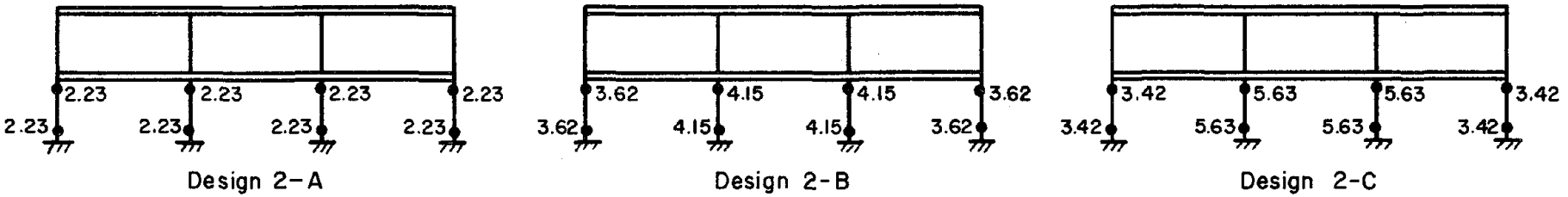

(a) Two-Story Shear Buildings

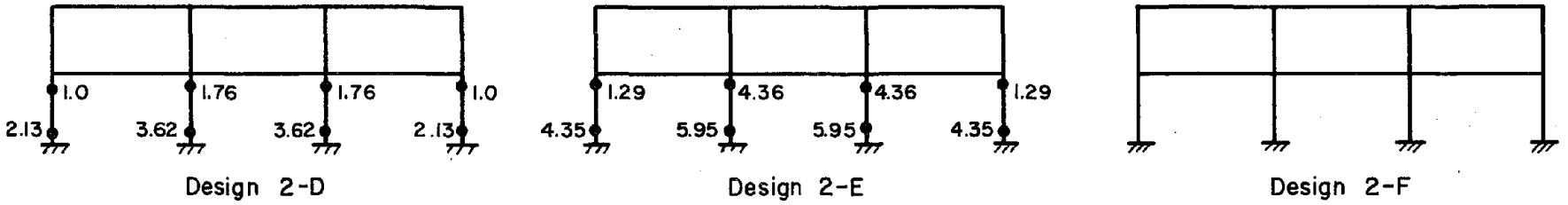

(b) Two-Story Moment Frame Buildings

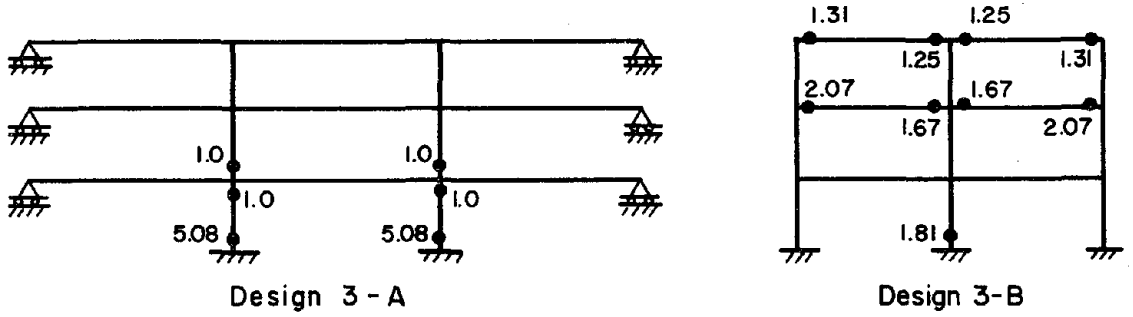

(c) Three-Story Moment Frame Buildings

FIG. F.1 CUMULATIVE/MAXIMUM HINGE ROTATIONS FOR INELASTIC CASE

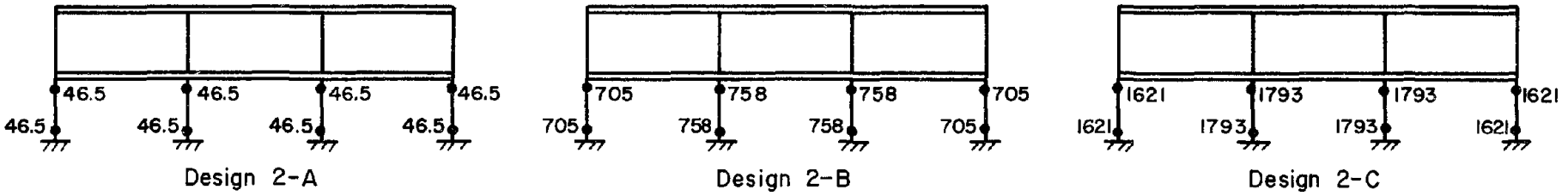

(a) Two-Story Shear Buildings

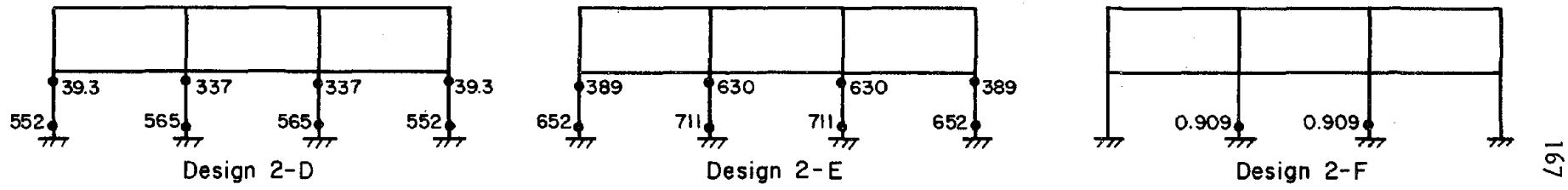

(b) Two-Story Moment Frame Buildings

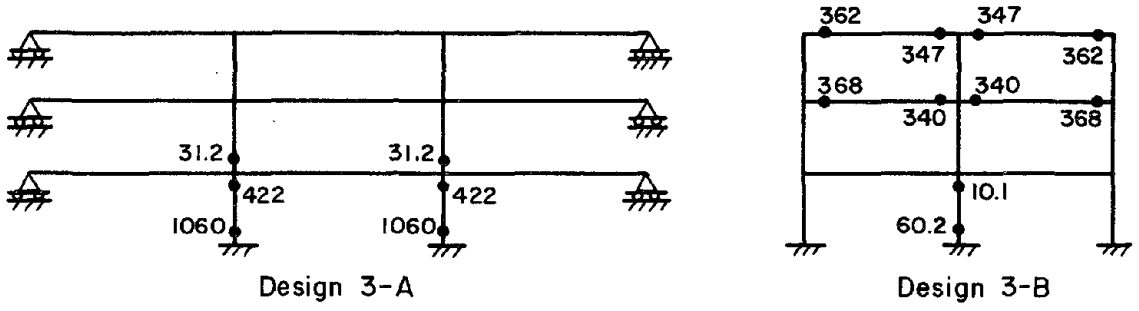

(c) Three-Story Moment Frame Buildings

FIG. F.2 MAXIMUM HINGE ROTATIONS FOR INELASTIC + PΔ CASE, 10^{-5} Rad

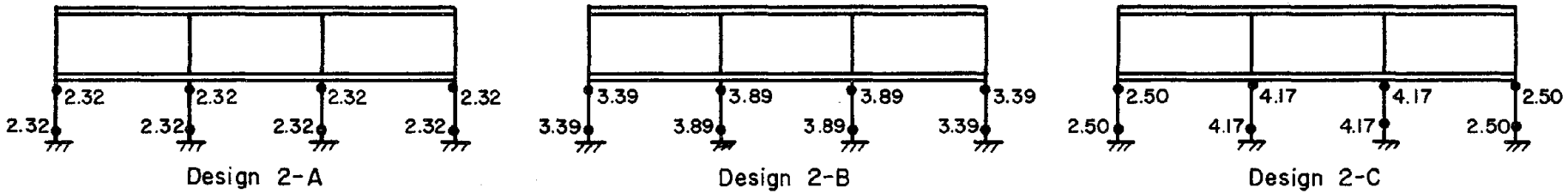

(a) Two-Story Shear Buildings

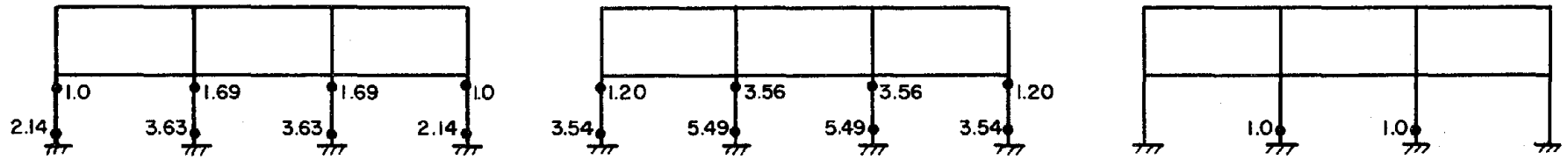

(b) Two-Story Moment Frame Buildings

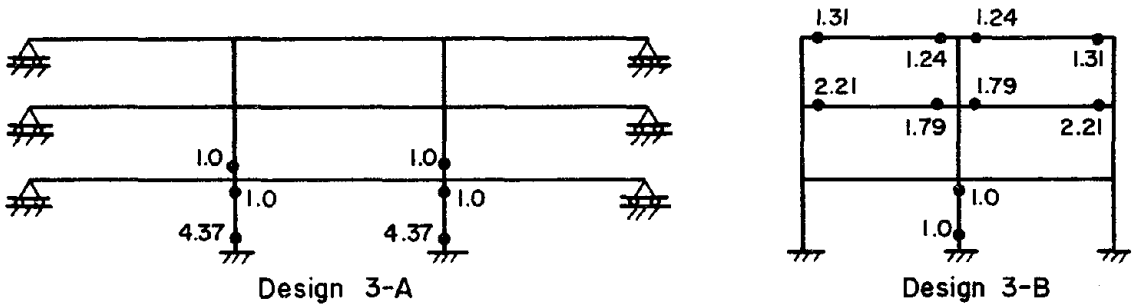

(c) Three-Story Moment Frame Buildings

FIG. F.3 CUMULATIVE/MAXIMUM HINGE ROTATIONS FOR INELASTIC + PΔ CASE

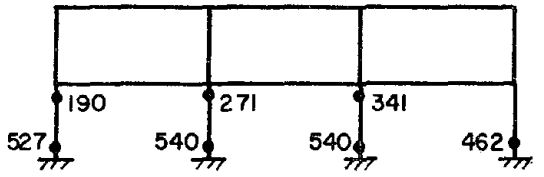

Design 2-D

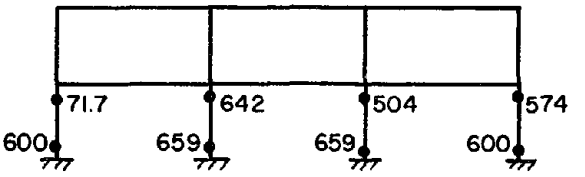

Design 2-E

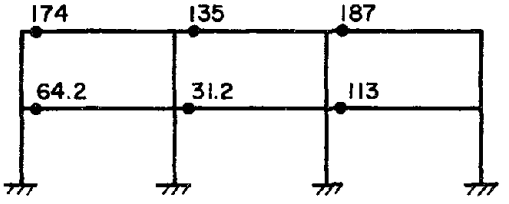

Design 2-F, Motion Left

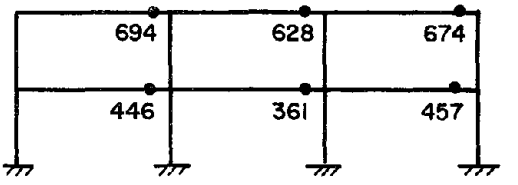

Design 2-F, Motion Right

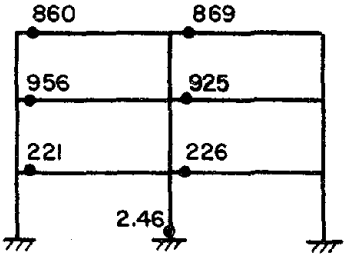

Design 3-B, Motion Left

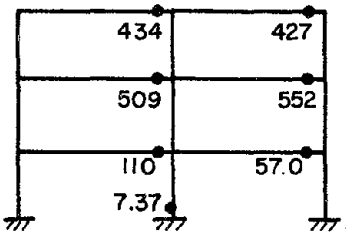

Design 3-B, Motion Right

(a) Maximum Hinge Rotations, 10^{-5} Rad.

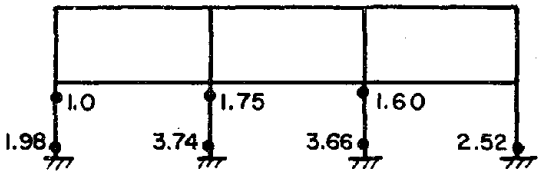

Design 2-D

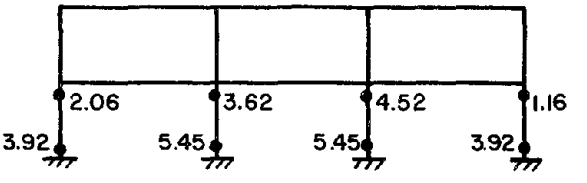

Design 2-E

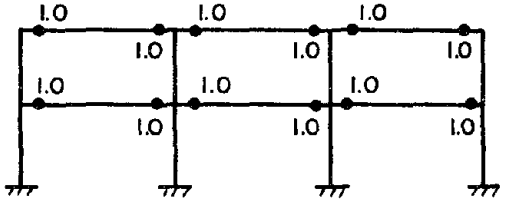

Design 2-F

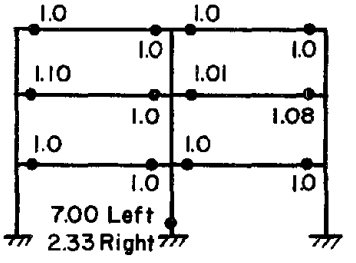

Design 3-B

(b) Cumulative/Maximum Hinge Rotations

FIG. F.4 HINGE ROTATIONS FOR INELASTIC + FEF CASE